# Anatomy and physiology of macaque visual cortical areas V1, V2 and V5/MT: bases for biologically realistic models

**Running title:** Neuroinformatics of macaque vision

**Simo Vanni*** simo.vanni@helsinki.fi
HUS Neurocenter, Neurology, Helsinki University Hospital, Finland.
Department of Neurosciences, University of Helsinki, Finland.

**Henri Hokkanen** henri.hokkanen@helsinki.fi
HUS Neurocenter, Neurology, Helsinki University Hospital, Finland.
Department of Neurosciences, University of Helsinki, Finland.

**Francesca Werner** francesca.werner@studio.unibo.it
HUS Neurocenter, Neurology, Helsinki University Hospital, Finland.
Department of Neurosciences, University of Helsinki, Finland.
Department of Biomedical and Neuromotor Sciences, University of Bologna, Italy.

**Alessandra Angelucci** alessandra.angelucci@hsc.utah.edu
Department of Ophthalmology and Visual Sciences,
Moran Eye Institute, University of Utah,
Salt Lake City, Utah, USA.

**Keywords:** microcircuit, neural network, neuroinformatics, biomimetic

*** Corresponding author:**

Email: simo.vanni@helsinki.fi Address: Biomedicum Helsinki, Neurology Research Unit, PO Box 700, 00290 Helsinki, Finland. Tel. +358 50 586 5530.

# Abstract

The cerebral cortex of primates encompasses multiple anatomically and physiologically distinct areas processing visual information. Areas V1, V2 and V5/MT are conserved across mammals and are central for visual behavior. To facilitate the generation of biologically accurate computational models of primate early visual processing, here we provide an overview of over 350 published studies of these three areas in the genus Macaca, whose visual system provides the closest model for human vision.

The literature reports 14 anatomical connection types from the lateral geniculate nucleus of the thalamus to V1 having distinct layers of origin or termination, and 194 connection types between V1, V2 and V5, forming multiple parallel and interacting visual processing streams. Moreover, within V1, there are reports of 286 and 120 types of intrinsic excitatory and inhibitory connections, respectively.

Physiologically, tuning of neuronal responses to 11 types of visual stimulus parameters have been consistently reported. Overall, the optimal spatial frequency of constituent neurons decreases with cortical hierarchy. Moreover, V5 neurons are distinct from neurons in other areas for their higher direction selectivity, higher contrast sensitivity, higher temporal frequency tuning and wider spatial frequency bandwidth.

We also discuss currently unavailable data that could be useful for biologically accurate models.

One of the fundamental aims of visual neuroscience is to understand the computational principles underlying biological vision. How do the biophysics of single neurons and network interactions generate neuronal receptive fields (RFs), process sensory inputs and cause visual behavior? Decades of studies have provided a wealth of data and multiple descriptive and quantitative models of vision. Nevertheless, we still lack the ability to construct accurate computational models that can reproduce a biologically meaningful visual system. Such models and related computer simulations could help bridge the gap between the physiological responses of single neurons and existing abstract models of vision, as well as provide a better understanding of cortical processing.

The continuous increase of computational power has recently enabled the first comprehensive microcircuit simulations of the rat somatosensory cortex (Markram et al. 2015). Recent simulations of macaque monkey visual cortex have explored large-scale interactions between visual cortical areas (Mejias et al. 2016), replicated natural firing rate statistics in a laminar network model of the primary visual cortex (V1; Rasch et al., 2011), or described the generation of orientation tuning and the dynamics of V1 sublayer 4C alpha (Chariker et al. 2016). However, we are still far from being able to replicate the multiplicity of cortical functions, let alone visual behavior, with biologically realistic model simulations.

Accurate numerical model simulations require quantitative data on the anatomy and physiology of the system, as well as on the structure and biophysical parameters of distinct cell types. With unavoidable gaps in available data, unknown parameters need to be explored against known neural RF properties, and eventually compared with visual behavior.

To facilitate the generation of realistic computational models of visual cortex, here we have collated data from more than 350 publications on connectivity, physiological RF

properties and single neuron biophysical properties in three visual cortical areas (V1, V2 and V5 or Middle Temporal –MT–) of the macaque monkey, one of the best studied animal genus in vision research, and the available animal model closest to humans (Kaas 1992; Preuss 2004).

In macaques, visual information drives a network of about 30 interconnected cortical areas organized into a hierarchical network according to laminar connectivity patterns (Maunsell and Van Essen 1983b; Ungerleider and Desimone 1986; Zeki and Shipp 1988; Felleman and Van Essen 1991; Merigan and Maunsell 1993; Barone et al. 2000; Van Essen 2003; Shipp 2007; Kravitz et al. 2011, 2013; Markov, Vezoli, et al. 2014). V1, at the bottom of this hierarchy, sends prominent connections to areas V2, V3, V4, V5/MT and V6; in turn these V1-recipient cortical areas are interconnected with each other.

Here we focus on areas V1, V2 and V5/MT, as there is general agreement on the location and macroscopic boundaries of these areas in primates and humans, and their anatomy and electrophysiological properties have been extensively characterized. In contrast, there is ongoing debate regarding the exact parcellation and function of the areas that occupy the cortical territory between V2 and V5 (Kaas 1992, 2003; Van Essen 2003; Wandell et al. 2007; Angelucci and Rosa 2015; Angelucci et al. 2015; Zhu and Vanduffel 2019). V1, V2 and V5 participate in early visual processing and are mutually connected. These areas represent multiple low- and middle-tier visual stimulus features at various scales, necessary for visually guided behavior (Hegdé and Van Essen 2003; Born and Bradley 2005; Sincich and Horton 2005; Vidyasagar and Eysel 2015; Zeki 2015). Phylogenetically, V1 and V2 are conserved in mammals, and V5 is found in all primate species studied (Kaas 1995, 2003; Large et al. 2016) suggesting that these three areas play a fundamental role in cortical processing of visual signals.

Despite challenges, such as the occurrence of multidimensional RFs, the complexity of

the cortical microcircuit, different definitions of the various parameters in different studies, and missing data, this review attempts to report the available data in a consistent way. We also attempt to provide a balanced overview of controversial issues, and to emphasize quantitative data. The latter are reported as numerical quantities, or best estimates of proportions or relative strengths, when these are available in the literature. When quantitative data are not available, we cover qualitatively topics, which we consider important for building computational models.

# Anatomical and physiological database and conventions

All data reported here are limited to the Old World monkey genus Macaca, including mainly the species *M. fascicularis*, *M. nemestrina*, *M. mulatta*, and *M. fuscata*. In addition, we report data from functional anatomy studies performed in *M. arctoides*, *M. assamensis*, *M. irus* or *M. radiata*. When different developmental stages were compared in a study, we extracted only data from young adult individuals.

For consistency and brevity, we have excluded data from New World monkeys which are phylogenetically more distant from humans than macaques [for phylogenetic comparison of primate visual cortices, see (Kaas 2003, 2005; Rosa and Tweedale 2005)]. However, for some experimental questions and methodological approaches, the New World primates are better suited animal models. For example, the smooth cortical structure of the marmoset cortex allows easier and simultaneous access to multiple visual cortical areas.

We have combined data from several species of the genus *Macaca*. Brain volume across the included species varies by a factor of about 1.7 (Marino 1998), which may introduce variability in quantifications between different datasets. Given the similar pattern of V1 layers across primate species (Balaram and Kaas 2014), we expect little

structural variation across macaque subspecies. Saleem et al (2007) studied the anatomical differences of medial temporal lobe areas between *M. fuscata*, *M. fascicularis* and *M. mulatta*. They found a similar anatomical organization of cortical layers, but one of the four areas studied showed a shift in areal boundary across sub-species. Similarly, the primary auditory cortex and its surrounding fields are smaller in *M. fascicularis* than in *M. fuscata*, whereas the laminar distributions of various histochemical stains were similar (Jones et al. 1995). These studies suggest that subtle differences in the macroscopic anatomy of visual cortical areas are likely to exist among macaque subspecies, but the general functional architecture is likely conserved.

Moreover, animal gender can introduce additional variability, as for example, in *M. mulatta*, the volume of the male brain is on average 1.26 times larger than that of the female (Franklin et al. 2000). However, the primary driver of variability is likely the body weight, as this is closely correlated with brain weight (Jerison 1955), therefore requiring knowledge of the body weight of the individual animals, more than their species or gender, in order to calibrate the data; unfortunately we lacked this information, therefore, our reports are not corrected for any of these factors.

Tuning properties of neuronal responses to eleven visual stimulus parameters were reported consistently across the literature and are summarized in the figures. For other parameter values in the text and tables, we report the mean and range of the mean values reported across studies (but no range if there was only one study). For a model system this can serve as the range of possible mean parameter values. The distribution of values behind the means were inconsistently reported across studies and, of course, it was impossible for us to control for outliers. These original distributions are omitted in this review, unless descriptive statistics, such as standard deviation, were available for the whole data in the original studies. The supplementary material comprises both anatomical

153 and physiological data in machine readable csv format.

154

## 155 Anatomical conventions

156 There are two different nomenclatures for V1 layers in the literature. We follow the
157 more widely used Brodmann's nomenclature, according to which layer (L) 4 has four
158 subdivisions (4A, 4B, 4Cα, 4Cβ; Brodmann 1909, translated by Garey, 2006). Hassler's
159 nomenclature is based on the same histological subdivisions, but layers 4A and 4B of
160 Brodmann are considered part of L3 (Hassler 1966).

161 Area V5 is also known as MT, for middle temporal, following its original naming in
162 the New World monkeys. In V1, we group L2 with L3A, as typical in many interlaminar
163 connectivity studies.

164 Here connection strength is defined mainly as the number of labeled neurons in
165 retrograde tracer studies, or density of axonal projections of singly labeled neurons. Such
166 anatomical definition of strength does not obviously reflect the actual physiological
167 strength of a connection, which depends on several other factors such as neuron identity,
168 and the number, strength and locations of pre-synaptic boutons on the postsynaptic
169 neuron. Note, also, that connection strength can only be compared within single tracer
170 injections, because the number of labeled cells varies across injections of different size.
171 When quantitative data were unavailable, connection strength was estimated from figures
172 or from the text and reported in Figure 2 and Supplementary Table 1 as sparse, medium or
173 dominant connection strength to indicate the approximate number of presynaptic somata
174 or axonal terminations. For interareal connections, the term "dominant" indicates the
175 combined dominant origin and termination of a given connection. In the absence of any
176 description of connection strength in the original publications, we set the strength to
177 medium. For contradicting results in different studies, we gave more weight to the data

that were more rigorously quantified. When quantitative data were available, sparse, medium and dominant connections (in Figure 2 and Supplementary Table 1) indicate <10%, 10-50% and >50%, respectively, of cells (for a given tracer injection), or of synapses/boutons/axonal length (for intracellular microinjections).

When axons of traced neurons were reported to terminate at a border between two cortical layers, the connection was marked as terminating in both layers. We included studies using glutamate uncaging (Sawatari and Callaway 2000; Briggs and Callaway 2001, 2005; Yabuta et al. 2001). This method reveals connections to neurons with somata and dendrites located within the postsynaptic layer, as well as to neurons with somata residing in other layers but with dendrites extending into the postsynaptic layer. Connectivity studies based on degeneration were not included.

For interareal connectivity studies, single tracer injections are typically not confined to a layer and therefore the layers of origin and termination within the injection site could not be identified. Therefore, in Supplementary Table 1, we report separately the literature references for the connections' origin and termination; moreover, for each laminar origin and termination the same reference is repeated for each laminar termination and origin, respectively. These data are visualized in Figure 2 reporting the existence and density of inter-areal connections between different layers of the connected areas. For example, Lund et al. (1981), following retrograde tracer injections across all V2 layers found labeled cells in V1 L2/3A, 4A and 4B, while following anterograde tracer injections into all V1 layers they found labeled terminations in V2 L4 and L3B with sparser spread into L3A, and at the L5 and 6 border. For the retrograde tracer injection of this study, in Supplementary Table 1 and Figure 2, we report 3 types of connections from V1 to V2, one arising from V1 L2/3A, the second from V1 L4A, and the third from V1 L4B, each terminating in V2 L3A , 3B, 4, 5B and 6, and cite this study five times for each of the

three V1 layers of origin.

## Description of physiological parameters.

Physiological RF data were reported as the total number or percent of cells in a given area as a function of a given RF parameter. This allowed us to combine different datasets if the reported values were comparable. To this goal, we extracted and digitized data from the figures in the original publications and reported in our figures the proportion of cells across studies as a function of a given physiological parameter value. Because we are not analyzing the original raw data, but summary histograms, the descriptive statistics we report here inevitably include some inaccuracies, for example errors in the centering of the bins on the X-axis of the original data, residual rotation, and calibration and digitization errors. As a quality control, we visualized all data-reporting figures, calibration and digitized points, and then re-digitized all data exceeding 10% mismatch between the total number of cells reported in the original study and that reported in our data.

Different studies used different metrics for data analysis. We included only data from one of these metrics, or data that could be converted into a standard metrics using a simple transformation. For example, different datasets report either circular variance (CV) or orientation selectivity index (OSI=1 – CV), as measures of orientation selectivity. In this case, we converted OSIs to CV.

# Anatomy

Anatomical data show significant individual variability, and many studies are based on only few monkeys. Thus, some of the mean values reported below may not reflect real population means.

Recently, mouse neocortical cells have been classified into 133 transcriptomic clusters based on single-cell RNA sequencing. These clusters included 61 GABAergic, 56 glutamatergic, and 16 non-neuronal types (Tasic et al. 2018). However, the number of such clusters depends on the cut point of the clustering method. Based on axonal projection patterns mainly in rodents, cortical excitatory cells have been classified into three major groups, intratelencephalic (projection to cortex and striatum), pyramidal tract (projections mainly to the brainstem, spinal cord and midbrain) and corticothalamic (projections mainly to the ipsilateral thalamus), with ongoing subgrouping efforts based on morphology, gene expression and physiology (reviewed in Shepherd 2013; Harris and Shepherd 2015). Following existing literature on the neuroanatomy of macaque visual cortex, largely from the 80's until the last decade (Gilbert 1983; Nieuwenhuys 1994; Douglas and Martin 2004), below we divide excitatory cells into two major morphological groups, spiny stellate and pyramidal cells. Further subgrouping pyramidal cell is challenging, due to the wide diversity of pyramidal cell dendritic and axonal morphologies, which could result in an intricate classification according to soma position, branching patterns or axonal targets (examples in Larkman 1991; Markram, Muller, Ramaswamy, Reimann, Schurmann, et al. 2015); moreover, such a subgrouping across layers has not been systematically applied to macaque visual cortex. The pyramidal and spiny stellate cells receive excitatory input predominantly onto their spines, and inhibitory input onto their somas, dendritic shafts and axon initial segments.

Likewise, a general system for GABAergic interneuron classification is missing [for reviews, see (Markram et al. 2004; Ascoli et al. 2008; DeFelipe et al. 2013)]. Cells immunoreactive for the calcium-binding proteins calbindin, calretinin, and parvalbumin are distributed non-uniformly across laminae in macaque V1 and V2 (DeFelipe et al. 1999), but these markers are not uniquely mapped to morphological cell types (Ascoli et

al. 2008; Markram et al. 2015). In rodent cortex, interneurons have been classified into three major types based on expression of parvalbumin, somatostatin and $5HT_{3A}$-receptor, each type having a different embryonal origin (Lee et al. 2010; Rudy et al. 2011). However, a similar classification has not been systematically applied to macaque visual cortex.

GABA-releasing inhibitory interneurons can be further classified based on the morphological, physiological or molecular phenotype (Ascoli et al. 2008; DeFelipe et al. 2013). At least eight morphological subtypes exist (Jones 1993; DeFelipe et al. 2013), with the double bouquet cell following a unique developmental path in primates (reviewed in DeFelipe, 2011; Betizeau et al., 2013). In the 80's and 90's, Jennifer Lund and colleagues published a series of Golgi-staining studies describing the various morphological inhibitory cell types in macaque V1 and their distinct laminar distributions of dendritic and axonal projections (Lund 1987; Lund et al. 1988; Lund and Yoshioka 1991; Lund and Wu 1997). These studies, however, did not quantify these cells' morphological features. Recently introduced automatic classifier methods might help generating a more unified classification of cell type morphologies (DeFelipe et al. 2013), but presently there exist no quantitative analyses of inhibitory cells in distinct areas and layers of macaque visual cortex.

## Area size and cell numbers, types and locations

***Lateral Geniculate Nucleus (LGN).*** In each LGN of *M. Mulatta*, the two magnocellular  Magno) layers, one for each eye, comprise on average 148 x $10^3$ neurons (range across monkeys 91–235 x $10^3$), and the four parvocellular (Parvo) layers, two for each eye, 1270 x $10^3$ neurons (range 900–1700 x $10^3$, Ahmad and Spear, 1993). Earlier

278 estimates of Magno- and Parvo LGN cell numbers, including data from undefined
279 macaque species, give values between the ranges above (le Gros Clark, 1941; Connolly
280 and Van Essen, 1984; reviewed in Peters et al., 1994). Of the numbers above, 35% of cells
281 in the Magno layers, and 25% of cells in the Parvo layers are immunoreactive for the
282 inhibitory neurotransmitter gamma-aminobutyric acid (GABA), therefore are local
283 inhibitory interneurons, the remaining being thalamocortical projection neurons (Montero
284 and Zempel 1986).

285 A neurochemically distinct population of koniocellular (Konio) cells was recognized
286 later (Hendry and Yoshioka 1994). It occupies primarily the spaces between and below
287 the Magno- and Parvo layers in LGN, forming six distinct layers, termed the intercalated
288 or K layers (reviewed in Hendry and Reid, 2000; Casagrande et al., 2007). These layers
289 comprise about 100 x $10^3$ projection neurons, and apparently no inhibitory interneurons.
290 In addition, small neurons with the chemical signature of K cells are also scattered within
291 the M and P layers and form bridges between the K layers (Hendry and Yoshioka 1994).

292 ***V1, V2, V5: Area size.*** The sizes and neuron numbers of cortical areas vary across
293 individual monkeys, being related to body weight, which has an allometric relation to
294 cortical surface (Maunsell and Van Essen 1987; Hofman 1989).

295 In the adult macaque monkey, the whole cortical surface of one hemisphere may
296 comprise up to 130-140 functionally distinct areas (Van Essen et al. 2012) and covers, on
297 average, an area of 10430 $mm^2$ (N = 10 hemispheres from 3 *M. mulatta* and 7 *M.*
298 *fascicularis*, range across monkeys 8286-14113 $mm^2$; Sincich et al., 2003). V1 represents
299 about 13% and V2 about 10% of this total area. Table 1 reports the surface areas for V1,
300 V2 and V5. The corresponding surface area ratios between these three areas are
301 1:0.80:0.042, respectively.
302

**Table 1.** Cortical surface areas ($mm^2$) from anatomical studies. N = total number of hemispheres. The mean values across studies were weighted by the N hemispheres in each study. Parenthesis enclose the range across the means of individual studies. Min and max values indicate the lowest and highest values in individual monkeys across all studies. References: 1. Gattass et al. 1981; Van Essen et al. 2. 1981, 3. 1986, 4. 2002; 5. O'Kusky and Colonnier 1982a; 6. Ungerleider and Desimone 1986a; 7. Maunsell and van Essen 1987; 8. Olavarria and Van Essen 1997; 9. Sincich et al. 2003.)

| | V1 | V2 | V5 |
|---|---|---|---|
| **Mean** | 1181 (797-1343) | 944 (730-1012) | 50 (33-73) |
| **Min** | 690 | 660 | 24 |
| **Max** | 1817 | 1412 | 99 |
| **N** | 58 | 17 | 37 |
| **Refs** | 1-5,9 | 1,3,8-9 | 2,6-7,9 |

***V1: neuron numbers and types.*** Pyramidal cell bodies occur in all V1 layers, except 4C and 1 (Lund 1973). Moreover, the apical dendrites of pyramidal cells residing in L5 and L6 have few spines in L4C. Spiny stellate cells occur in all V1 L4 subdivisions, and in L4C they constitute 85-95% of all neurons (Mates and Lund 1983; Fitzpatrick et al. 1987). Moreover, Briggs et al. (2016) have recently reported some spiny stellate cells in V1 L6A. Inhibitory stellate cells occur in all V1 layers.

Figure 1 depicts the modular organization of V1, which includes the ocular dominance columns (ODC) and cytochrome oxidase (CO) blobs, as well as the six layers of V1. Monocular RFs predominate in L4C, and the blob structure is most evident in L3. Above and below these layers, RFs are biased to represent the same ODC, blob/interblob compartment, and other RF properties such as preference for the orientation of edges,

316 usually referred to as columnar organization.

317

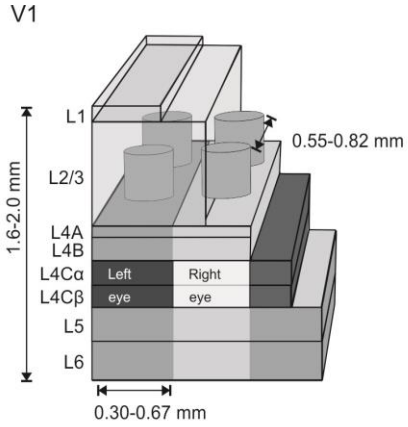


318

**Figure 1**. **Schematics of cytochrome oxidase (CO) and ocular dominance modules in V1.** The cylinders in L3 depict CO blobs, and the lighter and darker columnar gray bands the ocular dominance columns (ODC), most emphasized in L4C (Hubel and Wiesel 1968). References for cortical thickness (range of means; Chow et al. 1950; Lund 1973; O'Kusky and Colonnier 1982b); layer thickness is drawn approximately to scale (Lund 1973); reported distance between CO blobs is the range across monkeys (Horton 1984; Landisman and Ts'o 2002); reported width of ODC is the range across monkeys (LeVay et al. 1975; Horton and Hocking 1996).

319

320 Table 2 reports the total number of neurons and the relative number of inhibitory
321 neurons in each layer of area V1. The total number of neurons in one hemisphere of adult
322 macaque V1 (N=2 *M. fascicularis* and 4 *M. mulatta*) is 161 x $10^6$ (SD=18), and the total
323 number of synapses is 381 x $10^9$ (SD=53). V1 covers on average 841 $mm^2$ (SD=88)
324 surface area (N=7 hemispheres; O'Kusky and Colonnier, 1982). A recent study based on
325 rigorous stereological methods estimated V1 neuron numbers more than double the
326 original estimates. (Table 2; Giannaris and Rosene, 2012).

327

**Table 2.** Total number of neurons, synapses/neuron, and the proportion of inhibitory interneurons in each cortical layer of area V1. * Layers 2 and 3 together; ** Layers 4Cα and 4Cβ together. References: 1. O'Kusky and Colonnier 1982b; 2. Fitzpatrick et al. 1987; 3. Hendry et al. 1987; 4. Beaulieu et al. 1992; 5. Giannaris and Rosene 2012.)

| Layer | N neurons x $10^6$ | Synapses / neuron x $10^3$ | % inhibitory | N neurons x $10^6$ |
|---|---|---|---|---|
| **1** | 0.47 | 61.8 | 84 | Supragr. 215 |
| **2** | 44* | 2.6* | 20 | |
| **3** | | | 20 | |
| **4A** | 17 | 1.6 | 22 | Granular 121 |
| **4B** | 17 | 2.7 | 19 | |
| **4Cα** | 14 | 1.9 | 16** | |
| **4Cβ** | 24 | 1.4 | | |
| **5** | 20 | 1.7 | 20 | Infragr. 80 |
| **6** | 24 | 2.1 | 15 | |
| **Total** | 161 | 2.3 | | 416 |
| **Refs** | 1 | 1 | 2-4 | 5 |

In V1, 19% (range 18.5-19.6%) of neurons are GABA immunoreactive, while in extrastriate cortex surrounding V1, including area V2, the proportion of inhibitory neurons is 25% (range 24.2-25.3%, N=5 hemispheres, Hendry et al., 1987). No apparent difference in the density of GABAergic cells exists between the CO blobs and interblobs of V1 (Beaulieu et al. 1992).

In primate evolution, L4 of area V1 has become specialized into three sublayers (reviewed in Casagrande and Kaas, 1994), and correspondingly the number of neurons in V1 per unit surface area doubled compared with other cortical areas (Hendry et al. 1987). In addition, of all cortical areas, the density of neurons per unit volume is highest in V1.

The mean density of neurons across all layers in V1 is 230 x $10^3$/$mm^3$ (range 190–280 x $10^3$/$mm^3$; average of three *M. fascicularis* monkeys), and drops in V2 to 130 x $10^3$/$mm^3$ (range 110–140 x $10^3$/$mm^3$; average of two *M. fascicularis*, and one *M. mulatta*, Kelly and Hawken, 2017). The neuronal densities per unit mass show similar trends, being highest in V1 (130–177 x $10^6$/g) and somewhat lower in V2 (89–114 x $10^6$/g) and V5 (85 x $10^6$/g; *M. mulatta*, Collins, 2011).

Layer 4A has a unique honeycomb-like appearance consisting of parvocellular geniculate afferent axons, local groups of pyramidal neurons in cone-like arrangement (30-80 µm wide, mean 60 µm), separated by neuropil, and vertical apical dendritic clusters (1270 clusters/$mm^2$) arising from L5 pyramidal cells (Peters and Sethares 1991a, 1991b).

***V2: neuron numbers and types.*** Only sparse quantitative data exist for V2. Rockland (1997) estimated that beneath 1$mm^2$ area of V2 lay about 92600 neurons (of which 31200 in L3, 37200 in L4, 10600 in L6). In contrast to V1, there are no spiny stellate neurons in V2 L4 or elsewhere in cortex, and infragranular pyramidal cells in V2 have spines in L4, which further emphasizes the functional uniqueness of V1 among visual areas (Lund et al. 1981). In L4 of V2, over 90% of cells are pyramidal, with short apical dendrites, rising up to L3.

Data on neuron numbers and types for the individual layers of area V5 have not been reported.

Layer-specific quantifications of distinct neuron types would be of paramount importance for modeling.

# Connections between subcortical nuclei and V1, V2 and V5

## Geniculocortical and corticogeniculate connections

Three main pathways, Magno- Parvo- and Koniocellular streams, convey visual signals from the retina through the LGN to V1 (Figs. 2 *top*, 3 *top*, Supplementary Table 1A). These pathways are functionally distinct and computationally assumed to convey independent dimensions of visual information from the retina to the visual cortex (Derrington et al. 1984; Gegenfurtner 2003; Lennie and Movshon 2005). The Magno layers of the LGN, whose cells mediate achromatic vision, have high temporal but low spatial frequency tuning, and respond non-linearly to changes in luminance and contrast, send denser projections to V1 L4Cα, and sparser and fine axon collaterals to the lower part of L6. The Parvo layers, whose cells mediate red-green contrast, have high spatial but low temporal frequency tuning, and respond linearly to dynamic stimuli and contrast changes, send their most dominant projection to L4Cβ, and sparser projections from a separate population of cells to layers 4A and the upper part of L6 (Figs. 2 *top* and 3 *top*; Hubel and Wiesel 1972; Hendrickson et al. 1978; Blasdel and Lund 1983). In L4C, the thalamic afferents form arborizations covering one monocular column, with a complementary pattern of projection representing the other eye. The width of this periodic arborization shows individual variability from 0.5 to 1.2 mm (Hubel and Wiesel 1972).

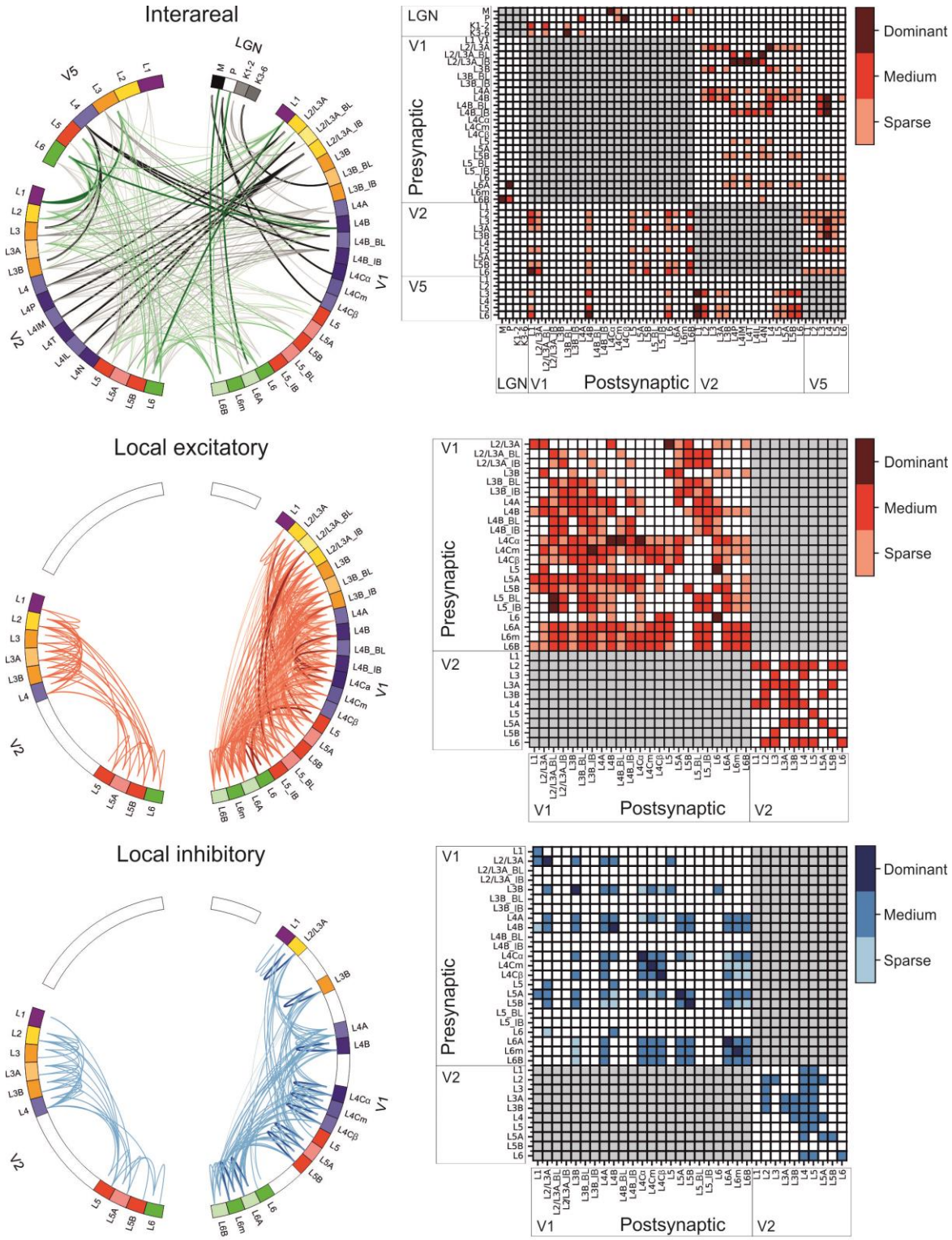
Interareal
LGN
V5
V1
V2
Presynaptic
Postsynaptic
Dominant
Medium
Sparse
Local excitatory
Local inhibitory

380

**Figure 2. Connections between LGN, V1, V2, and V5 and within V1 and V2**. For references, see Supplementary Table 1D. Top, middle and bottom rows indicate inter-areal, intra-areal excitatory and intra-areal inhibitory connections, respectively.

LEFT COLUMN: Connectograms (Krzywinski et al. 2009) showing connections between distinct layers. Each colored segment in the circular perimeter indicates a cortical layer, sublayer or CO compartment. Line width and color intensity indicate the robustness of the connection. Unknown strengths are marked as medium; for V2 interlaminar connections (middle and bottom connectograms), the paucity and qualitative character of the available studies did not allow us to estimate connection strength. The origin (soma) of a projection neuron is marked as a line slightly displaced from the outer edge of the circle, while its termination (axon terminals) is marked as a line reaching the outer edge of the circle. *Top Left:* Interareal connections and connections between LGN and areas V1, V2, V5. Black lines indicate FF connections, and green lines FB connections. V2 L4P = L4 pale stripe (no distinction between lateral/medial stripes), L4IM = L4 interstripe (or pale stripe) medial, L4T= L4 thick stripe, L4IL = L4 interstripe (or pale) lateral, L4N = L4 thin stripe. All interareal connections are excitatory. *Middle left*: Local excitatory connections. *Bottom Left:* Local inhibitory connections; none of the studies reviewed here identified the CO compartments.

RIGHT COLUMN: Matrix of the connections. No connection (*white squares*) indicates that the connection either does not exist or was not studied. *Red squares* indicate excitatory connections, and *blue squares* inhibitory connections. Color intensity indicates the strength of the connection.

381

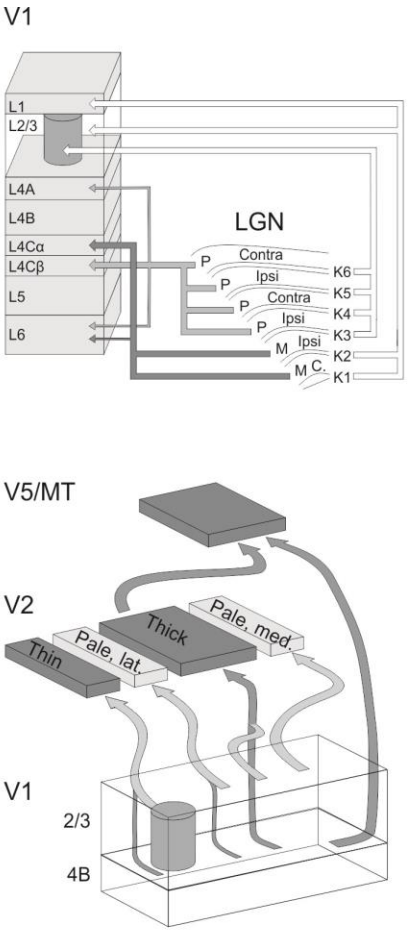


**V1** Blobs:
Color/Hue: 1-4
Lack of orientation specificity: 4
Low spatial frequency: 5-7
High contrast sensitivity: 5

Interblobs:
Orientation: 4
Mid and high SF: 5-7
Low contrast sensitivity: 5

Layer 4B:
High direction selectivity: 8

**V2** Pale medial (type II): contours
Orientation: 9, 10

Thick stripes: disparity, motion
Orientation: 4, 11-18
Low and High SF: 19
Illusory contours: 20
Retinal disparity: 12, 13, 17, 21
High contrast sensitivity: 19
Motion direction: 14, 18, 22

Pale lateral (type I): unknown
Orientation (weak): 9

Thin stripes: surface
Color, spectral sensitivity: 4, 11-15, 19, 23, 24
Luminance: 25
Low SF: 19
Brightness: 26, 27

Pale, undifferentiated (early data)
Illusory contours: 20, 28
Orientation: 4, 11, 13, 15, 16, 18
High SF: 19

**V5/MT** Speed tuning: 29-31
Orientation: 32
Direction tuning: 30, 32, 33
Disparity: 34, 35

382

**Figure 3. Feedforward pathways and specialization of functional compartments in LGN, V1, V2 and V5.** TOP: Main LGN to V1 pathways (Hendrickson et al. 1978; Blasdel and Lund 1983; Kaplan 2003; Casagrande et al. 2007). Arrow thickness indicates the relative contribution of Parvo and Magno geniculocortical afferents to the different V1 layers. BOTTOM: Main FF pathways between V1, V2 and V5 (Sincich and Horton 2002; Sincich et al. 2007, 2010; Federer et al. 2013). In both top and bottom schematics, additional sparse connections were omitted for clarity.

The CO compartments of V1 and V2 contain multiple functional feature maps and their constituent neurons show specific receptive field tuning properties, as indicated on the right. Numbers refer to the following references:

1, Tootell, Silverman, Hamilton, De Valois, et al. 1988; 2, Landisman and Ts'o 2002; 3, Xiao et al. 2007; 4, Lu and Roe 2008; 5, Edwards et al. 1995; 6, Silverman et al. 1989; 7, Tootell, Silverman, Hamilton, Switkes, et al. 1988; 8, Gur and Snodderly 2007; 9, Felleman et al. 2015; 10, Shipp and Zeki 2002a; 11, Shipp and Zeki 2002b; 12, DeYoe and Van Essen 1985; 13, Roe and Ts'o 1995; 14, Munk et al. 1995; 15, Gegenfurtner et al. 1996; 16, Vanduffel et al. 2002; 17, Ts'O et al. 2001; 18, Levitt, Kiper, et al. 1994; 19, Tootell and Hamilton 1989; 20, Peterhans and von der Heydt 1993; 21, Chen et al. 2008; 22, Lu et al. 2010; 23, Tootell et al. 2004; 24, Xiao et al. 2003b; 25, Wang et al. 2007; 26, Lu and Roe 2007; 27, Roe et al. 2005; 28, Heider et al. 2000; 29, Lagae et al. 1993; 30, Maunsell and Van Essen 1983c; 31, Perrone and Thiele 2001; 32, Albright 1984; 33, Dubner and Zeki 1971; 34, Maunsell and Van Essen 1983a; 35, DeAngelis and Newsome, 1999.

Data on single thalamocortical axon arborization patterns are very sparse. An individual Magno axon terminating in L4Cα may divide into two or perhaps more arbors. These arbors form a cluster, each covering 0.3-0.4 $mm^2$ surface area. Each cluster contains 6490 synapses (mean from Blasdel and Lund, 1983 and Freund et al., 1989; both studies reported data from one filled axon).

The corresponding coverage for the Parvo pathway axon terminal in L4Cβ is much smaller, 0.067 $mm^2$ (Blasdel and Lund 1983). Freund et al. (1989) filled two Parvo axons, and counted on average 3154 synapses/axon cluster. A single Parvo axon in L4A formed a single terminal field with a honeycomb-like pattern, including 764 boutons covering 0.058 $mm^2$ surface area (Blasdel and Lund 1983). Assuming an average of 2.2

synapses/bouton [mean of Parvo synapses per bouton, from (Freund et al. 1989)], this would result in 1681 synapses/axon cluster.

The Konio stream of the macaque LGN, a fraction of which mediates blue-yellow-contrast, is organized in 6 cellular layers (K1-K6), located between and below the four Parvo and two Magno layers (Figs. 2 *top* and 3 *top*; Casagrande et al. 2007). Layers K1-K2 project mainly to V1 L1 (47% of K1-K2 projecting boutons) and the upper part of L3 (38% of boutons; named 3A in Casagrande et al., 2007), with minor projections to L2 (3%) and the lower part of L3 (12%); each axon has on average 134 boutons (range 55-255, N=9 axons). Cells in the LGN layers K3-K6 project mainly to the lower part of V1 L3 (93% of boutons; named 3Bα in Casagrande et al., 2007), targeting mainly the CO-rich blobs (Hendry and Yoshioka 1994; Casagrande et al. 2007), with minor projections to L1 (2%), upper L3 (3%), and L4A (2%); each axon has on average 217 boutons (range 90-430, N=9 axons). The number of thalamocortical synapses per bouton in the Konio stream is unknown.

A subset of L6 neurons in V1 projects back to LGN (Wiser and Callaway 1996; Briggs et al. 2016) in a stream-specific manner (Lund et al. 1975), i.e. separate cells in L6A and 6B project to the Parvo and Magno layers, respectively, each with functional properties resembling their LGN targets (Briggs and Usrey 2009). In addition to V1, also some V2 L6 neurons project back to LGN (Briggs et al. 2016). Because the target layers in LGN are unknown for this V2 projections, these connections are omitted in Figure 2 and Supplementary Table 1A.

The LGN also projects directly to V2 (Bullier and Kennedy 1983; Markov et al. 2011), and about 1% of, or 8000, LGN neurons project directly to V5 (Sincich et al. 2004). Interestingly, these geniculate connections to V2 and to V5 both originate primarily from the intercalated Konio layers (Bullier and Kennedy 1983; Sincich et al. 2004), which

represent the phylogenetically older blue-yellow color system (Carlos and Silveira 2003). Unfortunately, we do not know the target layers in V2 and V5 for this LGN projection, and thus we have omitted these connections from Figure 2 and Supplementary Table 1A.

### Other subcortical afferents to V1, V2 and V5

Of all subcortical inputs to V1, one of the largest arises from the claustrum (0.3% of all retrogradely labeled neurons after injections in V1), whereas for LGN inputs this fraction does not exceed 0.2% (Markov et al. 2011). V1 receives also afferents from the pulvinar (to layers 1 and 2, Lund et al., 1981), and the amygdala (Markov et al. 2011). The largest fraction of subcortical projecting neurons to V2 arises from both inferior and lateral pulvinar (Benevento and Rezak 1976; Trojanowski and Jacobson 1976) [0.3% (Markov et al. 2011), terminating primarily in L3B (Lund et al. 1981)], and from the claustrum (0.5%; Markov et al. 2011). In addition, V1 and V2 receive sparse projections from thalamic intralaminar nuclei and the nucleus basalis of Meynert (Kennedy and Bullier 1985). Area V5 also receives projections from the pulvinar (Adams et al. 2000) and claustrum (Gattass et al. 2014). Unlike the very localized inputs from LGN and pulvinar, inputs from the claustrum and thalamic intralaminar nuclei show much larger spread (Perkel et al. 1986).

## Interareal Connections

### Overview of cortico-cortical connections

Interareal connections between V1, V2 and V5 have been reviewed previously (Zeki and Shipp 1988; Felleman and Van Essen 1991; Merigan and Maunsell 1993; Gattass et al. 2005; Sincich and Horton 2005; Angelucci and Bressloff 2006; Nassi and Callaway 2009). Later, quantitative studies have provided significant new information on the

444 relative connection strengths between cortical areas (Markov et al. 2011; Markov, Ercsey-
445 Ravasz, et al. 2014), and on-line databases have also enabled targeted searches of existing
446 literature (Kötter 2004; Bakker et al. 2012). In addition to visual inputs, V1 and V2
447 receive feedback from auditory and parietal cortices suggesting that multimodal signals
448 are available to all visual areas, not just to association areas positioned at higher levels of
449 the anatomical hierarchy (Falchier et al. 2002; Rockland and Ojima 2003).

450 The macaque cortex consists of a moderately dense network of functional areas, where
451 one estimate suggests that 66% of possible direct connections between two areas exist,
452 with the number of projecting neurons between any two areas spanning a scale of $10^5$
453 (Markov, Ercsey-Ravasz, et al. 2014). With the caution that these numbers are based
454 mainly on one species, *M fascicularis*, and thus cannot be applied to other macaque
455 species, these data suggest that the number of projecting neurons p(d) follows an
456 exponential cortical distance rule (Markov et al. 2013):

457

458 $$p(d) = c\, e^{-\lambda d};\ SD\ of\ p(d) = \sqrt{\mu + \frac{\mu^2}{\theta}}$$

459

460 where, c is a scaling constant, λ is the spatial decay constant, and d is distance across
461 white matter. Markov et al. (2013) reported λ = 0.19 $mm^{-1}$ for macaques, interpreting it to
462 reflect the cost of wiring. Variability of λ between monkeys was not reported, but
463 individual injections show SD which follows the mean, fitting best to negative binomial
464 model with dispersion parameter θ = 7.6. (Markov et al. 2011).

465 Between areas, the fraction of supragranular presynaptic projection neurons is
466 correlated with hierarchical distance from the target area, so that in lower-order areas
467 supragranular projection neurons predominate, whereas in higher order areas projection

468 neurons lay primarily in infragranular layers (Barone et al. 2000; Markov et al. 2013).

469 A large fraction of V1 excitatory cells sends their axons into the white matter. In a
470 study based on 9 monkeys (*Macaca radiata*;(Callaway and Wiser 1996), white matter-
471 projecting axons were found for 50% (3/6 cells) of excitatory cells in layers 2/3A, 60%
472 (3/5 cells) in L3B, 83% (5/6 cells) in L4B, and 19% in L5 (3/16 cells). In L6, 28% of
473 cells (16/56 cells; 8 monkeys; *Macaca radiata*) projected to white matter (Wiser and
474 Callaway 1996). Many projection neurons have also extensive intra- and interlaminar
475 local collaterals in V1 (Lund and Boothe 1975; Callaway and Wiser 1996; Yarch et al.
476 2017).

477 Markov et al. (2014a) have provided important quantitative data on corticocortical
478 connections (Table 3). They injected retrograde tracers in multiple areas, including V1,
479 V2 and V5, counted the number of cells projecting to these areas, and calculated each
480 area's relative input from different areas. V1 receives about three fourths of its interareal
481 input from V2, and vice versa V2 receives three fourths of its input from V1, representing
482 the densest mutual connectivity in the macaque brain. Rockland (1997) estimated that
483 under each $mm^2$ of cortex, 14600 V1 neurons send feedforward (FF) projections to V2
484 (range 8800-21600), whereas 11300 (range 8000-12800) V2 neurons send feedback (FB)
485 projections to V1. Moreover, 41-68% of V2 L6 neurons provide FB connections to V1
486 (Rockland 1994).

487

**Table 3.** Relative strength of mutual connections between V1, V2 and V5. Numbers indicate the percent of total presynaptic neurons, labeled in the source area after a retrograde tracer injection in the target area (e.g. after a tracer injection in V2, 76.4±2.7% of all labeled presynaptic cells reside in V1;(Markov, Ercsey-Ravasz, et al. 2014). Data from: http://core-nets.org/index.php?action=download. Data are from adult monkeys, five hemispheres were injected in V1 (four monkeys, all females), three in V2 (two monkeys, all males) and one in V5 (female).

| **V1 to V2** | | **V2 to V1** | |
|---|---|---|---|
| **Mean** | 76.4% | **Mean** | 73.2% |
| **Std** | 2.7% | **Std** | 3.5% |
| **Min** | 73.3% | **Min** | 68.3% |
| **Max** | 78.3% | **Max** | 76.6% |
| | | | |
| **V1 to V5** | | **V5 to V1** | |
| **Mean** | 1.9% | **Mean** | 5.9% |
| | | **Std** | 1.1% |
| | | **Min** | 5.2% |
| | | **Max** | 7.8% |
| | | | |
| **V2 to V5** | | **V5 to V2** | |
| **Mean** | 11.9% | **Mean** | 3.6% |
| | | **Std** | 0.6% |
| | | **Min** | 3.0% |
| | | **Max** | 4.1% |

Given this robust mutual connectivity between V1 and V2, it is interesting that these two areas exert rather different impacts on each other's neuronal responses; whereas inactivating V1 silences V2 (reviewed in Bullier et al. 1994), inactivating V2 has much subtler effects on V1 responses (Hupé et al. 1998, 2001; Nassi et al. 2013; Nurminen et al. 2018) indicating that the anatomical strength of a connection does not dictate its physiological strength. Other factors, such as the strength of synaptic connections and their location on the postsynaptic cell are likely important determinants of physiological strength of a connection.

The proportion of afferent connections to V5 arising from V1 and V2, as well as the FB connections from V5 to V1 and V2 are clearly sparser, but still significant (Table 3).

Many studies suggest that connections between V1 and V2, V2 and V5 and V1 and V5 are retinotopically organized in such a way that neighboring patches of cortex represent neighboring regions in the visual field (Ungerleider and Mishkin 1979; Weller and Kaas 1983; Ungerleider and Desimone 1986; Shipp et al. 1989). However, the cell populations projecting from V1 to V2 and V5 are largely distinct (Sincich and Horton 2003; Nassi and Callaway 2007).

Figure 2 *top,* 3 *bottom* and Supplementary Table 1A summarize the interareal connectivity between V1, V2 and V5. CO staining in V2 reveals a periodic stripe pattern consisting of dark thick and thin stripes with interleaving pale stripes (Fig. 3 *bottom*). A robust connection from V1 to V2 arises from L2/3A interblobs, followed by the projection from L2/3A blobs. A second robust, but generally sparser (except for the projection to thick CO stripes) pathway arises from L4B interblob and blob columns, and sparse inputs arise from layers 3B, 4A, 5B and 6A. In V2, the majority of V1 afferents terminate in L4 of the different CO stripes (thick, thin and pale), with minor terminations in layers 3A, 3B, 5A, 5B and 6. The FB projections from V2 to V1 arise predominantly

515 from L6, followed by layers 2-3A, with minor efferent connections from layers 3B and
516 5B. Earlier studies, using less sensitive anterograde tracers or bidirectional tracers
517 suggested that V2 FB projections terminate predominantly in L1 of V1, with only minor
518 projections or collaterals to other layers (2/3 and 5) (Rockland and Pandya 1979; Lund et
519 al. 1981; Rockland and Virga 1989; Rockland 1994; Gattas et al. 1997). Recent studies,
520 using more sensitive and exclusively anterograde viral vectors of fluorescent proteins,
521 however, have shown strong V2 FB projections not only to L1, but also to L5B and 6B of
522 V1, with sparser terminations in layers 2/3, 4B, 5A and 6A (Ta'afua et al. 2018). This
523 arrangement suggests that the layer-wise connectivity between V1 and V2 is largely
524 reciprocal, i.e. the same V1 layers sending FF projections to V2 receive direct FB
525 connections from V2. Such symmetry suggests the existence of FF-FB loops, for fast
526 modulation of incoming V1 FF signals by V2 FB connections. However, the lack of FB
527 connections arising from L4, the dominant FB arising from L6, and the dominant FB
528 terminations in L1 are exception to an exact FF-FB reciprocity, showing anatomical
529 asymmetry. How this asymmetry affects the cells' integrative function is unclear.
530 Connections to dendrites distant from the soma, such as the FB to L1, may contact the
531 apical dendrites of pyramidal cells with somata in deeper layers. However, studies in
532 rodents and modeling work have shown that the postsynaptic signals relayed at these
533 distal sites are attenuated (Rall 1962; Williams and Stuart 2002), and their effect may
534 depend on coincident inputs onto the proximal dendrite (Larkum et al. 2004; Larkum
535 2013). These dendritic intracellular interactions may affect the layer-specific timing of
536 visual responses carried by feedforward, horizontal and feedback connections (Self et al.
537 2013; Bijanzadeh et al. 2018).

538 FF connections from V1 to V5 arise from layers 4B (both blobs and interblobs) and 6
539 and target primarily L4 and less so L3 of V5. Similar to V2-to-V1 FB, FB connections

from V5 originate predominantly in L6, with smaller contributions from layers 5 and 3, while L4 sends no FB to V1. FB projections from V5 to V1 terminate predominantly in layers 4B and 6 (Maunsell and Van Essen 1983b; Ungerleider and Desimone 1986; Shipp et al. 1989), i.e. the source layers of the V1-to-V5 FF projection. Only in the peripheral visual field (>10° eccentricity), does V5 FB target also V1 L1 (Ungerleider and Desimone 1986; Shipp et al. 1989). FF connections from V2 to V5 arise predominantly from L3B, but also from layers 2, 3A and 5, with a minor contribution from L6. These connections terminate mainly in L4 of V5 with some spread into the neighboring layers 3 and 5. FB from V5 to V2 arises from V5 layers 3, 5 and 6, and terminates predominantly in V2 layers 1 and 6, but also 2, 3A, 5B, with minor terminations also in layers 3B and 5A. In contrast to V2, where the supragranular origin of FB connections is mainly from L2-3A, the supragranular FB from V5 seems to originate only from L3; while Rockland and Pandaya (1979) reported it to originate in L3A, Weller and Kaas (1983) did not specify from which subdivision of L3 V5 FB originates.

### Characteristics of connections between V1 and V2

The major target layer of V1-to-V2 projections is L4, where axon terminals form 0.2-0.5 mm wide clusters; 1-3 clusters are arranged in 0.2 (single cluster) to 1.2 mm (multiple clusters) long and 0.3 mm wide terminal fields (Rockland and Virga 1990; Anderson and Martin 2009). Sparse axonal terminations also occur contiguously in layers 3 and 5 (Rockland and Pandya 1979). In V2, the most frequent targets of V1 FF projections are the dendritic spines of excitatory neurons, with sparse terminations onto shafts, the latter mainly (about 60%) onto inhibitory neurons (Anderson and Martin 2009). Of the spines receiving V1 FF projections, only 19% receive a second inhibitory synapse in addition to excitatory synapses.

As mentioned above, macaque V2 has four CO stripe compartments (thick, thin, and 2 pale stripes), each with unique afferent and efferent connectivity (Fig. 2 *top*, 3 *bottom*, Supplementary Table 1A). Retrograde tracer injections confined to distinct V2 stripes result in spatially segregated clusters of labeled somata in V1, which align preferentially with distinct V1 CO compartments (blobs or interblobs), suggesting parallel FF pathways from V1 to V2 (Livingstone and Hubel 1984a, 1988a; Sincich and Horton 2002; Federer et al. 2013). Livingstone and Hubel (1984b, 1988) first proposed a tripartite model of V1-to-V2 projections. This model was later modified by Sincich and Horton (2002) and, subsequently, Federer et al. (2013) as illustrated in Figure 3 *bottom.* According to this model, thin stripes receive projections from CO blobs, and thick and pale stripes from interblobs. V1 projections to all stripes arise predominantly from L2-3 with sparse projections from layers 4A and 5-6; projections from L4B are densest to thick stripes, moderate to thin stripes and one set of pale stripes (type I, also termed pale-lateral as they are located laterally to thick stripes), and absent to the second set of pale stripes (type II, also termed pale-medial). Importantly, this segregation is not strict, as all stripe types receive sparser projections from both blobs and interblobs.

After paired injections of different retrograde tracers into thick and pale stripes, 16% of all V1 labeled neurons were double labeled in the interblobs (Sincich and Horton 2002); even smaller percentages of double labeled neurons were found after paired retrograde tracer injections into thin and pale stripes (Sincich and Horton 2002), or pale-lateral and pale-medial stripes (1-3% of all labeled neurons, Federer et al. 2013), demonstrating that different stripe types receive inputs predominantly from different V1 cells, but at least some common inputs from the same cells, and that the segregation of inputs is more marked for thin vs thick/pale stripes compared to thick vs. pale or pale-lateral vs. pale-medial stripes.

Using intra-V2 injections of a glycoprotein-deleted rabies virus carrying the gene for green fluorescent protein (GFP), Nassi and Callaway (2007) found that on average 17% of V1 L4B neurons projecting to V2 had spiny stellate morphology and 83% (N= 2 hemispheres, 82% and 85%, respectively) had pyramidal morphology. By confining injections of the same virus to thick or thin stripes, Yarch et al. (2019) reported that on average >60% of L4B inputs to thick stripes and about 40% to thin stripes arises from stellate cells, and the rest from pyramids. The difference between the results of Nassi and Callaway (2007) and those of Yarch and colleagues (2019) suggests that most V1 L4B stellate cells that project to V2 target the thick stripes, and that pale stripes receive dominant or exclusive V1 L4B inputs from pyramidal cells. Alternatively, viral injections in the two studies may have been confined to different subcompartments or layers within the stripes, or the virus differentially infected different populations of L4B cells in the two studies. Yarch et al. (2019) additionally fully reconstructed the intra-V1 axon arbors of single L4B neurons projecting to thick stripes; using unbiased cluster analysis of these neurons' intra-V1 laminar axon projection patterns, they identified at least two (possibly three) major classes within this L4B subpopulation. Most reconstructed neurons (65%, 15/23 neurons) belonged to Class 1, sending narrowly focused axonal projections to L2/3, and laterally extending projections to layers 4B and 5. Class 2 cells (26%), instead, sent collaterals mainly to L5, and the rare Class 3 cells (9%) predominantly to L6. The somata of all these cell classes lay preferentially outside CO blobs, and their axon projections in all layers also avoided CO blobs, indicating that the intra-V1 connections of L4B neurons projecting to thick stripes preserve segregation between blobs and interblobs.

Rockland and Virga (1989), reported that V2 to V1 FB axons form terminal clusters in V1 with extents of 4.0 x $10^6$ $\mu m^3$ (range 0.2 x $10^6$ - 15.4 x $10^6$), primarily in L1, with sparser terminations in layers 2 and 5. Most single FB axons travel 0.75-2 mm in L1,

615 sending clusters at 350-650 μm intervals (Rockland 1994). In L5, however, the terminals
616 travel <0.75 mm. The density of boutons varies from 3 to 15 boutons/100 μm of axon.
617 Using more sensitive viral vectors of GFP (AAV9) confined to distinct V2 stripes,
618 Angelucci and colleagues (Federer et al. 2015; Ta'afua et al. 2018) have recently reported
619 dominant V2 FB projections to V1 layers 1, 2A, 5B and 6B, and sparser projections to
620 2B, 3, 5A and 6A, from all stripe types. Sparse, but significant projections to L4B were
621 observed after thick and pale-lateral stripe injections but were virtually absent after thin
622 stripe injections. Moreover, V2 FB projections mimicked the parallel organization of the
623 reciprocal FF V1-to-V2 pathways: in all V1 layers of termination, thin stripes projected
624 predominantly to blobs and pale and thick stripes to interblobs.
625

626 Characteristics of V5 afferent pathways

627 The most direct LGN Magno inputs reach V5 tri-synaptically via V1 layers 4Cα and
628 4B. In contrast, most Parvo input travels a longer route, via V2, to reach V5 (see Fig. 3
629 in Nassi and Callaway 2006). More specifically, the pyramidal neurons in V1 L4B
630 receive Magno and Parvo inputs from both layers 4Cα (via direct 4Cα-to-4B projections)
631 and 4Cβ (via 4Cβ-to-3 projections contacting the apical dendrites of L4B pyramids in
632 L3), whereas the 4B spiny stellate neurons receive only Magno input from L4Cα (Yabuta
633 et al. 2001). L4B spiny stellates then carry Magno data directly to V5 (Nassi and
634 Callaway 2007). After injections of retrograde tracers into V5, Nassi and Callaway (2007)
635 found that on average 76% (N=3 hemispheres, range 67-93%) of the labeled cells in V1
636 L4B had spiny stellate morphology and only 24% had pyramidal morphology. This
637 contrasted with the much larger fraction of pyramids (~80%) projecting to V2. Moreover,
638 the V5-projecting V1 L4B neurons were larger in size compared to the V2-projecting
639 ones, and the V5-projecting pyramidal cells were more likely to reside under CO blobs

and have longer dendritic trees extending more often up to L1. Other studies found that L4B cells projecting to V5 are equally located under blobs and interblobs (Shipp et al. 1989; Sincich and Horton 2003), and that V1 projections to V5 arise predominantly from L4B (97.8% of V1 inputs), and sparsely from L6 projection (2.2%; Nhan and Callaway 2012).

Individual axons from V1 terminate into 1.0 – 1.8 mm wide patchy fields in L3, L4 and L6 of area V5 (Rockland 1989; Anderson et al. 1998). Each axonal branch forms up to 4 terminal arbors up to 250 μm in diameter in the L4 and L3, and up to 50-100 μm in L6 (Rockland 1989). The axons form excitatory synapses with dendritic spines (54%; with the largest synapses, mean area 0.127 $\mu m^2$, SEM 0.011), shafts (33%; 0.071 $\mu m^2$, SEM 0.07) and somata (13%; 0.031 $\mu m^2$, SEM 0.008). All connections to the soma and 26% of those on shafts were found to be on inhibitory postsynaptic cells, the reminder (78% of all connections) being on excitatory cells (Anderson et al. 1998). These authors estimated that of the 5-10 x $10^3$ synapses present on single V5 neurons, only few hundreds are made by V1 afferents, which is analogous to LGN-to-V1 projections where a small number of synapses have a disproportionally strong impact on the target neurons.

Similar to V1 projections, V2 afferent axons to V5 form terminal patches in L3-4, each patch being up to 200-250 μm in width, with an interpatch distance of up to 600 μm (Rockland 1995). Moreover, as in V1, most V2 afferent synapses land onto spines (67% in L4, 82% in L2/3), and only 4-6% of synapses onto L4 neurons are made by V2 afferent axons (Anderson and Martin 2002). In contrast to V1 projections, some V2 axon arbors extend from L4 upward into L1; moreover, V2 afferent axons are thinner than V1 afferents (diameter of about 3.0 μm in V1 vs. 1.0 μm in V2), and send no collaterals to L6 (Rockland 1995; Anderson and Martin 2002).

## Divergence and convergence in feedforward and feedback connections

Some of the earliest anatomical studies of interareal connections reported that the tangential extents of the FF and FB connectional fields were asymmetric (reviewed in Zeki and Shipp 1988). The forward connections converged to a local region in higher order areas, and it was hypothesized that they represent the anatomical substrate for the increasing RF size of neurons along the cortical hierarchy. In contrast, the backward projecting system was typically more divergent, thus possibly serving widespread modulation of low-order areas.

Angelucci et al. (2002) tested the hypothesis that widespread FB connections from extrastriate cortical areas provide an anatomical substrate for contextual modulation of V1 neuron responses arising from outside the neurons' classical RF (also termed the RF surround). By combining tracer injections with electrophysiological recordings at the injection site and in the cortical region of expected tracer transport, these authors were able to compare the spatial extent of extrastriate FB connections to V1 with the spatial extent of V1 neurons' classical and extra-classical RFs. Anterograde tracer injections confined to the V2 upper layers produced a pattern of labeled patchy FB terminations in V1 upper layers. Injections including also the deep V2 layers additionally produced less patchy, and more extensive terminal FB label in layers 5/6. The diameter of the V2 FB axon terminal field in V1 was 6.8 ± 0.4 mm (mean ± SEM, range 6.4-7.6 mm), while FB terminations from V5 extended over 13.4 ± 0.5 mm (range 12.9-13.9) mm in V1. These authors also made injections of retrograde tracers into V1 and measured the extent of the retrogradely-labeled fields of neurons in V2, and V5 sending convergent FB projections to the injected V1 region. When converted to visuotopic coordinates, on average, the V2 and V5 L5/6 FB neurons labeled by small injections of retrograde tracers in V1 encompassed a visual field region of 3.8° ± 0.6 and 26.6° ± 3.0, respectively, in diameter.

In contrast, the field of long-range intra-V1 horizontal connections converging to the same V1 injection sited was only 2.9° ± 0.4 in diameter. Expressed in units of V1 classical RF size, the visuotopic extents of V2 FB fields correspond to 4.0 ± 0.4 times (range 2.7-5.3; for FB from V2 L2/3) and 4.6 ± 0.2 times (4.0-5.1; for FB from V2 L5/6) the size of the classical RF of V1 neurons. FB from V5 L2/3 and 5/6, instead, extends 15.0, and 25.0 ± 4.0 (21-29) times, respectively, the V1 neurons' classical RF size. Importantly, the FB fields to V1 are much larger than the extent of visual field encompassed by the intra-V1 long-range horizontal connections, which, instead, encompass 2.7 (L2/3) to 3.7 (L4B) times the classical RF size of V1 cells. In conclusion, horizontal connections can mediate contextual integration of visual signals from just outside the V1 neurons' RF (the "near surround"), while FB connections provide V1 cells with a much larger area for integrating visual signals arising from the most distant regions of the RF surround (the "far surround").

## Intra-areal connections

Local cortical connectivity is complex. For example, a recently implemented model of the microcircuit of rat somatosensory cortex comprises almost 2000 connection types between 55 morphological cell types (Markram et al. 2015). For modeling purposes, the complex connectivity needs to be simplified to basic principles, including distance distributions, major local inter-laminar pathways, and main connection motifs for excitatory and inhibitory neurons. This information is only partially available for macaque cortex.

Overall, there seem to be two major categories of connections, long-range (millimeters-long) horizontal connections, which are most prominent within the lamina of origin (Fisken et al. 1975; Rockland and Lund 1983; Angelucci, Levitt, Walton, et al.

2002), and short local connections, which often cross layer boundaries.

## Horizontal connectivity

Most inputs to cortical neurons arise from their local neighborhood. On average 79% of incoming axons to any cortical point originate within the same functional area (Markov et al. 2011). In addition, the intra-areal intrinsic connectivity is highly local (Barone et al. 2000; Markov et al. 2011), i.e. following injection of a retrograde tracer in cortex, the number of resulting retrogradely labeled neurons drops as a function of distance (d) from the injected site:

$$Number\ of\ neurons \sim \frac{1}{e^{\lambda d}}$$

For example, in V1 lambda is 1/0.23 mm, resulting in 95% of labeled presynaptic neurons being located within 2.2 mm of the injection site; in V2 the corresponding value is 1.8 mm. On average, across the studied cortical areas, 95% of labeled intrinsic neurons are within 1.9 mm of the injected site (Markov et al. 2011). Moreover, on average 63% of these retrogradely labeled V1 neurons are supragranular, and the drop in number as a function of distance appears similar in the supra- and infragranular layers (Barone et al. 2000).

The extent of local horizontal connections varies in different layers of V1. Using bidirectional tracers (which label both axon terminals anterogradely and cell bodies retrogradely), Angelucci et al. (2002) showed average horizontal extents of 3 mm (radius from the injection site) in L2/3, 3.4 mm in L4B/upper 4Cα, and 4 mm in L5/6. The largest axonal extents in these layers were 4.5, 5.0 and 4.8 mm, respectively. In contrast, connections in the remainder of L4C seem to be highly local, extending laterally mainly

within one functional column (up to 0.2 mm radius, Fisken et al., 1975; Katz et al., 1989).

The number of synapses between any two horizontally connected cells appears to be very low: only 2 out of 33 postsynaptic dendritic branches (sample of two neurons) received two inputs from the same presynaptic neuron (McGuire et al. 1991). This study, however, looked only at single branches and, thus, could not exclude targets on different dendritic branches of the same postsynaptic cell.

## Functional organization of horizontal connections

Figure 4 depicts the relative extent of horizontal connections in V1, V2 and V5, and Table 4 summarizes key measurements. Horizontal connections extend over progressively larger distances in higher-order areas (Amir et al. 1993).

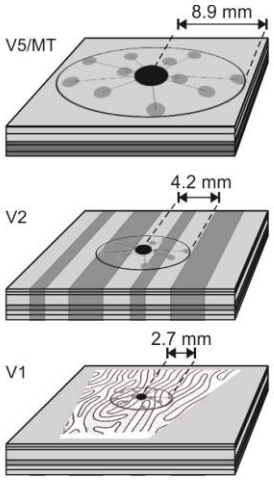

**Figure 4. Extent of intra-areal horizontal connections in the tangential domain of areas V1, V2 and V5.** Horizontal connections in V1 are most prominent in L2/3 and 5 but exist also in L4B/upper 4Cα and 6 (Amir et al. 1993; Angelucci, Levitt, Walton, et al. 2002). In V2, horizontally spreading connections emerge from L2, L3 and some from L5 and L6 (Levitt, Yoshioka, et al. 1994). In V5, locally projecting neurons are predominantly found in L2 and L3 and, following deep layer injections, also in L6 (Ahmed et al. 2012).

In the center of each cortical slab is a halo (*black dot*) of dense, unspecific local connectivity, surrounded by more specific patches of terminal clusters (*gray dots*). In V1, the ocular dominance pattern (modified from LeVay et al. 1975), and in V2 the schematics of the CO bands, are approximately at scale. In V5, the darker shading in layers 4-6 depicts heavier myelination. The horizontal connection extents are average maxima across studies from *M. Fascicularis* and *M. Mulatta*: V1, (Amir et al. 1993; Angelucci, Levitt, Walton, et al. 2002), V2 (Amir et al. 1993), V5 (Ahmed et al. 2012).

752

**Table 4.** Summary of horizontal connectivity. Mean (range) across studies. Distances are in mm. Data from 1. Amir et al. 1993; 2. Malach et al. 1993; 3. Levitt, Yoshioka, et al. 1994; 4. Yoshioka et al. 1996; 5. Angelucci, Levitt, Walton, et al. 2002; 6. Ahmed et al. 2012.)

| | V1 | V2 | V5 |
|---|---|---|---|
| **Most distant terminal cluster** | 2.7 (2.1-2.9) | 4.1 (4.0-4.2) | 8.9 |
| **Anisotropy ratio** | 1.7 (1.6-1.8) | 1.6 | 1.2 |
| **Cluster size** | 0.21 (0.18-0.23) | 0.25 (0.25-0.25) | 0.52 |
| **Inter-cluster separation** | 0.61 | 0.88 (0.60-1.15) | 2.3 |
| **References** | 1-2,4-5 | 1,3 | 6 |

753

754 In layers 2/3 of V1, horizontal connections labeled by retrograde tracer injections into
755 V1 form patches of axon terminals and somata around the injection site (Rockland and
756 Lund 1983; Angelucci, Levitt, Walton, et al. 2002; Tanigawa et al. 2005). Single tracer
757 injections label on average 11 (range 3-21) patches (Yoshioka et al. 1996; Tanigawa et al.
758 2005), each about 0.1-0.2 mm wide, which repeat at 0.5-0.6 mm intervals (Rockland and

759 Lund 1983). The 0.2 mm patch diameter matches the width of the dendritic fields of
760 pyramidal cells in the supragranular layers, and, together with the characteristic interpatch
761 distance, reflects the preference of these connections to link V1 domains with similar
762 functional tuning (Malach et al. 1993; Yoshioka et al. 1996). Patchy horizontal
763 connections are also prominent in L5 (Lund et al. 1993).

764 Tracer injections targeted to specific orientation-preference domain in the V1
765 orientation map send horizontal connections preferentially (70%) to other V1 domains
766 with similar orientation preference (±45°) as that of the injected site. In the local
767 neighborhood of the injected site the connection targets show wider orientation diversity
768 (Malach et al. 1993).

769 Horizontal connections in V1 layer 2/3 also prefer domains of similar ocular
770 dominance (OD) and CO compartment (blob/interblob, Livingstone and Hubel 1984b;
771 Yoshioka et al. 1996). Tracer injections targeted to a specific OD column resulted in
772 labeled patches of horizontal connections, of which on average 54% resided in the
773 surrounding OD columns representing the same eye territory, 18% at the border between
774 the left and right eye representation, and 28% in the opposite eye territory. For tracer
775 injections targeted to blob/interblob domains, 71% of connection targets remained in the
776 same domain, the rest were located at blob/interblob borders or into the opposite CO
777 compartment (Yoshioka et al. 1996).

778 Taken together, in layers 2 and 3 of V1 the horizontal connectivity is locally (within
779 dendritic and axonal field) not specific to functional domains, but long-range connections
780 form terminal patches with a preference for similar-domain cells.

781 In thalamorecipient L4Cβ, the dendritic fields of both spiny and non-spiny stellate
782 cells seem to avoid crossing OD boundaries, whereas axons of both cell classes cross to
783 the opposite domain. Since these axons are only about 100 μm long, they nevertheless

784 mainly remain in their home eye column (Katz et al. 1989). Functionally, this results in
785 strictly monocular cells in this layer (Hubel and Wiesel 1968).
786 Horizontal connections in layers 4B/upper4Cα also show some domain-specific
787 clustering. When columnar tracer injections encompass L2 to upper L4Cα, the clusters of
788 horizontal connections in L2/3 and those in L4B/upper4Cα are vertically aligned, but
789 clusters in L4B/upper4Cα are band-like rather than patch-like as in L2/3 (Angelucci,
790 Levitt, and Lund 2002; Lund et al. 2003).
791 In L6, a specialized class of large pyramidal Meynert cells shows little clustering of
792 their horizontal connections and appear to form diffuse terminations (Li et al. 2003). In
793 other layers, the horizontal connectivity in relation to functional domains has not been
794 systemically studied.
795 The distribution of horizontal connections is anisotropic. The ratio between the long
796 and short axes of the antero- and retrogradely-labeled connection fields ranges from 1.5 in
797 L4B/upper 4Cα to 1.8 in L5/6 (Angelucci, Levitt, Walton, et al. 2002). Interestingly, the
798 visual field representation of these horizontal connection fields appears isotropic, i.e. their
799 spatial anisotropy in cortex translates to an isotropic distribution in visual field. This
800 results from the anisotropic columnar organization in V1, primarily due to the OD
801 columns, interrupting an otherwise smooth retinotopic representation (Blasdel and
802 Campbell 2001).
803 In V2, horizontal connections are also patchy (Rockland 1985; Amir et al. 1993;
804 Levitt, Yoshioka, et al. 1994). From each injection site, efferent axons travel in layers 1-3
805 to form 10-15 terminal patches, each 0.25-0.3 mm wide. The patches are found up to 4
806 mm away from the injection site, with a gamma-like, positively skewed, distribution,
807 peaking at 1 mm distance. The patches form an oval field, with median longer/shorter
808 axis ratio of 1.6 (range 1-3.8), and the longer axis of the field being oriented orthogonal to

809 the CO stripes. Given the anisotropy of visual field representation in V2, due to the
810 presence of CO stripes, the connections seem to connect roughly a circular area of visual
811 field. After tracer injections confined to the upper layers, some labeled horizontal
812 connection are also observed in L5.

813 The stripe specificity of horizontal connections in V2 remains unclear. It appears that
814 over short distances, they cross CO stripe boundaries (Levitt, Yoshioka, et al. 1994), but
815 over longer projection distances they preferentially target the same stripe type as that of
816 the injected site (Baldwin et al. 2012). Interestingly, GABAergic connections seem to
817 create an oval-shaped connectivity along, rather than across, the CO stripes, in contrast to
818 excitatory connections (Kritzer et al. 1992); their maximum lateral spread is also shorter,
819 1.4 mm in superficial layers and 1.1 mm in the infragranular layers. Functionally, this
820 difference in excitatory vs. inhibitory topography would seem to indicate that V2
821 excitatory horizontal connections combine signals from different visual processing
822 streams, while the more local inhibitory connections suppress nearby activation within
823 one stream.

824 In V5, horizontal connections form the longest-range connections, with clusters up to
825 10 mm from the injection site (Ahmed et al. 2012). A tracer injection in the upper layers
826 labels horizontal connections that are restricted to supragranular layers, whereas a tracer
827 injection in the deep layers labels horizontal axons in both supragranular and L6 neurons
828 with a similar distribution of clusters (mean space between clusters 2 mm).

829

830 Overview of interlaminar connections

831 Interlaminar connections in V1 and V2 (Figs. 2 *middle, bottom*, Supplementary Table
832 1B-D) have been previously reviewed (Gilbert 1983; Lund 1988; Lund et al. 1994; Levitt
833 et al. 1996; Callaway 1998a; Douglas and Martin 2004). We found no intrinsic

834 interlaminar connectivity studies of macaque V5.

835 From a modeling perspective, it is interesting that lamination might reflect a
836 developmental hierarchy. The major laminar borders and layer-specific connections
837 develop first, guided by ontogenetic molecular markers, whereas sublamina-specific
838 connectivity (e.g. axons targeting 3 vs. 4B, 4Cα vs. 4Cβ) might emerge postnatally,
839 guided by either molecular markers or visual input (Callaway 1998b). Eventually,
840 interlaminar connectivity becomes highly complex with multiple unique combinations of
841 layer inputs (Sawatari and Callaway 2000; Nassi and Callaway 2009).

842 The excitatory and inhibitory local circuit neurons have been clearly distinguished in
843 the literature, as light and electron microscopic observations allow straightforward
844 identification of excitatory cells, as having spinous dendrites and forming asymmetric
845 synapses, in contrast to inhibitory cells which instead have smooth dendrites and form
846 symmetric synapses. However, there are sparser data describing the extent of axonal
847 spread in a target layer. Moreover, in these studies, cell samples were typically small,
848 precluding statistical analyses, and the distance covered by the projecting axons is often
849 reported only as largest extent within the small sample. An even greater challenge is the
850 classification of inhibitory and excitatory cells into different morphological subtypes and
851 describing the subtype-specific connectivity. While attempts to classify neurons into
852 distinct subtypes have been made, the relative proportions of the different subtypes and
853 the statistics of their inputs and outputs is sporadic and largely missing in macaques.
854 However, a general rule that has emerged from these studies is that both excitatory and
855 inhibitory neuron types typically project strongly within their home layer.

856

857 ## Excitatory interlaminar connections

858 In Figure 2 (*Middle*) and in Supplementary Table 1 B, we report, separately for V1 and

V2, the layer location of the somata giving rise to interlaminar projections and a semi-quantitative description of their axonal target layers.

***V1 excitatory neuron connectivity.*** Excitatory neurons in L4Cα and L4Cβ project strongly to their home layer, but they also target 4Cm, a sub-layer of cells which occupies the middle of L4C between the α and β sub-layers, and which receives only sparse direct LGN connections. L4Cα sends robust projections to layers 3B and 4B, which align with CO blobs, but sparser projections also to other layers, except L1 and 5B. L4Cβ sends a robust projection to L3B, which instead aligns with both interblobs and blobs. L4Cβ also sends more moderate projections to other layers, except 1 and 5B. The L3B blob and interblob compartments seem to distribute efferent connections primarily to corresponding blob or interblob compartments, respectively, in other layers (2/3A, 4B (sparse) and 5), and L3B interblob neurons in addition project to 5A. L2/3A interlaminar connections are partially selective for blob/interblob divisions, emphasizing connections within their home compartment, but not totally avoiding crossing CO boundaries. L4A, which receives direct LGN Parvo input, projects to L3B interblobs, but also to layers 2/3A, 4B and 5A. Cells in L4B blobs seem to be targeting mainly interblobs within 4B itself and in L5; in contrast, cells in L4B interblobs target primarily interblobs in these layers. L4B projections to layers 2/3A and 3B, instead, terminate in CO blobs, regardless of whether their soma sits in a blob or interblob column. However, Yarch et al. (2017) have recently shown that the L4B output cells that project to the thick CO stripes of V2 do not obey this local L4B to L3-blob connectivity rule; instead, these cells have somata that typically lay at a blob border or an interblob, and in L3 they avoid blobs but project to the same CO compartment where their soma resides, i.e. blob border or interblob.

L5A and 5B neurons seem to be widely projecting to supragranular and granular layers, avoiding, however, L4Cm. L5A and 5B both send some axons to L6, too. L6 cells

884 are connected to almost all other layers, with some emphasis on L4C.

885 In V1, the mutual connectivity between the L5 and 6 sublayers has not been studied.
886 Sub-layers 5A and 5B are most likely highly interconnected (Kisvarday et al. 1989;
887 Briggs and Callaway 2005), but this has not been explicitly studied. The illustrations in
888 Wiser and Callaway (1996), together with the quantification of pyramidal cell types in
889 L6A, L6m and L6B seem to suggest that there is dense mutual sublayer connectivity
890 between these L6 subdivisions.

891 L6 pyramidal cells have been classified into subgroups based on their specific laminar
892 targets (Wiser and Callaway 1996). L6 neurons target either the L4C sublayers and L4A
893 in different combinations avoiding all other layers (type I) or avoid L4C and show strong
894 mutual connectivity within L6 (type II). The L6 projections to CO blobs vs. interblobs
895 seem to be nonspecific (Wiser and Callaway 1996) and only a subset of type I pyramids
896 project selectively to particular OD columns in L4C (Wiser and Callaway 1997).

897 ***V2 excitatory neuron connectivity.*** For V2 interlaminar connections, we found only
898 three studies (Valverde 1978; Lund et al. 1981; Levitt, Yoshioka, et al. 1994), limiting the
899 robustness of the connectivity graph and especially the classification of connection
900 strength (Fig. 2 *Middle*, Supplementary Table 1B). First, local excitatory connections
901 show the typical intralaminar self-connectivity. Input layer 4 sends projections to
902 supragranular layers, whereas no direct infragranular projection has been reported from
903 this layer. L3B connects to layers 3A, 5A and 2. L3A projects to L3B, 2 and 5B. L2 sends
904 axonal projections to every layer except 5A. L5A connects back to L4 and sends
905 projections to both 3A and 3B. L5B projects to layers 3A and 3B. Finally, L6 sends
906 efferent axons to all other layers, except L1.
907

## Inhibitory interlaminar connections

Jennifer Lund and colleagues studied the inhibitory neurons and their interlaminar connections of V1 in a series of four papers (Lund 1987; Lund et al. 1988; Lund and Yoshioka 1991; Lund and Wu 1997), based on Golgi impregnation of thick tissue sections and reconstructions of single neurons within single sections. The limitations of these studies are the incomplete impregnation and the fact that neurons cannot be reconstructed beyond individual impregnated sections, therefore leading to incomplete neuron reconstructions. The inhibitory local circuit neurons of V2, instead, have been studied mainly together with excitatory neurons (Valverde 1978; Lund et al. 1981; Levitt, Yoshioka, et al. 1994). Kritzer et al. (1992) used 3H-nipecotic acid to retrogradely label GABAergic cells. Their data suggest that inhibitory connections are made nearly across all layers in both V1 and V2, with the probability of connections decreasing with laminar distance. This is consistent with data in rodents (Markram et al. 2015). Due to poor confinement of tracer injections to single layers in Kritzer et al. (1992), in Figure 2 and Supplementary Table 1 we have omitted most data from this study.

***V1 inhibitory neuron connectivity.*** The dendritic fields of inhibitory interneurons often spread vertically outside the layer where the parent soma is located (Lund 1987). Albeit spreading to other layers, the dendritic fields spread uniformly, sampling apparently unselectively across their depth. Horizontally, the dendritic fields of smooth inhibitory neurons in supragranular layers 1-4B are local, measuring 250-350 μm in diameter (Lund and Yoshioka 1991; Lund and Wu 1997).

It is safe to claim that more than half of the inhibitory synapses are formed within the layer of the parent soma. The exceptions in Figure 2 (*bottom*) and Supplementary Table 1 are L1, for which sparse data do not allow quantitative estimates, and L4A, which is too narrow to include most of the local axonal tree. In contrast to dendrites, the axons may

933 also cross layers, but without sprouting, targeting specific upper or lower layers. A subset
934 of inhibitory neurons with somata either in L4Cα or L4Cβ sends axons to the opposite
935 geniculo-cortical stream (i.e. L4Cα => L4Cβ, L4A or L4Cβ => L4Cα), potentially
936 causing cross-inhibition between the Magno and Parvo streams (Lund 1987).
937 Horizontally, the axons of inhibitory neurons may spread considerable distances, albeit
938 much less than the horizontal spread of excitatory cells; the largest distances are reached
939 by the L2/3 wide-arbor Basket cells, whose axon terminals may reach up to 1.5 mm from
940 the soma (Lund and Wu 1997).

941 The layer-specific connectivity in relation to CO compartments has not been
942 extensively studied for inhibitory interneurons, thus this is omitted in Fig. 2 (*bottom*).
943 Overall, however, the few available studies seem to indicate that inhibitory connections
944 preserve CO specificity (Kritzer et al. 1992), similar to excitatory neurons.

945 L4Cα interneurons connect to all 4C sublayers, as well as to layers 4B, 4A, 3B, 5A,
946 and the bottom of L6. Sparse axonal projections from L4Cα target, in addition, layers 5B
947 and 6A. L4Cβ interneurons show similar connectivity as those of 4Cα, but with emphasis
948 on L6A instead of 6B, and a missing projection to L4B.

949 L4B interneurons target layers 3B, 4A, both 5A and 5B and all L6 sublayers. Sparse
950 projections reach L1 and L2/3A. L4A inhibitory neurons have similar targets as those of
951 L4B. In contrast to L4B, L4A inhibitory neurons send weaker projections to L6, while
952 targeting L4C (4Cm, as well as, weakly, 4Cα and 4Cβ). L3B inhibitory neurons target
953 predominantly L4A, and moderately layers 2/3A, 4B, 4Cm, 5A and 5B, and all three
954 sublayers of L6. L2/3A interneurons send dominant projections to layers 1, 3B, 4A, 4B
955 and 5B, and sparse connections to L6. L1 interneurons send axons to layers 2/3A, 3B and
956 4B, but not to L4C or infragranular layers. L5A sends inhibitory axons to layers 1, 3B, as
957 well as to all L4C and L6 sublayers. L5B is very different from 5A, as it sends inhibitory

axon projections to layers 2/3A, 5A and 6A, and sparse projections to 3B, 4A, 4B, and the bottom two L6 sublayers. L6 interneurons project to layers 4A, all 4C sublayers, 5, and heavily to all L6 sublayers.

The two most apparent distinctions between inhibitory and excitatory intrinsic connectivity within V1 are in L1, which has more extensive inhibitory than excitatory connectivity, and in L6, which inhibits only the thin L4A, but excites most supragranular layers. Horizontally, the inhibitory connections do not seem to form terminal axon clusters, as excitatory neurons do, but their axon density decreases continuously as a function of distance (Kritzer et al. 1992).

Lund et al. (1988) suggested that some L5B inhibitory neurons send axons to the white matter, which would be an important exception to the rule that all white matter tracts are excitatory. Later, long-range inhibitory projections have been found in many species and systems (Caputi et al. 2013) but they are sparse, originating from about 0.5% of neocortical GABA neurons in mice (Tamamaki and Tomioka 2010). In macaques, long-distance projecting inhibitory neurons are predominantly inside the white matter (81%) and in the gray matter they reside predominantly in L3 (12%; L1 0.5%, L2 3%, L5 2%, L6 1.5%, L4 none, Tomioka and Rockland 2007). The functional role of these neurons has remained unknown.

***V2 inhibitory neuron connectivity.*** In V2, the inhibitory connectivity graph is sparse due to availability of only sparse data and will likely need to be modified when new data will become available. The extensive connectivity of L4 is mainly reported in Kritzer et al. (1992), but the $^{3}$H-nipecotic acid retrograde tracing data seem to show an overall more diffusely connected system across layers than, e.g. the Golgi stained single cell data of Lund et al. (1981).

## Interlaminar feedback

Despite the paucity of data on V2 excitatory interlaminar connectivity compared to V1, some similarities between the two areas are apparent.

The input layers 4C and 4 in V1 and V2, respectively, preferentially target the supragranular layers, particularly 3B, but also 3A and 2. In contrast, L2 avoids projecting back to these input layers. Given the lack of direct L2 FB to L4, it may be interesting to investigate whether L2 provides FB-like inputs to other layers.

L6 projects to all layers containing excitatory neurons. Given the large RFs and their broader tuning in L6 (Gur et al. 2005), L6 interlaminar projections could provide fast intracolumnar FB inputs relaying local contextual information to more sharply tuned cells in other layers. Moreover, as V1 L6 (together with L1) is a major recipient of inter-areal FB projections arising from higher visual areas (as discussed above), L6 is also in a position to relay global contextual information (arising from the “far surround” of V1 neurons) to all V1 layers to which it projects. This idea is consistent with the observation that V1 L6 (but also L1) shows the shortest onset latency of local field potential (LFP) responses (i.e. is activated earlier than other layers) following presentation of a visual stimulus in the far RF surround of neurons in a recorded V1 column (Bijanzadeh et al. 2018). These early far-surround responses in V1 L6 (and L1) are thought to be generated by inter-areal FB connections from extrastriate cortex (Angelucci, Levitt, Walton, et al. 2002; Angelucci and Bressloff 2006; Angelucci et al. 2017).

Anatomical reconstruction of microcircuits remains a challenge. Here, we have reviewed studies, most of which are based on injections of neuroanatomical tracers followed by microscopy analysis of labeled tracts or reconstructions of single labeled neurons across serial tissue sections. These approaches have well recognized limitations, for example difficulty and errors in serial section reconstruction of single neurons,

variability in tracer transport across injections and animals, etc. Serial block surface imaging with electron microscopy (EM) allows for accurate and high resolution 3D reconstruction of circuits, at the level of synapses (Denk and Horstmann 2004), and recently automated transmission EM has allowed synapse-level analysis of excitatory network in rodents (Lee et al. 2016). These methods are, however, difficult to apply to large tissue blocks, e.g. encompassing macaque V1, let alone the whole macaque visual cortex. Recently developed methods based on viral vector-mediated high-resolution fluorescent labeling of neuronal circuits (Luo et al. 2008), followed by tissue clearing , to render intact tissue blocks optically transparent (Chung et al. 2013), and deep-tissue imaging (Denk et al. 1990; Stelzer 2015), to image labeled neurons through intact tissue blocks, are making it possible to characterize primate and even human (Mortazavi et al. 2019) brain circuits at cellular resolution. However, lack of algorithmic and computational solutions to visualize, analyze and reconstruct the massive amount of neuronal data that are being collected remains a major challenge that requires development of cyberinfrastructure and computational approaches (Venkat et al. 2016; Petruzza et al. 2017, 2018).

# Functional anatomy

## Cell structure and synaptic coverage

The heterogeneity of cellular structures and their development across brain areas has been previously reviewed (Elston 2003; Elston and Fujita 2014). In V1, dendritic morphology does not seem to change as a function of RF eccentricity. V1 L3 pyramidal neurons show similar number of dendritic branches, total dendritic length, and basal dendritic fields across eccentricities (Oga et al. 2016).

In contrast, along the hierarchy of visual areas dendritic field size and complexity

increase. For L3 pyramidal cells, the area of basal dendrites, which form the largest extent of horizontal dendritic field coverage, increases from V1 (36 ± 5.5 x $10^3$ $\mu m^2$; range 27-49 x $10^3$ $\mu m^2$) to V2 (45 ± 10 x $10^3$ $\mu m^2$; range 18-66 x $10^3$ $\mu m^2$), to V5 (84 ± 11 x $10^3$ $\mu m^2$; range 56-104 x $10^3$ $\mu m^2$; Elston and Rosa 1997). Moreover, there are more dendritic branches per unit area in V5 than in V1 or V2.

The L3 pyramidal neuron basal dendritic field area is somewhat larger in the CO blobs (27 ± 11 x $10^3$ $\mu m^2$; range 5-49 x $10^3$ $\mu m^2$) of V1 compared with the interblobs (20 ± 10 x $10^3$ $\mu m^2$; range 6-51 x $10^3$ $\mu m^2$; Elston and Rosa 1998). There was a similar trend for larger dendritic fields in the V2 thin stripes compared with pale stripes, but without statistical significance.

The V1 L5 pyramidal cell basal dendritic area (40 ± 19 x $10^3$ $\mu m^2$; Oga et al. 2017) is comparable to that of L3 mentioned above.

The total length of the apical dendrite of V1 L3 pyramidal neurons averages (mean ± SD) 1,530 ± 114 μm (trunk 9% of total length, oblique branches 50% and tuft 41%) with 15.3 ± 1.2 branch points, and the total length of the basal dendrites averages 1,659 ± 138 μm with 16.8 ± 1.8 branch points (Gilman et al. 2017). The apical dendrites have on average 855 ± 92 spines, and the basal dendrites 1,030 ± 157 spines.

The apical dendrite spine necks, retrieved from two pyramidal cells in V1 L3, range from 0.2 to 1.2 μm in width, most being 0.4-0.8 μm (McGuire et al. 1991).

The proportion of LGN afferent synapses relative to the total number of synapses (summarized in Peters et al., 1994) in Magno-recipient L4Cα was originally reported to be between 1.3-1.9% (18-40/neuron), and in Parvo-recipient L4Cβ 3.7-8.7% (37-191/neuron; O'Kusky and Colonnier 1982b; Beaulieu et al. 1992). The corresponding number of synapses per number of neurons were (mean±SD) 1.9±0.2 x $10^3$ in L4Cα, and 1.4±0.2 x $10^3$ in L4Cβ (O'Kusky and Colonnier 1982b). A recent quantitative 3D

microscopy study (Garcia-Marin et al. 2017) reported higher average thalamocortical synaptic densities: 0.46 (range 0.39-0.53) x $10^8$/$mm^3$ in L4Cα, and 0.82 (range 0.70-0.93) x $10^8$/$mm^3$ in L4Cβ. These densities correspond to 15% of all excitatory synapses in L4Cα (197 /neuron), and 20% in L4Cβ (200 /neuron) being thalamocortical synapses, suggesting a much stronger thalamocortical drive than previously assumed. In L4A the thalamocortical synapses had an anisotropic honeycomb arrangement, with thalamocortical synaptic density of 0.35 (0.23-0.49) x $10^8$/$mm^3$. In L6 the corresponding density was 0.13 (0.08-0.16) x $10^8$/$mm^3$.

There might be a trend for higher inhibitory synaptic coverage of the spiny stellate cell somas compared with pyramidal cell somas. Otherwise different layers and animals showed variable (between 20-60% of circumference) inhibitory synapse coverage of their somata (Lund et al. 2001).

Although V1 L2-3 CO blobs and interblobs differ in several physiological properties, their pyramidal neurons show no significant difference in soma area, spine density, number of basal dendrites, dendritic radius, or dendritic branching pattern (Hubener and Bolz 1992). Moreover, the dendritic fields of the pyramidal cells cross blob boundaries suggesting continuous dendritic sampling.

### Proportions and synaptic densities of excitatory and inhibitory connections in V1

About 85-90% of V1 connections are excitatory, forming asymmetric synapses with postsynaptic cells, the rest being inhibitory, i.e. forming symmetric synapses (Fisken et al. 1975; Medalla and Luebke 2015). The horizontal and interlaminar connections seem target dendritic spines and shafts in similar proportions. Labeling single V1 L3 pyramidal cells by intracellular injections of HRP (N=2), McGuire et al. (1991) studied both local

and long-range excitatory connections of layer 2/3 PCs and found that 75% of synapses are made onto dendritic spines and 25% onto shafts. This is consistent with the overall population of V1 layer 2/3 excitatory neurons, which make 75% of their synaptic contacts onto dendritic spines, with a mean density of 365±54 x $10^6$ synapses / $mm^3$ (mean±SEM), and 25% with shafts, with a mean density of 119±10 x $10^6$ / $mm^3$ (Medalla and Luebke 2015). Inhibitory neurons, instead, target spines more seldom (34%; mean density of 33±7 x $10^6$ / $mm^3$) than dendritic shafts (66%; 62±24 x $10^6$ / $mm^3$, Medalla and Luebke, 2015). Although lower in volumetric density, the density of synapses along inhibitory cells' dendritic shafts (average of 1.9 synapses/µm, range 0.8-3.9 synapses/µm) is much higher than the density of synapses along excitatory cells' dendrites (average of 0.3 synapses/µm, range 0.1-0.5 synapses/µm, McGuire et al., 1991). A similar synaptic density was found on the cell bodies of the smooth inhibitory cells, with about 200-300 synapses over the whole soma surface.

### Diversity of response properties in V1 and V2 layers

Layers 4Cα and 4Cβ show response properties similar to those of their respective afferent Magno and Parvo LGN neurons (Blasdel and Fitzpatrick 1984). The minimum response field size of neurons (defined as the RF size measured using small bar or square stimuli) is about two times larger in L4Cα than in L4Cβ. Correspondingly, the contrast threshold increases up to 3.5-fold from the top of L4Cα to the bottom of L4Cβ. In supragranular layers, in both blob and interblob regions, cells receive input from both Magno- and Parvo streams (Nealey and Maunsell 1994).

Gur and colleagues (Gur et al. 2005; Gur and Snodderly 2007, 2008) measured RF properties of neurons in different V1 layers in alert monkeys and found significant variability. Orientation and direction tuning in V1 show high laminar variability, with the

input layers, 4Cα and 4Cβ, 4A and 6 housing less selective units (Gur et al. 2005). In addition, the input layers show higher spontaneous firing rates [layer: mean (range across cells) in light / mean (range) in darkness, Hz: L4A: 27 (1-74) / 24 (3-113); L4Cα: 13 (<1-52) / 10 (<1-28); L4Cβ: 30 (11-59) / 17 (5-28); L6: 13 (<1 – 27Hz) /10 (<1-25) Hz] compared to the output layers whose mean firing rates are generally <1 Hz [L3: 3 (<1 – 14) / <1 (one cell); L4B: 1 (<1 – 3) / 1 (<1-3); L5: <1 (<1 – <1) / <1 (<1 – <1), from Fig 5 top in Snodderly and Gur 1995)]. The high spontaneous firing rate in the input layers may be inherited from the LGN, where the mean spontaneous firing rate is about 13Hz (Spear et al. 1994). Mapping RF size with bars of light increments or decrements, Gur et al. (2005) found that V1 layers receiving direct input from LGN (L4A, L4Cα, L4Cβ, L6) have larger RFs than other layers (L2/3, L4B, L4Cm, L5). These findings challenged earlier studies of layer 4C which reported much smaller RF sizes (Schiller et al. 1976; Hubel and Wiesel 1977; Blasdel and Fitzpatrick 1984). This discrepancy can perhaps be attributed to the effects of anesthesia in the earlier studies, which is known to alter LGN activity and multiple RF properties downstream of LGN (Gur et al. 2005). As an alternative explanation, the discrepancy may emerge from less accurate laminar differentiation and RF mapping in awake animals. Moreover, the method and visual stimuli used to map RF size affect the measurements (Angelucci and Bressloff 2006). For example, estimates of RF sizes based on the cortical spread of deoxyglucose uptake (Tootell, Switkes, et al. 1988) allows accurate laminar definition and indicate that layers 2 and 6 have the widest RFs (spread could not be quantified), followed by L5 (half the spread from the edge of the stimulus, about 0.5 mm). L4Cα and L4B show intermediate spread (0.35 and 0.33 mm, respectively), followed by L3 (0.24 mm), and last L4Cβ (0.14 mm). Importantly, RF sizes vary by a factor of over 10 within layers (Dow et al. 1981; Van Essen and Newsome 1984). Given the inverse relationship between spatial frequency

and the RF size (Teichert et al. 2007) spatial frequency data suggests that large RFs are horizontally clustered into CO blobs (Tootell, Silverman, et al. 1988).

Most V1 laminae have a median circular variance, a measure of orientation selectivity (CV = 1 – orientation selectivity index), close to 0.5, but in L3B CV reaches up to 0.75, i.e. L3B is less orientation selective (Ringach et al., 2002). L4 has an intricate parcellation, with layers 4A, 4Cα and 4Cβ having higher CV values, and 4Cm much smaller values (Gur et al. 2005). Overall, L4Cm, the sublayer located between 4Cα and 4Cβ, behaves like a non-input layer: it has small RFs, sharp orientation and direction tuning and low spontaneous activity.

Direction selectivity emerges first in layer 4Cα, and thereafter highly direction selective cells are found in L4Cm, L3, L4B and L6 (Gur and Snodderly 2007). Downstream from L4Cα, the L4Cm projects to L3, and it has been proposed to represent a third motion pathway from V1 to V2, in addition to the monosynaptic motion pathways arising from direction selective cells in layers 4B and 6 (Gur and Snodderly 2007). In addition to high direction selectivity, cells in L3 show high orientation selectivity and small RFs.

Although typically studied together, L2 is functionally distinct from L3. L2 has higher levels of ongoing activity, less spatially selective RFs, lower orientation selectivity and no direction selectivity (Gur and Snodderly 2008), thus, resembling more the input than output layers of V1.

In V2, the tuning properties of neuronal RFs in different layers show greater similarity than in V1 (Tootell and Hamilton 1989), but L3 has the largest proportion of neurons tuned for visual stimulus parameters (Shipp and Zeki 2002a). The layers receiving feedback (L1, L2, L5 and L6), show more often (27 vs 18%) combined tuning to chromatic and spatial features, suggesting higher-order feature binding in these layers

than in the layers receiving the feed-forward input (L4 and L3; Shipp et al. 2009).

## Diversity of response properties in parallel pathways

As reviewed in Schiller et al. (1976), the input from the LGN is transformed into five main ways within V1. First, the concentric center-antagonistic surround RFs become a minority in V1, while orientation selectivity emerges. Second, many units become selective for motion direction. Third, many cells acquire “complex” RFs, i.e. they respond to both light increments and decrements in their RFs. Fourth, most cells become driven by both eyes and, fifth, become more selective for spatial frequency. In addition, some cells show double color opponency (Livingstone and Hubel 1984a), and most cells sum contrast non-linearly as a function of visual stimulus size (Sceniak et al. 1999; Angelucci, Levitt, Walton, et al. 2002; Cavanaugh et al. 2002).

The functional architecture of the macaque visual cortex and parallel processing strategies have been more extensively reviewed previously (Casagrande and Royal 2004; Roe 2004; Sincich and Horton 2005; Nassi and Callaway 2009). In brief, Figure 3 *top* depicts the parallel FF pathways from LGN to V1. Afferent geniculate connections from the two eyes remain segregated into OD columns in the input layers of V1 (Hubel and Wiesel 1968). CO blobs are prominent in layers 2/3, but to some extent visible also in layers 1, 4B, 5 and 6 in register with the L2/3 blobs (Horton 1984).

In V2, the CO stripes run orthogonally to the V1/V2 border (Tootell et al. 1983), and are visible, albeit weakly, in most layers and moderately in L4 (Balaram et al. 2014). Across V2, there are about 28 complete sets of CO stripes, a full stripe cycle encompassing on average 4 mm (Olavarria and Van Essen 1997). Table 5 presents a quantitative overview of early electrophysiological single unit recording studies showing the prevalence of various visual stimulus tuning properties in the different V2 stripes

(modified from Shipp and Zeki 2002a). Electrophysiological recordings have demonstrated that many visual response properties are present, albeit with differing prevalence, in all stripe types, and there has been much debate and controversy over the functional specificity, or lack thereof, of distinct stripes (Shipp and Zeki 2002a).

Intrinsic signal optical imaging (OI) is better suited than single unit recordings to reveal the predominant response within a neuronal population and, in addition, it allows investigations of the spatial layout of particular visual responses (Blasdel and Salama 1986; Grinvald et al. 1986; Ts'o et al. 1990). This technique has revealed that while neuronal responses to the various visual stimulus parameters are present in most CO compartments, only some of these parameters are systematically mapped within a given compartment.

Figure 3 *right* lists the functional feature selectivity and maps found in the various CO compartments of V1 and V2. Unfortunately, macaque V5 is buried within the superior temporal sulcus, and thus is not accessible to OI. In V1, OI has revealed multiple, and at least partially independent, spatial representations or maps of visual stimulus features, including ocular dominance (Blasdel and Salama 1986; Bartfeld and Grinvald 1992; Blasdel 1992), orientation (Bartfeld and Grinvald 1992; Blasdel 1992; Ramsden et al. 2014; Felleman et al. 2015), motion direction (Lu et al. 2010; Hu et al. 2018), binocular disparity (Ts'O et al. 2001; Chen et al. 2008), color (Ts'O et al. 2001; Landisman and Ts'o 2002; Xiao et al. 2003, 2007; Lu and Roe 2008) and brightness/luminance (Roe et al. 2005; Wang et al. 2007) maps.

Based on microelectrode recordings by Hubel and Wiesel (1974a) Braitenberg and Braitenberg (1979) suggested that iso-orientation domains are arranged around orientation singularities. This local "pinwheel-like" organization of orientations was later confirmed by optical imaging of intrinsic signal (Blasdel and Salama 1986; Ts'o et al. 1990; Malach

et al. 1993; Landisman and Ts'o 2002; Nauhaus et al. 2008) and two-photon imaging (Nauhaus et al. 2012); for a critical and quantitative analysis of data and models, see (Obermayer and Blasdel 1993; Erwin et al. 1995).

Many studies have examined the relative spatial relationships between these various feature maps in V1. CO blobs (Horton and Hubel 1981) and orientation pinwheel centers (Bartfeld and Grinvald 1992) lie close to the center of OD bands [(the latter 300-670 μm wide (LeVay et al. 1975; Horton and Hocking 1996)], but it has remained controversial whether CO blobs and pinwheel centers align with each other (Bartfeld and Grinvald 1992; Blasdel 1992; Obermayer and Blasdel 1993; Lu and Roe 2008). This controversy may have been aggravated by spatial low-pass filtering of neural responses by optical imaging method which may cause systematic shift of pinwheel centers (Polimeni et al. 2005). In our unpublished data (Merlin et al. 2012), we find a strong association between CO blobs and pinwheel centers, with 85-90% of blobs containing a pinwheel center. However, as pinwheel centers are more numerous than CO blobs in V1, only about 50% of pinwheel centers reside in blobs, therefore suggesting at least partially independent representations of orientation and CO blob maps. The CO blobs seem to coincide with color patches revealed by OI (Lu and Roe 2008), and each color patch contains an orderly and overlapping mapping of responses to distinct hues (Xiao et al. 2007). Despite this partially independent spatial arrangement between orientation pinwheels and color patches, many neurons in V1 are tuned both to color and orientation (Garg et al. 2019).

OI studies have shown that in V2 each CO stripe contains distinct feature maps. Each thick stripe contains one or more (200 μm wide x 1 mm long) topological representation of horizontal retinal disparities (Chen et al. 2008), and a pinwheel-like (about 1 mm wide) or linear representation of different motion directions (Lu et al. 2010). In addition, thick stripes contain ordered orientation maps which have diameter of 0.7-1.5 mm (Ts'O et al.

2001). Orientation domains are also found in the pale stripes, in response to both real and illusory contours (Ramsden et al. 2014). Thin stripes represent hue in a systematic fashion [0.07-0.32 wide x 1.3 mm long bands of varying shape (Xiao et al. 2003)], as well as brightness increments/decrements, the latter forming distinct domains about 0.7 mm apart (Wang et al. 2007).

**Table 5.** Functional selectivity of V2 stripes. Median % (range) of cells tuned to the specific visual stimulus parameter (single or multi-unit recordings) across seven electrophysiological studies published up to 2002. Modified from the summary of (Shipp and Zeki 2002a). The definitions of tuning and stripe type varied between studies. * Disparity or binocular interaction. Data originally from: 1. DeYoe and Van Essen 1985; 2. Peterhans and von der Heydt 1993; 3. Levitt, Kiper, et al. 1994; 4. Munk et al. 1995; 5. Roe and Ts'o 1995; 6. Gegenfurtner et al. 1996; 7. Shipp and Zeki 2002a.

| | Thick | Thin | Pale | References |
|---|---|---|---|---|
| **Orientation** | 85 (51-88) | 41 (20-73) | 80 (17-96) | 1-7 |
| **Direction** | 29 (11-60) | 6 (0-21) | 13 (0-34) | 1-4, 6-7 |
| **Color** | 16 (7-39) | 63 (53-86) | 27 (12-64) | 1,3-7 |
| **Disparity*** | 68 (38-77) | 21 (10-33) | 15 (1-22) | 1-2,5 |

# Physiology

## Conduction velocities and latencies

The hierarchy of anatomical connections suggests that areas higher in the hierarchy have increasingly longer response latencies to visual stimulation. Experimental evidence supports this claim to some extent for the areas in the occipitotemporal ventral stream, but

not for the areas in the parietal and frontal dorsal stream (Schmolesky et al. 1998). In the LGN, the Magno pathway has about a 20-ms lead in response onset relative to the Parvo pathway. In V1, magnorecipient L4Cα has a corresponding 20-ms lead relative to parvorecipient L4Cβ (Nowak et al. 1995). This segregation of latencies continues in the distinct functional compartments of V2 (Bullier and Nowak 1995). Interestingly, the inhibitory responses are as early as the excitatory responses, and the shortest latencies in V2 are in the infragranular layers (Nowak et al. 1995). Thereafter, cortical latencies show a wide distribution (Nowak and Bullier 1997; Schmolesky et al. 1998).

Intracortical conduction velocity has been measured for connections between V1 and V2 (Girard et al. 2001). The following values are a lower bound for the true velocities, because they were estimated assuming direct connections in Cartesian 3D space. The median FF conduction velocity was 3.7 m/s (range 3 – 6 m/s), and the FB conduction velocity 3.4 m/s (range 1.5 – 9.5 m/s). This is very fast compared to the conduction velocity of upper layer local V1 axons (0.33 m/s) enabling a rapid FF-FB loop between V1 and V2, particularly faster for the Magno signals which are conveyed to V2 and back to V1 even before the Parvo signals (80% of optic nerve fibers) arrive to V1. Functionally, Magno signals may prime V1 with contextual/top-down information before Parvo signals arrive to V1, and the loop via extrastriate cortices would be necessary in particular for long-distance interactions (reviewed in Bullier, 2001; Bullier et al., 2001; Angelucci and Bressloff, 2006). It is noteworthy that Girard et al. (2001) briefly reported that intrinsic horizontal connections within the infragranular layers of V1 may conduct signals faster than upper layer axons (up to 1m/s), albeit still slower than interareal V1-V2 connections; however, layer differences were not thoroughly characterized in that study and will need further investigation.

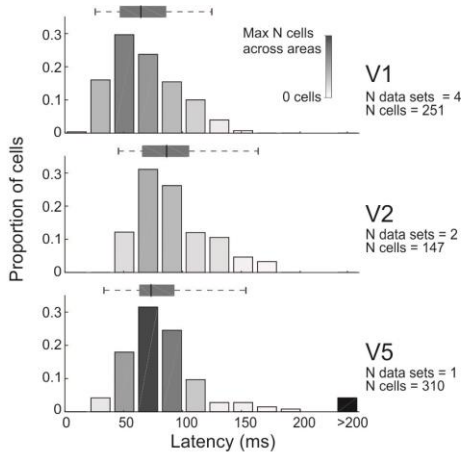


1271

**Figure 5. Onset latencies of spiking responses to visual stimulation**. The proportions of cells are displayed as a function of latency. The number of distinct figures providing the source data, some in the same papers, are indicated on the right (N data sets), together with the total number of cells across the data sets. Bar darkness reflects the number of cells in each bin normalized to largest number of cells in any of the bins across the three cortical areas. The black bar on the right contains outlier values above the reported cutoff at the tick mark value. The whisker plots indicate the 2.5, 25, 50, 75 and 97.5 percentiles of the data, calculated from the histograms in the original data. Data for V1 are from (Maunsell and Gibson 1992; Nowak et al. 1995), for V2 from (Nowak et al. 1995), and for V5 from (Raiguel et al. 1989).

1272

1273 Figure 5 shows response onset latencies in areas V1, V2 and V5, and Supplementary
1274 Figure 1 shows the cumulative density functions and pairwise uncorrected Mann-Whitney
1275 U tests between the areas' median latency values. Response onset latencies overlap in the
1276 different areas, but median latency increases from V1 to V5 to V2 (65, 73 and 86 ms,
1277 respectively). Onset latencies are strongly dependent on various visual stimulus
1278 parameters, especially luminance, which affects integration time in the retina (Mansfield
1279 1973). Moreover, there is significant variability between individual animals in onset
1280 latencies (Maunsell and Gibson 1992), which complicates comparison across studies. The
1281 study of Schmolesky et al. (1998) compared latencies in different cortical areas. Mean
1282 latencies were shortest in V1, 66 ms (SD 10.7, range 34-97), longest in V2 82 ms (SD
1283 21.1, range 56-118) and intermediate in V5 72 ms (SD 10.3, range 49-98). These latencies

resemble our summary data from multiple studies.

The earliest responses at the top of L4C of V1 cause oscillations at 50-100 Hz (Maunsell and Gibson 1992). Within V2, the thick (median multi-unit onset latency 63 ms) and pale (70 ms) stripes show earlier response onset compared to the color-sensitive thin stripes (81 ms; Munk et al. 1995).

## Firing rate statistics

The ability of a neural system to provide the same response with high temporal precision is highly dependent on the variance of the input, suggesting neural systems have low intracellular noise (Mainen and Sejnowski 1995). High temporal precision enables a system to transmit information using less resources. Because neuronal response statistics differs in alert vs. anesthetized monkeys, in the discussion below we specify the state of anesthesia.

In alert monkeys, individual V1 neurons show high temporal precision of spike latency in response to an optimal stimulus, with the median Fano factor (variance/mean) across layers ranging between 0.2 and 0.35, and the mean across V1 being 0.33 ± 0.17 (SD, range across cells <0.1-1). However, when stimulus contrast is reduced to near threshold, variability increases, and Fano Factors grow closer to 1 (Gur and Snodderly 2006).

The spontaneous spike rate in V1 has an exponential distribution across cells with very low average rates (simple cells 1.2 Hz, N=137, complex cells 4.9 Hz, N=245, anesthetized; Schiller et al. 1976).

Rasch et al. (2011) studied the statistics of V1 spiking during movie viewing in anesthetized monkeys. They found a mean firing rate of 5.1 ± 0.8 (SD) Hz, and an exponential distribution of firing rates, with the exponent being on average -0.8 ± 0.6 s

(range -2.4 s – -0.2 s). For individual neurons, the Fano factor across multiple presentations of the same stimulus was close to 1 for very short ≤10 ms epochs and increased for longer epochs. The population response was, as expected, more reliable for short epochs (smaller Fano factor than for individual neurons), but increased again with longer epochs, suggesting that the firing rates of individual neurons go up and down together. There are probably important differences in firing rate statistics due to anesthesia. First, the Fano factors are significantly lower in awake than anesthetized animals (Gur and Snodderly 2006); moreover, when fixational eye movements are carefully controlled in awake animals (Gur and Snodderly 2006; McFarland et al. 2016), Fano factors cease to increase at longer epochs. In summary, response variability might be significantly smaller in awake visual cortex than previously assumed and stay constant over time.

There are few studies on the firing rate statistics of extrastriate areas. Because Fano factor is affected by anesthesia, epoch length and, in awake animals, fixational eye movements, areas V1, V2 and V5 need to be compared under identical conditions. Yang et al (2009) compared anesthetized young and old adult monkeys and found that Fano factors in V1 and V5 during drifting grating stimulation are very similar, but increase with age in both areas. Mean Fano factors were (young/old) 1.4/2.4 in V1, and 1.5/2.5 in V5.

## Visual field representation in cortex

The representation of the visual field in cortex can be characterized by three parameters, namely RF size, magnification factor (or it's 2D generalization log conformal mapping), and cortical point image. These representations are however not smooth, because local discontinuities arise from RF scatter and additional dimensions, such as

ocular dominance (V1;(LeVay et al. 1975) and cytochrome oxidase (V2) bands (Roe and Ts'o 1995; Shipp and Zeki 2002b).

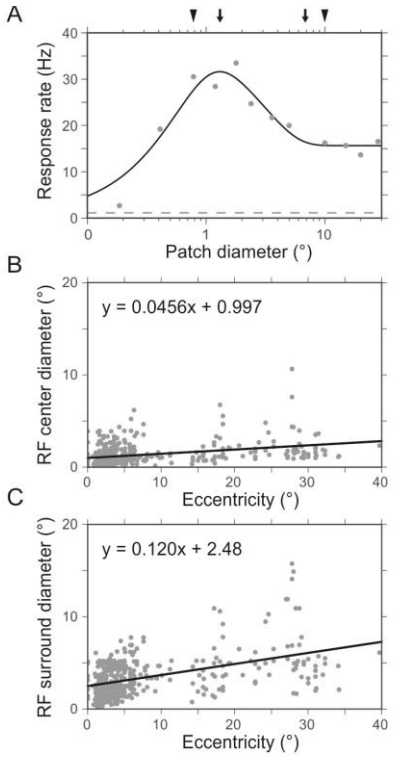


**Figure 6. Area summation function in V1.** A: Area summation function for an example V1 neuron. Solid line represents fit to the data (dots) using the difference of Gaussians (DoG) model. Dashed line indicates the mean spontaneous firing rate. Arrows indicate the center and surround diameters obtained using the DoG fit. Arrowheads indicate the center and surround diameters extracted from the empirically measured responses (without any fit). Data from (Shushruth et al. 2009). B: RF center diameter with respect to eccentricity. Solid line represents linear fit to the data (dots, N=425). C: RF surround diameter with respect to eccentricity. Solid line represents linear fit to the data (dots, N=425). B, C data from (Cavanaugh et al. 2002).

## Receptive field size

In macaque V1, a typical single-cell response to an enlarging stimulus first shows an increase, then a decrease, until an asymptote is reached (Fig. 6A). The RF size is defined as the stimulus radius at peak response, and the region beyond peak response, where the

cells response is suppressed is termed the surround. This patch-size tuning curve, also called the area summation function (ASF), has been modeled as antagonistic excitatory and inhibitory Gaussian mechanisms, interacting either divisively (ratio of Gaussians, RoG, model; Cavanaugh et al., 2002) or subtractively (difference of Gaussians, DoG, model; Sceniak et al. 1999). In the DoG model, the area summation function is:

$$R(dia) = R_0 + K_c \int_{-dia/2}^{dia/2} e^{-(2x/w_c)^2} dx - K_s \int_{-dia/2}^{dia/2} e^{-(2x/w_s)^2} dx$$

Here, dia is the diameter of the stimulus, $R_0$ the spontaneous firing rate, $K_c$, $K_s$, the gain and $w_c$, $w_s$ the extent of the receptive field center and surround, respectively. The center and surround mechanisms are thought to be generated by distinct connections: the excitatory center primarily by geniculocortical FF and intra-V1 horizontal connections, while the inhibitory surround primarily by both local intra-V1 and interareal FB connections (Angelucci, Levitt, Walton, et al. 2002; Schwabe et al. 2006). A recent review (Angelucci et al. 2017) discusses how the cortical microcircuit might give rise to the area summation function.

Neurons show significant variability in their ASFs and the center and surround extents vary with visual field eccentricity (Fig. 6B, C). In parafoveal V1 (at 3-7° eccentricity) using a high contrast grating patch increasing in size, the RF radius measured on average 0.36° ± 0.13° (N=79; range 0.11° – 0.82°, Shushruth et al. 2009), and in a different study 0.39° (N=148; eccentricity < 5°, Cavanaugh et al. 2002). These same studies estimated the surround radius to be 1.62° ± 0.62° (N=79; range 0.55° – 2.66°) and 2.5° (N=148) respectively. The extents were determined using the DoG fits to the spatial summation data (Shushruth et al. 2009), or directly from the data (Cavanaugh et al. 2002), and defining RF extent as the smallest stimulus radius at the peak of the fitted function, or (for

cells that did not show surround suppression) that elicited 95% of the maximum response, and the surround extent as the smallest stimulus for which the response was reduced to 5% of its asymptotic value.

Similarly, in parafoveal V2 (up to 10° eccentricity), the RF radius has been reported to average 0.74° ± 0.50° (N=91; range 0.16° – 2.43°) and the surround radius 3.56° ± 1.94° (N=83; range 1.06° – 10.55°). Thus in V2, the RF sizes are on average double the sizes of V1 RFs (Shushruth et al. 2009).

For V5, similar nonlinear ASFs as in V1 and V2 have been reported (Pack et al. 2005; Hunter and Born 2011). The peak response appears to be larger than in V1 or V2, in many cases larger than the largest stimulus diameter used for the measurements (30°). The "classical RF" for V5 cells, which is measured using small stimuli rather than gratings of increasing size, was defined by the following equation: size (deg) = 0.72E + 1.35 (Desimone and Ungerleider 1986). The optimal RF size, corresponding summation field, is about 10 times larger in V5 than in V1 (Albright and Desimone 1987; Maunsell and van Essen 1987).

## Mapping of visual field in cortex

The representation of foveal and parafoveal visual field in V1 can be characterized as (Schwartz 1980, 1994) :

$$w = k * \log(z + a) \qquad \text{Eq 1}$$

where $w$ is the position in cortex, and z is the position in visual field. The real part of z represents the eccentricity, and the imaginary part the polar angle (azimuth) in visual field. The parameters $k$ and $a$ scale the transformation, and $a$ defines the foveal part of the

visual field, respectively. For the existing macaque data (Daniel and Whitteridge 1961), Schwartz (1980) used a value of $a$=1 (in his Figure 1), and $k$ would scale for the individual V1 size.

Schwartz's log mapping has been generalized to cover full field V1, V2 and V3, and to account for shear that conformal (i.e. angle-preserving) mappings cannot model (Polimeni et al. 2006). For numerical simulations, the log mapping provides a straightforward way to map the visual field into cortical coordinates, and it has recently been applied to visual cortical prosthetics as well (Li 2015).

Several previous studies have provided quantitative data on the one-dimensional derivative of the log conformal map, i.e. the magnification factor. This is the distance in cortex that represents a given distance in visual field (Daniel and Whitteridge 1961). The parameters $k$ and $a$ of the log conformal mapping are related to the magnification factor (M), because the inverse of the magnification factor can be defined as a linear function of eccentricity (Schwartz 1994):

$$\frac{1}{M} = \frac{a}{k} + \frac{1}{k} * \text{eccentricity} \qquad \text{Eq. 2}$$

Although none of the cortical areas show smooth mappings of the visual field, as they all have some sub-structure, V1 has in early studies been characterized with a single magnification value. Nevertheless, the relation of eccentricity to $M^{-1}$ is not fully linear (Dow et al. 1981), and additionally shows significant horizontal-vertical anisotropy (Tootell, Switkes, et al. 1988). This anisotropy calls for the aforementioned more comprehensive 2D mapping of the visual cortex than what the M factor allows (Polimeni et al. 2006). However, since these parameters are nonexistent for V5, here we only report magnification factor.

The area V1 magnification factor, M, as a function of eccentricity is 1/(0.077 + 0.082 x E) mm/deg, as determined using the 2 deoxyglucose method (2DG) method within the central 10° (Tootell et al. 1982), and 1/(0.0404 + 0.116 x E) mm/deg, as determined using electrophysiological recordings within the central 2.5° (Dow et al. 1981) or 1/(0.109 + 0.0637 x E) mm/deg outside the foveal representation (Hubel and Wiesel 1974b; Hubel and Freeman 1977). The slope of $M^{-1}$ at the fovea is about half the slope outside the fovea. The OD columns cause anisotropy by reducing the M factor to about half the value in the direction orthogonal to the OD bands (LeVay et al. 1975).

Early V2 studies reported that the three CO stripes have separate maps of the visual field. The representations are, however, continuous within the same type of stripe (Roe and Ts'o 1995; Shipp and Zeki 2002b). Each of the V2 CO compartments had similar values of magnification factor (interstripes 1.44 mm/deg, thin stripes 1.4 mm/deg and thick stripes 1.25 mm/deg; Roe and Ts'o 1995).

The magnification factor for area V5 is 1.14 x $E^{-0.76}$ (Gattass and Gross 1981; Albright and Desimone 1987). Because the sizes of cortical areas vary across individuals (as also shown for humans in Amunts et al., 2000), the magnification factors show also individual variability.

## Cortical point image

The literature on cortical point image, *i.e.* the cortical representation of one point in visual field, is a function of the average cortical RF size and scatter. In V1, the cortical point image shows discrepant values, depending on whether it was measured by electrophysiological recordings or by optical imaging with voltage sensitive dyes (VSDI). Electrophysiological recordings demonstrate an exponential reduction of the cortical point image with increasing eccentricity. At the fovea the point image approaches 10 mm,

whereas in the periphery it is about 1 mm (Dow et al. 1981). In contrast, VSDI shows a constant point image, at least in the parafoveal representation (2°-5°, Palmer et al., 2012). The former method measures action potentials, i.e. the output of neurons, whereas the latter measures the subthreshold voltage variations. The discrepancy may, thus, be related to differences in neuronal tuning of synaptic vs. action potentials (Jia et al. 2010), and may partially reflect non-linear mapping from subthreshold to suprathreshold responses (Anderson et al. 2000; Miller and Troyer 2002).

Including LGN in a computational model requires mapping the visual field onto LGN cells, and then LGN cells onto visual cortex. The visual field forms retinotopic representation in each Parvo- and Magno layer. The LGN represents the visual field with a smaller number of cells than V1, and the ratio of LGN/V1 cell numbers changes as a function of eccentricity (Connolly and Van Essen 1984). The number of cells per square degree of visual field ($M_c$, cells/deg$^2$) as a function of eccentricity (E) is given by:

$$M_c = k(a + E)^{-x}$$

where k=83700, a=1.28 and x=1.96, for Parvo layers, and k=3520, a=3.12 and x=1.56, for Magno layers. These results suggest that the Magno/Parvo cell ratio in LGN increases by a factor of up to 20 from the fovea to the periphery.

Livingstone and Hubel (1988b), instead, found an approximately equal M/P-ratio across eccentricities, and suggested that the Connolly and Van Essen (1984) analysis was flawed. The anatomical data of Livingstone and Hubel (1988b) were later challenged by Malpeli et al. (1996), who attributed the discrepancy to a number of potential factors, such as technical issues related to the retrograde transport of the tracers, the omission of the Koniocellular channel (which was discovered in 1994, after the Livingstone and

Hubel's study), or a plateau in the magnitude of the magnification factor of the Magno channel at the eccentricities where the tracer injections were placed. Malpeli et al. (1996) showed that the M/P cell ratio in LGN grows by a factor of at least 14 from the fovea to the periphery, thus confirming the original study by Connolly and Van Essen (1984).

Based on the results by Connolly and Van Essen (1984), Schein and de Monasterio (1987) estimated the point images from LGN cells onto V1. Point images are very different for the LGN Parvo and Magno cells' mapping onto the cortex, which results from the different type of scaling of N neurons/unit area as a function of eccentricity. Outside the fovea, the ratio of LGN Parvo cells to unit area of cortex is close to constant, being 550/mm$^2$ at 1° eccentricity, and increasing to 872/mm$^2$ at 80°. In contrast, the density of Magno cells increases steeply, from 13/mm$^2$ at 1° to 206/mm$^2$ at 80° eccentricity. The point image in V1 behaves exactly the opposite, namely for Parvo cells it decreases steeply with eccentricity, whereas it is almost constant for the Magno cells.

The cortical point image size grows along the ventral stream hierarchy, but stays constant along the dorsal stream, including V5 (Gattass et al. 2005).

## Orientation selectivity

In V1 about 70% of cells are tuned to the orientation of edge stimuli, the rest having non-orientation-sensitive RFs (Bullier and Henry 1980). The distribution of orientation selectivity across V1 layers is discussed in the section "Diversity of response properties in V1 layers" under "Functional anatomy". Quantitatively, orientation selectivity can be defined by two parameters, circular variance (CV) and bandwidth (BW). The circular variance is a global measure, based on firing rate responses (r) to all orientations (Θ).

$$Circular\ Variance = 1 - \left|\frac{\sum r e^{i2\theta}}{\sum r}\right| \qquad \text{Eq. 3}$$

A CV of zero indicates high orientation selectivity, and CV of 1 no selectivity.

Figure 7 and Supplementary Figure 1 show that the CV in V1 is somewhat higher than in V2. All datasets in V1 and V2 were from (Goris et al. 2015), and were originally reported as orientation selectivity index (OSI), which we have converted into CV (1-OSI) for the data shown in Fig. 7. For V5, Albright (1984) reported that 83% (74/89) of units were tuned for orientation, but, because he quantified orientation tuning as the difference between the max and min responses, this data could not be converted to CV.

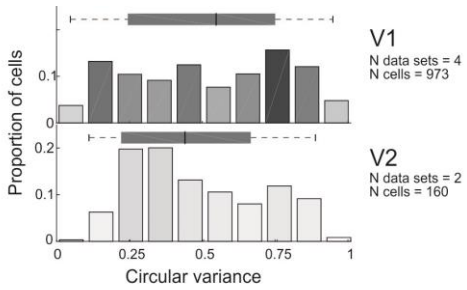


**Figure 7. Circular variance.** Conventions are as in Figure 5. Data for V1 are from (Ringach et al. 2002; Gur et al. 2005; Goris et al. 2015) and for V2 from (Goris et al. 2015).

Orientation bandwidth is a local measure, defined as the response distribution close to the orientation causing the peak response (Figure 8, Supplementary Fig 1).

$$BW_\theta = \theta_{r_{1/2}max} - \theta_{r_{1/2}min} \quad \text{Eq. 4}$$

where

$\theta_{r_{1/2}max}$ is the max (min) orientation producing half of the response strength. Studies reporting BW at $1/2^{1/2}$, or 70.7%, of the peak response (Ringach et al. 2002; Gur et al. 2005) instead of the half-height, were transformed to half-height values by assuming a Gaussian distribution of the tuning, and multiplying the BW values by the square root of

two. The full bandwidth was reported only by Albright et al. (1984), whereas we doubled the values from other studies which reported the half-bandwidth. The outlier cutoff was set at 160 deg. Fig. 8 and Supplementary Fig. 1 demonstrate that orientation bandwidth is slightly wider in V1 than V2, but bandwidth in V5 is not significantly different from V1 and V2.

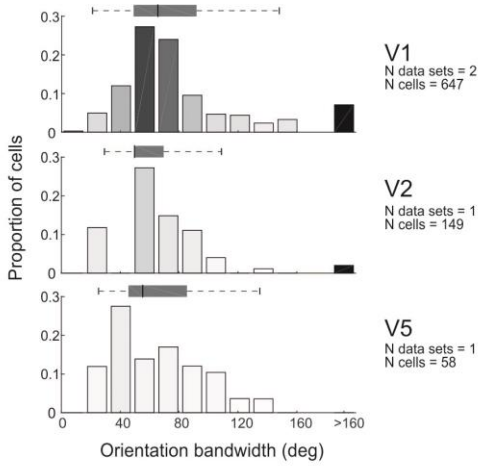


**Figure 8. Orientation bandwidth.** Conventions are as in Figure 5. Data for V1 are from (Ringach et al. 2002; Gur et al. 2005), for V2 from (Levitt, Kiper, et al. 1994), and for V5 from (Albright 1984).

## Direction selectivity

The direction selectivity index (DSI) reported in Figure 9, is based on nine previous studies. The DSI is defined as follows:

$$DSI = 1 - \frac{r_{null\ direction}}{r_{preferred\ direction}} \qquad \text{Eq. 5}$$

A DSI = 0 indicates a non-direction selective cell and a DSI =1 a highly directionally selective cell. Values >1 appear when the minimal response to stimuli moving in the non-preferred direction is below the spontaneous firing rate. One study (De Valois, Yund, et al.

1530 1982) reported V1 DSI as null/preferred response; in this case were recalculated the DSI
1531 values according to Eq. 5. De Valois et al. did not report values when the null response
1532 was below baseline, leading to a max DSI value of 1. However, a similar secondary peak
1533 at 1 in V1 was observed in two other data sets. The distribution in Figure 9 did not change
1534 much with the De Valois et al. dataset removed (222 cells).
1535

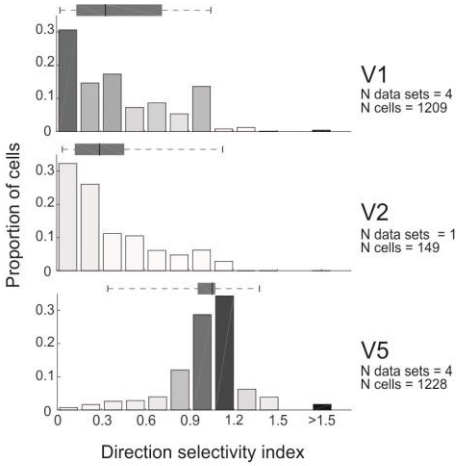


1536

**Figure 9. Direction selectivity index.** Conventions are as in Figure 5. Data for V1 are from (De Valois, Yund, et al. 1982; Albright 1984; Movshon and Newsome 1996; Wang and Movshon 2016), for V2 from (Levitt, Kiper, et al. 1994), and for V5 from (Maunsell and Van Essen 1983c; Albright 1984; Movshon and Newsome 1996; Wang and Movshon 2016).

1537

1538 Direction selectivity clearly differs in different areas. Most cells in V1 and V2 are
1539 poorly or moderately directionally selective, and the two areas show overlapping
1540 distribution, whereas most cells in V5 are strongly directionally selective.
1541

## 1542 Spatial frequency selectivity

1543 In contrast to the retinogeniculate pathway, where most cells show low-pass
1544 characteristics, in visual cortex the majority of cells are band-pass tuned (De Valois,
1545 Albrecht, et al. 1982). Spatial frequency (SF) has typically been described by two

parameters, the optimal response (peak) and the bandwidth.

Figure 10 shows the distribution of peak SFs in the three cortical areas. The eccentricities of the recorded neurons varied a little between studies, but the range was similar: 2-5° in V1, 0-5° in V2, and 0-8° in V5. The large variability in peak SF precluded setting the outlier threshold at the same cutoff value for all areas, because the low outlier cutoff in V1 (<0.5, De Valois et al., 1982a) encompassed most data in V5. The number of outliers in the original data were low, 4 cells (1.5%) in V1, 22 (9.4%) in V2, and none in V5, thus them could only minimally skew the data in Figure 10.

The peak SF differed significantly between areas, with the highest values in V1, and progressively lower values in V2 and V5 (Suppl. Fig. 1). Functionally this suggests that the three areas co-operate to detect a wide range of SFs. Because the low SFs would be lost after band-pass filtering in V1, these data in addition suggest either that V2 and V5 have direct access to visual information from LGN (as, indeed, reported in the anatomy section above) or that the few units in V1 tuned to low SFs have high response gain.

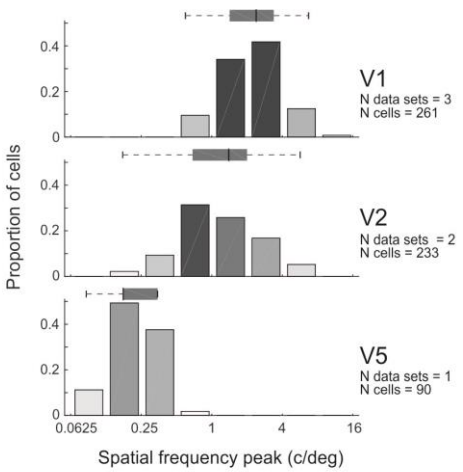


**Figure 10. Spatial frequency peak.** Conventions are as in Figure 5. Data for V1 are from (De Valois, Albrecht, et al. 1982; Foster et al. 1985), for V2 from (Levitt, Kiper, et al. 1994), and for V5 from (Yuan et al. 2014).

Datasets on the SF bandwidth are limited, due to different metrics used to report it in different studies (Fig. 11). The bandwidth in Fig. 11 is reported as full width at half-height, on a logarithmic scale (octaves, *i.e.* $\log_2$):

$$BW_{SF} = SF_{r_{1/2}max} - SF_{r_{1/2}min} \quad \text{Eq. 6}$$

V5 has significantly wider SF bandwidth compared to V1 and V2 (Suppl. Fig. 1). In addition, higher areas showed increasingly higher numbers of cells whose SF bandwidth could not be defined (black bars), as their response did not drop to half of the maximum response on either side of the peak. Cells with such wide-band tuning could be sensitive to sharp edges.

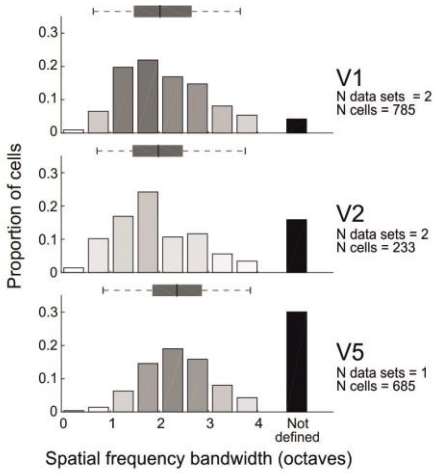


**Figure 11. Spatial frequency bandwidth.** Conventions are as in Figure 5. Data for V1 are from (Foster et al. 1985; Wang and Movshon 2016), for V2 from (Foster et al. 1985; Levitt, Kiper, et al. 1994), and for V5 from (Wang and Movshon 2016).

## Temporal frequency selectivity

Peak temporal frequency (TF) was characterized in five studies (Fig. 12). The original

data have sparse bins, and small numbers of cells, hampering comparison between areas. V5 significantly prefers higher optimal TFs compared to V1 and V2, whereas V2 shows a distribution with somewhat lower TF values than V1 (Suppl. Fig. 1).

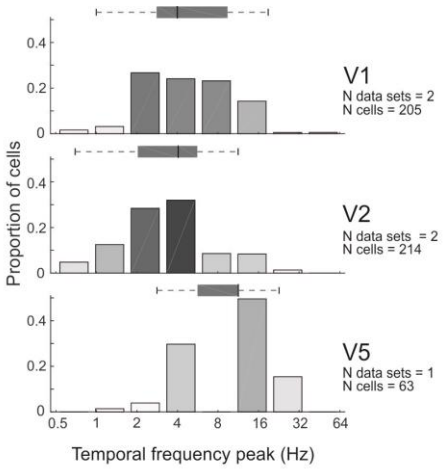


**Figure 12. Temporal frequency peak.** Conventions are as in Figure 5. Data for V1 are from (Foster et al. 1985; Hawken et al. 1996), for V2 from (Foster et al. 1985; Levitt, Kiper, et al. 1994), and for V5 from (Yuan et al. 2014).

The TF bandwidth (Fig. 13) was characterized in the literature only for a minority of cells, most not reaching the threshold of 50% response strength, and most of them having low-pass temporal response function. The TF bandwidth was significantly wider in V1 than in V2 (Suppl. Fig. 1). We found no published data for V5.

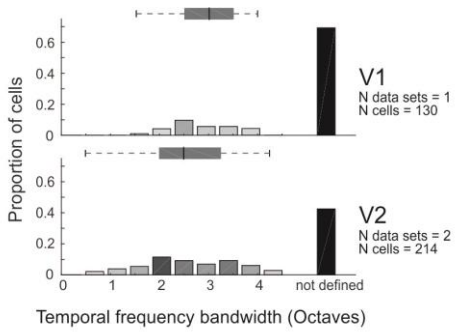


**Figure 13. Temporal frequency bandwidth.** Conventions are as in Figure 5. Data for V1 are from (Foster et al. 1985), and for V2 from (Foster et al. 1985; Levitt, Kiper, et al. 1994).

## Contrast response function

The contrast response function is quantified using the following equation

$$R = b + \frac{C^{\gamma}}{C^{\gamma} + C_{50}^{\gamma}} \quad \text{Eq. 7}$$

where $R$ is response, $b$ baseline firing rate and $C$ contrast (independent variable). The fitted variables are $\gamma$, the exponent, and $C_{50}$, the semisaturation contrast, i.e. the contrast value at which the response curve reaches 50% of its maximum value.

Figure 14 shows the distributions of semisaturation contrast and contrast exponent for areas V1, V2 and V5. For each study we reviewed both parameters. The only logarithmic semisaturation contrast plot (V2) in (Levitt, Kiper, et al. 1994) was turned into a linear scale, for comparison.

Figure 15 visualizes the normalized contrast response functions attainable with the median exponent and semisaturation contrast for each area. Figures 14 and 15 as well as Suppl. Fig 1 demonstrate that V5 has significantly higher contrast sensitivity than the two other areas, followed by V2 and V1. This is due to the varying semisaturation contrast, whereas the median exponents are similar in the three areas.

Figure 16 shows that there is a similar distribution of maximum firing rates across the cell population in V1 and V5. The original data were binned at 10 spikes/s and peaked between 10 and 20 Hz in both V1 and V5, with about 50% drop in the 0-10 Hz bin (Sclar et al. 1990).

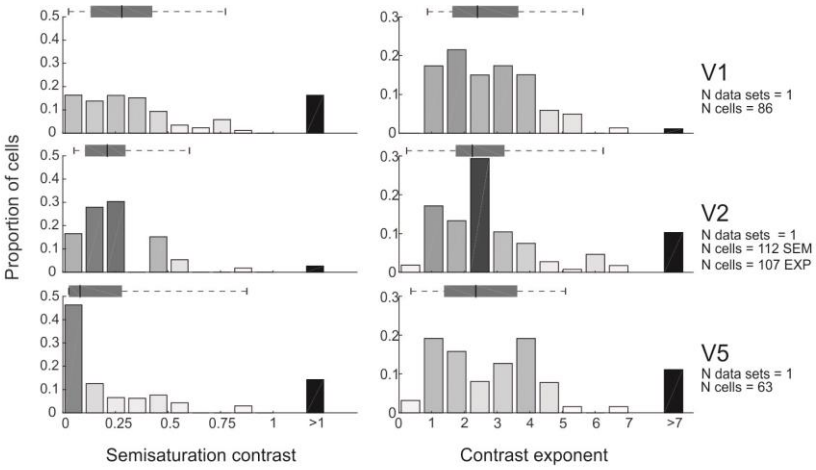


1615

**Figure 14. Semisaturation contrast and contrast exponent of the contrast response function.** Conventions are as in Figure 5. Data for V1 are from (Sclar et al. 1990), for V2 from (Levitt, Kiper, et al. 1994), and for V5 from (Sclar et al. 1990).

1616

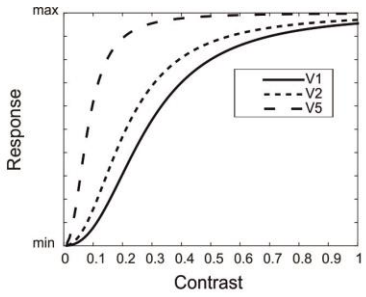


1617

**Figure15. Contrast response function**. Based on the median parameters of the data reported in Figure 14.

1618

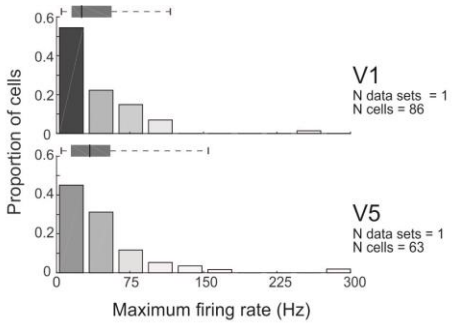


1619

**Figure 16. Maximum firing rate.** Stimuli were sinusoidal gratings at 120 cd/m2 luminance and saturating contrast; the grating orientation, spatial frequency, motion direction and speed were optimized for each cell. Conventions are as in Figure 5. Data for V1 and V5 are from (Sclar et al. 1990).

1620

## Higher-order feature selectivity in V2 and V5

In addition to the low-level feature selectivity, neurons in V2 and V5 become selective to more complex RF features. These higher-order features are related presumably to pattern, object, speed and depth computations in V2 and V5.

About one third of V2 cells are selective for complex gratings or forms (Hegdé and Van Essen 2000). These responses are dependent on anisotropic orientation sensitivity in the classical RF and its surroundings (Ito 2004; Anzai et al. 2007). Most V2 cells (63%) are sensitive to natural texture statistics, i.e. in the higher order correlation of image features across spatial frequencies, orientations and positions. This is in sharp contrast to V1, where only 15% show such selectivity (Freeman et al. 2013). Interestingly, this increased sensitivity in V2 derives from stronger surround suppression from non-natural (gratings, noise) than from natural texture stimuli (Ziemba et al. 2018).

Stereoscopic depth perception is dependent on relative disparity between the retinal images of the two eyes. While V1, V2 and V5 all have cells which are tuned for retinal disparity, only the cells in V2 and V5 contribute to depth perception (Maunsell and Van Essen 1983a; DeAngelis et al. 1998; Nienborg 2006). Another depth cue, motion parallax, arises from self-motion in stationary surroundings. Eighteen percent of V5 cells contribute significantly to behavioral judgments based on motion parallax (Kim et al. 2015).

The V2 cells assign contrast edges to particular object, or code “border ownership”, more often than V1 cells (59% in V2 vs 18% in V1; Zhou et al. 2000). This may be related to emergent segregation of objects from background in V2.

Many V5 cells become more sensitive to motion of a whole pattern than motion of the components of the pattern. Estimates for the proportion of cells which prefer pattern motion in macaque V5 range from 23-25%, whereas such cells are rare in V1 (Movshon

et al. 1985; Wang and Movshon 2016).

## Neuronal membrane physiology

The neuronal membrane physiology has not been systemically studied in macaque visual cortex. Some parameters have been extracted from prefrontal cortex, but given the structural differences of neurons in different areas (Elston 2003; Luebke 2017) it is unclear whether such values are relevant for the visual areas considered in this review, therefore, those data were excluded. In visual cortices, some biophysical parameters are available for V1 L3 pyramidal neurons (Table 6, Amatrudo et al., 2012; Luebke et al., 2015; Gilman et al., 2017). While all neurons have tonic regular spiking patterns, many also show phasic activity. Amatrudo et al. (2012) tuned a model neuron to the structure of a single pyramidal cell providing an example table of biophysical model parameters (their Table 1).

**Table 6.** Biophysical parameters for area V1 L3 pyramidal neurons. Data from Amatrudo et al., 2012; Luebke et al., 2015; Gilman et al., 2017). sEPSC, sIPSC= spontaneous EPSP, IPSP. Mean (range) across studies.

| | |
|---|---|
| **Membrane time constant (ms)** | 23 (19– 28) |
| **Input resistance (Mohm)** | 238 (205– 285) |
| **Resting membrane potential (mV)** | -66 (-66.4 – -65.8) |
| **Action potential threshold (mV)** | -42 (-42.8 – -41.8) |
| **Rheobase (pA)** | 82 (79– 87) |
| **sEPSC freq (Hz)** | 1.4 (1.2 – 1.5) |
| **rise (ms)** | 1.1 (1.0 – 1.2) |
| **decay (ms)** | 4.7 (4.2 – 5.4) |
| **amplitude (pA)** | 6.7 (6.4 – 7.3) |
| **sIPSC_freq (Hz)** | 0.33 |
| **rise (ms)** | 2.8 |
| **decay (ms)** | 7.6 |
| **amplitude (pA)** | 20 |

In V1 L3 pyramidal cells, a depolarizing current step of 80 pA evokes on average (SD) a 14.9 (1.8) Hz response, and a 180 pA current step evokes a 19.6 (2.4) Hz response, clearly higher than in prefrontal cortex (Gilman et al. 2017). This is likely due to the smaller cell size, and thus membrane capacitance, in visual than prefrontal cortex, resulting in more responsive neurons to the same input current.

# The need for future quantitative studies

We have reviewed the literature and summarized quantitative data about the structure and function of, and interactions between macaque visual areas V1, V2 and V5. Although available data are insufficient to support a complete quantitative microcircuit diagram, it, however, allows to construct a binary diagram, including partial data on relative connection strength, which allows to identify dominant and sparse connections in a microcircuit, helping to constrain the parameter search spaces for numerical simulations.

This review omits several areas in the occipital lobe, such as V3, V3A, V6/PO and V4. These areas lack either a unique definition (Angelucci and Rosa 2015; Angelucci et al. 2015; Gamberini et al. 2015; Zhu and Vanduffel 2019), clear homologues between humans and macaques (Kaas 1992; Tootell et al. 1997; Hadjikhani et al. 1998), thus precluding prospective generalization of the model system to humans, or have not been sufficiently studied to justify their inclusion into a quantitative review. The exclusion of these visual areas naturally limits the type of visual analysis that can be expected from a model and may also lead to inaccuracies in the model receptive fields, if the latter are shaped by feedback in the real biological system.

In the early nineties, Felleman and Van Essen (1991) provided a binary diagram of connections between macaque visual cortical areas and studied their mutual hierarchy. The CoCoMac database (Stephan et al. 2001; Kötter 2004; Bakker et al. 2012) later provided online access to interareal anatomical tract tracing data. Later these connections were studied quantitatively, revealing the dense connectome between areas (Barone et al. 2000; Markov et al. 2011; Markov, Ercsey-Ravasz, et al. 2014). The macroscopic scale is however insufficient for model simulations aiming to replicate single neuron function. Instead, we need a model at the microcircuit level.

## Missing parts for a synthetic blueprint

Much information is still missing in order to build a comprehensive model of the macaque visual cortex. First, we need information on which cell types contact which other cell types, making how many synapses, and the probability distribution of synapses along the dendritic tree. Unfortunately, the construction of such a detailed connectome directly from anatomical data is not technically possible, because no current method allows reading and visualizing massive anatomical volumes at synaptic resolution.

Fortunately, partial data samples may allow us to extract statistical rules which could lead to the establishment of a representative connectome and synaptome of a neural system (DeFelipe 2010, 2015). Two studies, both in rat somatosensory cortex, have presented approaches to build a comprehensive model from sparse connectivity data. In the first study, Egger et al. (2014) combined experimental anatomical volumetric data, soma distributions, examples of neuron type specific morphologies (axonal and dendritic fields), relative frequency of neuron types, and subcellular structural connectivity data between cell types. This subcellular connectivity included neuron-type specific density of postsynaptic targets, separately for the soma and apical- and basal dendrites. Using these data, the software calculated dense instantiations of a microcircuit, which were available for numerical simulations (such as Landau et al., 2016). In the second study, Reimann et al. (2015) build microcircuit models based on five types of data. The first defines morphological neuron types, and their local density distributions. Then, they estimate the total length of axons, and the density of boutons on the axons for each type of neuron. For each connection between two neuron types, the approach requires connection probability and the mean and standard deviation of number of synapses per connection. This algorithm was later used to build a comprehensive microcircuit model of rat somatosensory cortex (Markram et al. 2015).

Table 7 lists some of the key data that are still missing for macaque. In the literature there are many anatomical tracing studies of interareal connections. Unfortunately, there are only partial data on the densities of distinct morphological neuron types in different layers for V1 and none for V2 or V5. Moreover, inhibitory cell types have not been quantified by layer, and quantitative data of dendritic length and bouton or synapse numbers on different cell types, and in different layers, are missing.

A recent cluster analysis of V1 L6 neurons provides a sense of the correlations between functional parameters (Hawken et al. 2019). The study reports six major clusters of RF properties, on the basis of simple/complex RFs (f0/f1 modulation;(Skottun et al. 1991), direction selectivity, and temporal frequency tuning. Such cluster analyses for other layers could reveal the inter-parameter correlations, which may significantly limit a model's parameter search space.

In addition, we are missing subcellular data on synaptic connection strengths, although it is likely that the latter are also dynamically adjusted by homeostasis (Turrigiano et al. 1998; van Rossum et al. 2000; Turrigiano 2008). For state-of-the-art Hodgkin-Huxley membrane voltage dynamics, we would, additionally, need information on the relative density of distinct ion channels. For a comprehensive multicompartmental model, the detailed dendritic morphology of distinct cell types would be required in digital format. Some data are available at http://neuromorpho.org/index.jsp mainly for V1 L6 pyramidal and spiny stellate neurons (Briggs et al. 2016) and L3 pyramidal cells (Luebke et al. 2015).

**Table 7.** Missing data for macaque V1, V2, V5 needed for microcircuit reconstruction. PC: pyramidal cell

| Parameter | Missing data |
|---|---|
| **Total N neurons by layer** | V2, V5 |
| **Excitatory cell type counts by layer** | PC subtypes sparse for V1, missing for V2 and V5 |
| **Inhibitory cell type counts by layer** | V1, V2, V5 |
| **Interlaminar cell type specific connectivity** | Partial data for V1, sparse for V2, missing for V5 |
| **Horizontal distribution of local axons** | Partial data for V1, V2 and V5 |
| **Axonal structure, incl. N boutons** | Sparse data for V1, missing for V2 and V5 |
| **Dendritic structure** | Partial data for V1, V2, missing for V5 |
| **Neural membrane electrophysiology** | Sparse data for V1, missing for V2 and V5 |
| **Cell type specific neural structural model** | V1, V2, V5 |

Fortunately, a complete microcircuit connectome is not necessary for simplified model simulations. Simplified models allow avoiding unnecessary complexity for some research questions and increase computational efficiency (Hokkanen et al. 2019). Figure 17 presents two levels of connection detail that can be implemented in a model. If the neural model is point-like, with fixed synaptic dynamics and firing patterns, the required level of description of the system is the identification of pre- and postsynaptic neuron types, the fraction of pre- and postsynaptic neurons contacting each other, the number of synapses per connection, and the amount of divergence and convergence in interareal connectivity (Fig. 17 *top*). However, more detailed and biologically realistic models require additional details on the morphology and firing rate statistics of the presynaptic neuron, as well as synapse location and dynamics of the postsynaptic neurons (Fig. 17 *bottom*).

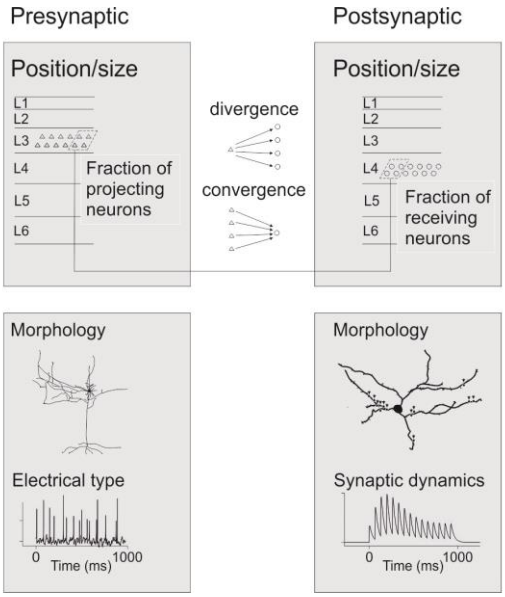


**Figure 17. Describing connections between two neuron groups in silico.** A) A simple point-like phenomenological neural model with fixed synaptic dynamics only needs to incorporate data on position and population size as well as data on the divergence and convergence of connections. B) A more comprehensive, biophysically meaningful, multicompartmental model requires, in addition, data on the cellular morphology, distribution of synapses, and electrical types of neurons and synaptic dynamics.

Studies on anatomical tracer injections targeted to specific CO compartments of V1 or V2, have typically reported the percentages of resulting labeled neurons in each compartment. To calibrate such measures, we need data on the density of projecting fibers/mm$^2$ of cortical surface area for each V2 compartment. For V1, where distinct layers have unique projection patterns, such data should also indicate the amount of projecting fibers/mm$^3$ of cortex. Given the known layer thickness, one would thus be able to estimate the amount of projecting fibers.

## Filling in missing macaque data for numerical simulations

For missing local connectivity data for macaque visual cortex, a theoretician is forced to use available data from other mammalian species, such as cat, rat and mouse, whose

local connections have been studied more extensively (Thomson and Lamy 2007; Markram et al. 2015). In addition, neural cell membrane electrophysiology has been studied more extensively in rodents (Markram et al. 1998; Thomson and Destexhe 1999; Gupta et al. 2000), and there is a clear underrepresentation of monkey data in the neuroinformatics databases, such as NeuroElectro at http://neuroelectro.org/.

Binzegger et al. (2004) collected local structural data for cat primary visual cortex, and suggested a canonical microcircuit diagram based on those data and remaining assumptions. For this diagram one needs essentially three quantities: the number of each neuron type in each layer, each neuron type's average dendritic length in each layer, and the number of synapses formed by each cell type in each layer. Moreover, one needs to assume that synapses form between cell types with equal probability (Peters' rule, Braitenberg and Schuz, 1998). However, many parameters remain uncertain in such a diagram. For example, how synapses are distributed onto the postsynaptic cells' dendritic trees, the short-term synaptic dynamics and potential for long-term plasticity in distinct neuron types, potential local anatomical anisotropies, such as those of patchy local horizontal connections.

Thomson et al (2002) provided local structural network data for rat and cat cortex, together with connection strength measured by dual or triple intracellular electrophysiological recordings in cortical slices. Most differences between species were just scale differences. Thomson et al (2002) reported apparent deviations from Peter's rule, particularly an asymmetry between interlaminar FF (e.g. L4 to 3 and L3 to 5) and FB projections (e.g. from L3 to L4, and from L5 to L3). The excitatory targets of FF connections were primarily the larger pyramidal neurons; the FB targets were horizontally more diffuse than the FF targets, and the FB-induced EPSPs were very small, below threshold. Moreover, FB connections were stronger onto inhibitory than onto excitatory

neurons, the latter being generally very sparse. The authors suggested that this asymmetry prevents reverberating excitation within the local circuit.

Interspecies differences may unfortunately hamper the ability to supplement a monkey model with rodent data (Luebke 2017). For example, the basket cells show lower input resistance and higher firing thresholds in rat compared to monkey, causing them to have lower excitability in rats than monkeys (Povysheva et al. 2008).

Schmidt et al. (2017) estimated the quantitative anatomical connectivity of macaque visual areas by combining CoCoMac databases (Stephan et al. 2001; Bakker et al. 2012) with the fraction of supragranular presynaptic neurons in a source area (Barone et al. 2000; Markov et al. 2011; Markov, Vezoli, et al. 2014) and an exponential distance rule (Ercsey-Ravasz et al. 2013). As local connectivity data from macaque were largely missing, the model of Schmidt et al. (2017) used Potjans and Diesmann's (2014) local microcircuit model, which was based on data from rats and cats. While Schmidt et al. (2017) provided a full graph of connections of macaque visual cortex, as well as explicit tables of the heuristics and assumptions included in their model, our reported anatomical data are different. We provide the details of published experimental data, including the rich substructure and layer-specific connectivity. Although we provide relative rather than absolute connection strengths, and there are uncertainties about the completeness of layer-specific connectivity graphs between two areas, our work goes one step forward compared to existing interareal connectivity graphs (Felleman and Van Essen 1991; Markov, Ercsey-Ravasz, et al. 2014).

In conclusion, here we have collated data from the literature with the goal of facilitating construction of biophysically meaningful models of macaque visual cortex and validation of such models by numerical simulation of neuronal RF properties. In the short run, it will be challenging to establish how the model structure gives rise to RF

properties that resemble those measured in the real cortex, because multiple unknown factors affect RF responses. In the long run, however, a comprehensive model could nevertheless help elucidate the relation between macroscopic activation, local spiking and signal processing in a neural population.

# Funding

This work was supported by Helsinki University Hospital research funds (TYH2016257, Y1249NEUR1) to S.V.; grants from the NIH (R01 EY026812, R01 EY019743, BRAIN U01 NS099702), NSF (IOS 1355075 and 1755431, EAGER 1649923), and University of Utah Neuroscience Initiative, to A.A.; grants from Research to Prevent Blindness, Inc. and a core grant from the NIH (EY014800) to the Department of Ophthalmology, University of Utah.

# Acknowledgments

We thank Vafa Andalibi for technical support and prof Patrizia Fattori and Dr Michela Gamberini for help with physiological data analysis.

# References

Adams MM, Hof PR, Gattass R, Webster MJ, Ungerleider LG. 2000. Visual cortical projections and chemoarchitecture of macaque monkey pulvinar. J Comp Neurol. 419:377–393.

Ahmad A, Spear PD. 1993. Effects of aging on the size, density, and number of rhesus monkey lateral geniculate neurons. J Comp Neurol. 334:631–643.

Ahmed B, Cordery PM, McLelland D, Bair W, Krug K. 2012. Long-range clustered connections within extrastriate visual area V5/MT of the rhesus macaque. Cereb Cortex. 22:60–73.

Albright TD. 1984. Direction and orientation selectivity of neurons in visual area MT of the macaque. J Neurophysiol. 52:1106–1130.

Albright TD, Desimone R. 1987. Local precision of visuotopic organization in the middle temporal area (MT) of the macaque. Exp Brain Res. 65:582–592.

Amatrudo JM, Weaver CM, Crimins JL, Hof PR, Rosene DL, Luebke JI. 2012. Influence of Highly Distinctive Structural Properties on the Excitability of Pyramidal Neurons in Monkey Visual and Prefrontal Cortices. J Neurosci. 32:13644–13660.

Amir Y, Harel M, Malach R. 1993. Cortical hierarchy reflected in the organization of intrinsic connections in macaque monkey visual cortex. J Comp Neurol. 334:19–46.

Amunts K, Malikovic A, Mohlberg H, Schormann T, Zilles K. 2000. Brodmann´s areas 17 and 18 brought into stereotaxic space–where and how variable. Neuroimage. 11:66–84.

Anderson JC, Binzegger T, Martin KAC, Rockland KS. 1998. The connection from cortical area V1 to V5: A light and electron microscopic study. J Neurosci. 18:10525–10540.

Anderson JC, Martin KAC. 2002. Connection From Cortical Area V2 to MT in Macaque

1861 Monkey. J Comp Neurol. 443:56–70.
1862 Anderson JC, Martin KAC. 2009. The Synaptic Connections between Cortical Areas V1
1863 and V2 in Macaque Monkey. J Neurosci. 29:11283–11293.
1864 Anderson JS, Lampl I, Gillespie DC, Ferster D. 2000. The Contribution of Noise to
1865 Contrast Invariance of Orientation Tuning in Cat Visual Cortex. Science. 290:1968–
1866 1972.
1867 Angelucci A, Bijanzadeh M, Nurminen L, Federer F, Merlin S, Bressloff PC. 2017.
1868 Circuits and Mechanisms for Surround Modulation in Visual Cortex. Annu Rev
1869 Neurosci. 40:425–451.
1870 Angelucci A, Bressloff PC. 2006. Contribution of feedforward, lateral and feedback
1871 connections to the classical receptive field center and extra-classical receptive field
1872 surround of primate V1 neurons. Prog Brain Res. 154:93–120.
1873 Angelucci A, Levitt JB, Lund JS. 2002. Anatomical origins of the classical receptive field
1874 and modulatory surround field of single neurons in macaque visual cortical area V1.
1875 Prog Brain Res. 136:373–388.
1876 Angelucci A, Levitt JB, Walton EJ, Hupe JM, Bullier J, Lund JS. 2002. Circuits for local
1877 and global signal integration in primary visual cortex. J Neurosci. 22:8633–8646.
1878 Angelucci A, Roe AW, Sereno MI. 2015. Controversial issues in visual cortex mapping:
1879 Extrastriate cortex between areas V2 and MT in human and nonhuman primates. Vis
1880 Neurosci. 32:e025.
1881 Angelucci A, Rosa MGP. 2015. Resolving the organization of the third tier visual cortex
1882 in primates: A hypothesis-based approach. Vis Neurosci. 32:e010.
1883 Anzai A, Peng X, Van Essen DC. 2007. Neurons in monkey visual area V2 encode
1884 combinations of orientations. Nat Neurosci. 10:1313–1321.
1885 Ascoli GA, Alonso-Nanclares L, Anderson SA, Barrionuevo G, Benavides-Piccione R,

1886 Burkhalter A, Buzsáki G, Cauli B, DeFelipe J, Fairén A, Feldmeyer D, Fishell G,
1887 Fregnac Y, Freund TF, Gardner D, Gardner EP, Goldberg JH, Helmstaedter M,
1888 Hestrin S, Karube F, Kisvárday ZF, Lambolez B, Lewis DA, Marin O, Markram H,
1889 Muñoz A, Packer A, Petersen CCH, Rockland KS, Rossier J, Rudy B, Somogyi P,
1890 Staiger JF, Tamas G, Thomson AM, Toledo-Rodriguez M, Wang Y, West DC, Yuste
1891 R. 2008. Petilla terminology: nomenclature of features of GABAergic interneurons
1892 of the cerebral cortex. Nat Rev Neurosci. 9:557–568.
1893 Bakker R, Wachtler T, Diesmann M. 2012. CoCoMac 2.0 and the future of tract-tracing
1894 databases. Front Neuroinform. 6:Article 30.
1895 Balaram P, Kaas JH. 2014. Towards a unified scheme of cortical lamination for primary
1896 visual cortex across primates: Insights from NeuN and VGLUT2 immunoreactivity.
1897 Front Neuroanat. 8:Article 81.
1898 Balaram P, Young N a, Kaas JH. 2014. Histological features of layers and sublayers in
1899 cortical visual areas V1 and V2 of chimpanzees, macaque monkeys, and humans.
1900 Eye Brain. 6:5–18.
1901 Baldwin MKL, Kaskan PM, Zhang B, Chino YM, Kaas JH. 2012. Cortical and
1902 subcortical connections of V1 and V2 in early postnatal macaque monkeys. J Comp
1903 Neurol. 520:544–569.
1904 Barone P, Batardiere A, Knoblauch K, Kennedy H. 2000. Laminar distribution of neurons
1905 in extrastriate areas projecting to visual areas V1 and V4 correlates with the
1906 hierarchical rank and indicates the operation of a distance rule. J Neurosci. 20:3263–
1907 3281.
1908 Bartfeld E, Grinvald A. 1992. Relationships between orientation-preference pinwheels,
1909 cytochrome oxidase blobs, and ocular-dominance columns in primate striate cortex.
1910 Proc Natl Acad Sci. 89:11905–11909.

1911 Beaulieu C, Kisvarday Z, Somogyi P, Cynader M, Cowey A. 1992. Quantitative
1912 distribution of gaba-immunopositive and -immunonegative neurons and synapses in
1913 the monkey striate cortex (area 17). Cereb Cortex. 2:295–309.
1914 Benevento LA, Rezak M. 1976. The cortical projections of the inferior pulvinar and
1915 adjacent lateral pulvinar in the rhesus monkey (macaca mulatta): An
1916 autoradiographic study. Brain Res. 108:1–24.
1917 Betizeau M, Dehay C, Kennedy H. 2013. Conformity and Specificity of Primate
1918 Corticogenesis. In: Werner JS,, Chalupa LM, editors. The New Visual
1919 Neurosciences. Cambridge, Massachusetts: The MIT Press. p. 1407–1422.
1920 Bijanzadeh M, Nurminen L, Merlin S, Angelucci A. 2018. Distinct Laminar Processing of
1921 Local and Global Context in Primate Primary Visual Cortex. Neuron. 100:259–274.
1922 Binzegger T, Douglas RJ, Martin KA. 2004. A quantitative map of the circuit of cat
1923 primary visual cortex. J Neurosci. 24:8441–8453.
1924 Blasdel GG. 1992. Differential Imaging of Ocular Dominance and Orientation Selectivity
1925 in Monkey Striate Cortex. J Neurosci. 12:3115–3138.
1926 Blasdel GG, Campbell D. 2001. Functional retinotopy of monkey visual cortex. J
1927 Neurosci. 21:8286–8301.
1928 Blasdel GG, Fitzpatrick D. 1984. Physiological organization of layer 4 in macaque striate
1929 cortex. J Neurosci. 4:880–895.
1930 Blasdel GG, Lund JS. 1983. Termination of afferent axons in macaque striate cortex. J
1931 Neurosci. 3:1389–1413.
1932 Blasdel GG, Salama G. 1986. Voltage-sensitive dyes reveal a modular organization in
1933 monkey striate cortex. Nature. 321:579–585.
1934 Born RT, Bradley DC. 2005. Structure and function of visual area MT. Annu Rev
1935 Neurosci. 28:157–189.

1936 Braitenberg V, Braitenberg C. 1979. Geometry of orientation columns in the visual cortex.
1937 Biol Cybern. 33:179–186.
1938 Braitenberg V, Schuz A. 1998. Cortex: Statistics and geometry of Neuronal connectivity.
1939 2nd ed. Berlin: Springer.
1940 Briggs F, Callaway EM. 2001. Layer-specific input to distinct cell types in layer 6 of
1941 monkey primary visual cortex. J Neurosci. 21:3600–3608.
1942 Briggs F, Callaway EM. 2005. Laminar patterns of local excitatory input to layer 5
1943 neurons in Macaque primary visual cortex. Cereb Cortex. 15:479–488.
1944 Briggs F, Kiley CW, Callaway EM, Usrey WM. 2016. Morphological Substrates for
1945 Parallel Streams of Corticogeniculate Feedback Originating in Both V1 and V2 of
1946 the Macaque Monkey. Neuron. 90:388–399.
1947 Briggs F, Usrey WM. 2009. Parallel Processing in the Corticogeniculate Pathway of the
1948 Macaque Monkey. Neuron. 62:135–146.
1949 Brodmann K, Garey LJ. 2006. Brodmann's Localisation in the Cerebral Cortex, Springer.
1950 Bullier J. 2001. Integrated model of visual processing. Brain Res Brain Res Rev. 36:96-
1951 107.
1952 Bullier J, Girard P, Salin P-A. 1994. The role of area 17 in the transfer of visual
1953 information to extrastriate visual cortex. In: Peters A,, Rockland KS, editors.
1954 Cerebral Cortex. New York: Plenum Press. p. 301–330.
1955 Bullier J, Henry GH. 1980. Ordinal position and afferent input of neurons in monkey
1956 striate cortex. J Comp Neurol. 193:913–935.
1957 Bullier J, Hupe JM, James AC, Girard P. 2001. The role of feedback connections in
1958 shaping the responses of visual cortical neurons. Prog Brain Res. 134:193–204.
1959 Bullier J, Kennedy H. 1983. Projection of the Lateral Geniculate Nucleus onto Cortical
1960 Area V2 in the Macaque Monkey. Exp Brain Res. 53:168–172.

1961 Bullier J, Nowak G. 1995. Parallel versus serial processing: new vistas on the distributed
1962 organization of the visual system. Curr Biol. 5:497–503.
1963 Callaway EM. 1998a. Local circuits in primary visual cortex of the macaque monkey.
1964 Annu Rev Neurosci. 21:47–74.
1965 Callaway EM. 1998b. Prenatal development of layer-specific local circuits in primary
1966 visual cortex of the macaque monkey. J Neurosci. 18:1505–1527.
1967 Callaway EM, Wiser AK. 1996. Contributions of individual layer 2-5 spiny neurons to
1968 local circuits in macaque primary visual cortex. Vis Neurosci. 13:907–922.
1969 Caputi A, Melzer S, Michael M, Monyer H. 2013. The long and short of GABAergic
1970 neurons. Curr Opin Neurobiol. 23:179–186.
1971 Carlos L, Silveira L. 2003. Comparative study of primate retina. In: Kaas JH,, Collins CE,
1972 editors. The primate visual system. London: CRC Press. p. 29–51.
1973 Casagrande VA, Kaas JH. 1994. The afferent, intrinsic and efferent connections of
1974 primary visual cortex in primates. In: Peters A,, Rockland KS, editors. Cerebral
1975 Cortex, Volume 10, Primary visual cortex in primates. New York: Plenum Press. p.
1976 201–259.
1977 Casagrande VA, Royal DW. 2004. Parallel visual pathways in a dynamic system. In: Kaas
1978 JH,, Collins CE, editors. The primate visual system. London: CRC Press. p. 1–27.
1979 Casagrande VA, Yazar F, Jones KD, Ding Y. 2007. The morphology of the koniocellular
1980 axon pathway in the macaque monkey. Cereb Cortex. 17:2334–2345.
1981 Cavanaugh JR, Bair W, Movshon JA. 2002. Nature and interaction of signals from the
1982 receptive field center and surround in macaque V1 neurons. J Neurophysiol.
1983 88:2530–2546.
1984 Chariker XL, Shapley R, Young L. 2016. Orientation Selectivity from Very Sparse LGN
1985 Inputs in a Comprehensive Model of Macaque V1 Cortex. J Neurosci. 36:12368–

12384.

Chen G, Lu HD, Roe AW. 2008. A Map for Horizontal Disparity in Monkey V2. Neuron. 58:442–450.

Chung K, Wallace J, Kim SY, Kalyanasundaram S, Andalman AS, Davidson TJ, Mirzabekov JJ, Zalocusky KA, Mattis J, Denisin AK, Pak S, Bernstein H, Ramakrishnan C, Grosenick L, Gradinaru V, Deisseroth K. 2013. Structural and molecular interrogation of intact biological systems. Nature. 497:332–337.

Collins CE. 2011. Variability in neuron densities across the cortical sheet in primates. In: Brain, Behavior and Evolution. p. 37–50.

Connolly M, Van Essen D. 1984. The representation of the visual field in parvicellular and magnocellular layers of the lateral geniculate nucleus in the macaque monkey. J Comp Neurol. 226:544–564.

Daniel PM, Whitteridge D. 1961. The representation of the visual field on the cerebral cortex in monkeys. J Physiol. 159:203–221.

De Valois RL, Albrecht DG, Thorell LG. 1982. Spatial frequency selectivity of cells in macaque visual cortex. Vis Res. 22:545–559.

De Valois RL, Yund EW, Hepler N. 1982. The orientation and direction selectivity of cells in macaque visual cortex. Vis Res. 22:531–544.

DeAngelis GC, Cumming BG, Newsome WT. 1998. Cortical area MT and the perception of stereoscopic depth. Nature. 394:677–680.

DeFelipe J. 2010. From the Connectome to the synaptome: An epic love story. Science. 330:1198–1201.

DeFelipe J. 2011. The Evolution of the Brain, the Human Nature of Cortical Circuits, and Intellectual Creativity. Front Neuroanat. 5:Article 29.

DeFelipe J. 2015. The anatomical problem posed by brain complexity and size: a

2011 potential solution. Front Neuroanat. 9:Article 104.
2012 DeFelipe J, González-Albo MC, Del Río MR, Elston GN. 1999. Distribution and patterns
2013 of connectivity of interneurons containing calbindin, calretinin, and parvalbumin in
2014 visual areas of the occipital and temporal lobes of the macaque monkey. J Comp
2015 Neurol. 412:515–526.
2016 DeFelipe J, López-Cruz PL, Benavides-Piccione R, Bielza C, Larrañaga P, Anderson S,
2017 Burkhalter A, Cauli B, Fairén A, Feldmeyer D, Fishell G, Fitzpatrick D, Freund TF,
2018 González-Burgos G, Hestrin S, Hill S, Hof PR, Huang J, Jones EG, Kawaguchi Y,
2019 Kisvárday Z, Kubota Y, Lewis DA, Marín O, Markram H, McBain CJ, Meyer HS,
2020 Monyer H, Nelson SB, Rockland K, Rossier J, Rubenstein JLR, Rudy B, Scanziani
2021 M, Shepherd GM, Sherwood CC, Staiger JF, Tamás G, Thomson A, Wang Y, Yuste
2022 R, Ascoli GA. 2013. New insights into the classification and nomenclature of
2023 cortical GABAergic interneurons. Nat Rev Neurosci. 14:202–216.
2024 Denk W, Horstmann H. 2004. Serial block-face scanning electron microscopy to
2025 reconstruct three-dimensional tissue nanostructure. PLoS Biol. 2:e329.
2026 Denk W, Strickler JH, Webb WW. 1990. Two-photon laser scanning fluorescence
2027 microscopy. Science. 248:73–76.
2028 Derrington AM, Krauskopf J, Lennie P. 1984. Chromatic mechanisms in lateral geniculate
2029 nucleus of macaque. J Physiol. 357:241–265.
2030 Desimone R, Ungerleider LG. 1986. Multiple visual areas in the caudal superior temporal
2031 sulcus of the macaque. J Comp Neurol. 248:164–189.
2032 Douglas RJ, Martin KAC. 2004. Neuronal Circuits of the Neocortex. Annu Rev Neurosci.
2033 27:419–451.
2034 Dow BM, Snyder AZ, Vautin RG, Bauer R. 1981. Magnification Factor and Receptive
2035 Field Size in Foveal Striate Cortex of the Monkey. Exp Brain Res. 44:213–228.

2036 Egger R, Dercksen VJ, Udvary D, Hege H-C, Oberlaender M. 2014. Generation of dense
2037 statistical connectomes from sparse morphological data. Front Neuroanat. 8:Article
2038 129.
2039 Elston GN. 2003. Cortex, cognition and the cell: new insights into the pyramidal neuron
2040 and prefrontal function. Cereb Cortex. 13:1124–1138.
2041 Elston GN, Fujita I. 2014. Pyramidal cell development: postnatal spinogenesis, dendritic
2042 growth, axon growth, and electrophysiology. Front Neuroanat. 8.
2043 Elston GN, Rosa MGP. 1997. The occipitoparietal pathway of the macaque monkey:
2044 Comparison of pyramidal cell morphology in layer III of functionally related
2045 cortical visual areas. Cereb Cortex. 7:432–452.
2046 Elston GN, Rosa MGP. 1998. Morphological variation of layer III pyramidal neurones in
2047 the occipitotemporal pathway of the macaque monkey visual cortex. Cereb Cortex.
2048 8:278–294.
2049 Ercsey-Ravasz M, Markov NT, Lamy C, Van Essen DC, Knoblauch K, Toroczkai Z,
2050 Kennedy H. 2013. A predictive network model of cerebral cortical connectivity
2051 based on a distance rule. Neuron. 80:184–197.
2052 Erwin E, Obermayer K, Schulten K. 1995. Models of orientation and ocular dominance
2053 columns in the visual cortex: A Critical Comparison. Neural Comput. 7:425–468.
2054 Falchier A, Clavagnier S, Barone P, Kennedy H. 2002. Anatomical evidence of
2055 multimodal integration in primate striate cortex. J Neurosci. 22:5749–5759.
2056 Federer F, Merlin S, Angelucci A. 2015. Anatomical and functional specificity of V2-to-
2057 V1 feedback circuits in the primate visual cortex. In: Soc. Neurosci. Abstr. p.
2058 Online: 699.602.
2059 Federer F, Williams D, Ichida JM, Merlin S, Angelucci A. 2013. Two Projection Streams
2060 from Macaque V1 to the Pale Cytochrome Oxidase Stripes of V2. J Neurosci.

33:11530–11539.

Felleman DJ, Lim H, Xiao Y, Wang Y, Eriksson A, Parajuli A. 2015. The Representation of Orientation in Macaque V2: Four Stripes Not Three. Cereb Cortex. 25:2354–2369.

Felleman DJ, Van Essen DC. 1991. Distributed hierarchical processing in the primate cerebral cortex. Cereb Cortex. 1:1–47.

Fisken RA, Garey LJ, Powell TP. 1975. The intrinsic, association and commissural connections of area 17 on the visual cortex. Philos Trans R Soc L B Biol Sci. 272:487–536.

Fitzpatrick D, Lund JS, Schmechel DE, Towles AC. 1987. Distribution of GABAergic neurons and axon terminals in the macaque striate cortex. J Comp Neurol. 264:73–91.

Franklin MS, Kraemer GW, Shelton SE, Baker E, Kalin NH, Uno H. 2000. Gender differences in brain volume and size of corpus callosum and amygdala of rhesus monkey measured from MRI images. Brain Res. 852:263–267.

Freeman J, Ziemba CM, Heeger DJ, Simoncelli EP, Movshon JA. 2013. A functional and perceptual signature of the second visual area in primates. Nat Neurosci. 16:974–981.

Freund TF, Martin KAC, Soltesz I, Somogyi P, Whitteridge D. 1989. Arborisation pattern and postsynaptic targets of physiologically identified thalamocortical afferents in striate cortex of the macaque monkey. J Comp Neurol. 289:315–336.

Gamberini M, Fattori P, Galletti C. 2015. The medial parietal occipital areas in the macaque monkey. Vis Neurosci. 32:e013.

Garcia-Marin V, Kelly J, Hawken M. 2017. Major Feedforward Thalamic Input Into Layer 4C of Primary Visual Cortex in Primate. Cereb Cortex. 29:134–149.

2086 Garg AK, Li P, Rashid MS, Callaway EM. 2019. Color and orientation are jointly coded
2087 and spatially organized in primate primary visual cortex. Science. 364:1275–1279.
2088 Gattas R, Sousa APB, Mishkin M, Ungerleider LG. 1997. Cortical projections of area V2
2089 in the macaque. Cereb Cortex. 7:110–129.
2090 Gattass R, Gross CG. 1981. Visual topography of striate projection zone (MT) in
2091 posterior superior temporal sulcus of the macaque. J Neurophysiol. 46:621–638.
2092 Gattass R, Nascimento-Silva S, Soares JGM, Lima B, Jansen AK, Diogo ACM, Farias
2093 MF, Botelho MM, EP, Mariani OS, Azzi J, Fiorani M. 2005. Cortical visual areas in
2094 monkeys: location, topography, connections, columns, plasticity and cortical
2095 dynamics. Philos Trans R Soc B Biol Sci. 360:709–731.
2096 Gattass R, Soares JGM, Desimone R, Ungerleider LG. 2014. Connectional subdivision of
2097 the claustrum: two visuotopic subdivisions in the macaque. Front Syst Neurosci.
2098 8:Article 63.
2099 Gegenfurtner KR. 2003. Cortical mechanisms of colour vision. Nat Rev Neurosci. 4:563–
2100 572.
2101 Giannaris EL, Rosene DL. 2012. A stereological study of the numbers of neurons and glia
2102 in the primary visual cortex across the lifespan of male and female rhesus monkeys.
2103 J Comp Neurol. 520:3492–3508.
2104 Gilbert CD. 1983. Microcircuitry of the Visual Cortex. Annu Rev Neurosci. 6:217–247.
2105 Gilman JP, Medalla M, Luebke JI. 2017. Area-Specific Features of Pyramidal Neurons-a
2106 Comparative Study in Mouse and Rhesus Monkey. Cereb Cortex. 27:2078–2094.
2107 Girard P, Hupe JM, Bullier J. 2001. Feedforward and feedback connections between areas
2108 V1 and V2 of the monkey have similar rapid conduction velocities. J Neurophysiol.
2109 85:1328-31.
2110 Goris RLT, Simoncelli EP, Movshon JA. 2015. Origin and Function of Tuning Diversity

in Macaque Visual Cortex. Neuron. 88:819–831.

Grinvald A, Lieke E, Frostig RD, Gilbert CD, Wiesel TN. 1986. Functional architecture of cortex revealed by optical imaging of intrinsic signals. Nature. 324:361–364.

Gupta A, Wang Y, Markram H. 2000. Organizing Principles for a Diversity of GABAergic Interneurons and Synapses in the Neocortex. Science. 287:273–278.

Gur M, Kagan I, Snodderly DM. 2005. Orientation and direction selectivity of neurons in V1 of alert monkeys: Functional relationships and laminar distributions. Cereb Cortex. 15:1207–1221.

Gur M, Snodderly DM. 2006. High response reliability of neurons in primary visual cortex (V1) of alert, trained monkeys. Cereb Cortex. 16:888–895.

Gur M, Snodderly DM. 2007. Direction selectivity in V1 of alert monkeys: Evidence for parallel pathways for motion processing. J Physiol. 585:383–400.

Gur M, Snodderly DM. 2008. Physiological differences between neurons in layer 2 and layer 3 of primary visual cortex (V1) of alert macaque monkeys. J Physiol. 586:2293–2306.

Hadjikhani N, Liu a K, Dale a M, Cavanagh P, Tootell RB. 1998. Retinotopy and color sensitivity in human visual cortical area V8. Nat Neurosci. 1:235–241.

Harris KD, Shepherd GMG. 2015. The neocortical circuit: themes and variations. Nat Neurosci. 18:170–181.

Hassler R. 1966. Comparative anatomy of the central visual system in dayand night-active primates. In: Hassler R,, Stephan H, editors. Evolution of the forebrain. Stuttgart: Thieme. p. 419–434.

Hawken MJ, Shapley RM, Disney AA, Garcia-Marin V, Henrie JA, Henry CA, Johnson EM, Joshi S, Kelly JG, Ringach DL, Xing D. 2019. Functional clusters of neurons in layer 6 of macaque V1. bioRxiv. doi: https://doi.org/10.1101/685990.

2136 Hegdé J, Van Essen DC. 2000. Selectivity for complex shapes in primate visual area V2. J
2137 Neurosci. 20:RC61.
2138 Hegdé J, Van Essen DC. 2003. Strategies of shape representation in macaque visual area
2139 V2. Vis Neurosci. 20:313–328.
2140 Hendrickson AE, Wilson JR, Ogren MP. 1978. The neuroanatomical organization of
2141 pathways between the dorsal lateral geniculate nucleus and visual cortex in Old
2142 World and New World primates. J Comp Neurol. 182:123–136.
2143 Hendry SH, Reid RC. 2000. The koniocellular pathway in primate vision. Annu Rev
2144 Neurosci. 23:127–153.
2145 Hendry SH, Schwark HD, Jones EG, Yan J. 1987. Numbers and proportions of GABA-
2146 immunoreactive neurons in different areas of monkey cerebral cortex. J Neurosci.
2147 7:1503–1519.
2148 Hendry SHC, Yoshioka T. 1994. A neurochemically distinct third channel in the macaque
2149 dorsal lateral geniculate nucleus. Science. 264:575–577.
2150 Hofman MA. 1989. On the evolution and geometry of the brain in mammals. Prog
2151 Neurobiol. 32:137–158.
2152 Hokkanen H, Andalibi V, Vanni S. 2019. Controlling Complexity of Cerebral Cortex
2153 Simulations-II: Streamlined microcircuits. Neural Comput. 31:1066–1084.
2154 Horton JC. 1984. Cytochrome oxidase patches: a new cytoarchitectonic feature of
2155 monkey visual cortex. Philos Trans R Soc Lond B Biol Sci. 304:199–253.
2156 Horton JC, Hocking DR. 1996. Intrinsic variability of ocular dominance column
2157 periodicity in normal macaque monkeys. J Neurosci. 16:7228–7339.
2158 Horton JC, Hubel DH. 1981. Regular patchy distribution of cytochrome oxidase staining
2159 in primary visual cortex of macaque monkey. Nature. 292:762–764.
2160 Hu J, Ma H, Zhu S, Li P, Xu H, Fang Y, Chen M, Han C, Fang C, Cai X, Yan K, Lu HD.

2161 2018. Visual Motion Processing in Macaque V2. Cell Rep. 25:157-167.e5.
2162 Hubel D, Wiesel T. 1968. Receptive fields and functional architecture of monkey striate
2163 cortex. J Physiol. 215–243.
2164 Hubel DH, Freeman DC. 1977. Projection into the visual field of ocular dominance
2165 columns in macaque monkey. Brain Res. 122:336–343.
2166 Hubel DH, Wiesel TN. 1972. Laminar and columnar distribution of geniculo-cortical
2167 fibers in the macaque monkey. J Comp Neurol. 146:421–450.
2168 Hubel DH, Wiesel TN. 1974a. Sequence regularity and geometry of orientation columns
2169 in the monkey striate cortex. J Comp Neurol. 158:267–294.
2170 Hubel DH, Wiesel TN. 1974b. Uniformity of monkey striate cortex: A parallel
2171 relationship between field size, scatter, and magnification factor. J Comp Neurol.
2172 158:295–305.
2173 Hubel DH, Wiesel TN. 1977. Ferrier lecture. Functional architecture of macaque monkey
2174 visual cortex. Proc R Soc London Ser B, Biol Sci. 198:1–59.
2175 Hubener M, Bolz J. 1992. Relationships between Dendritic Morphology and
2176 Cytochrome-Oxidase Compartments in Monkey Striate Cortex. J Comp Neurol.
2177 324:67–80.
2178 Hunter JN, Born RT. 2011. Stimulus-Dependent Modulation of Suppressive Influences in
2179 MT. J Neurosci. 31:678–686.
2180 Hupé J-MM, James AC, Girard P, Bullier J. 2001. Response modulations by static texture
2181 surround in area V1 of the macaque monkey do not depend on feedback connections
2182 from V2. J Neurophysiol. 85:146-63.
2183 Hupé JM, James AC, Payne BR, Lomber SG, Girard P, Bullier J. 1998. Cortical feedback
2184 improves discrimination between figure and background by V1, V2 and V3 neurons.
2185 Nature. 394:784–787.

2186 Ito M. 2004. Representation of Angles Embedded within Contour Stimuli in Area V2 of
2187 Macaque Monkeys. J Neurosci. 24:3313–3324.
2188 Jerison HJ. 1955. Brain to body ratios and the evolution of intelligence. Science.
2189 121:447–449.
2190 Jia H, Rochefort NL, Chen X, Konnerth A. 2010. Dendritic organization of sensory input
2191 to cortical neurons in vivo. Nature. 464:1307–1312.
2192 Jones EG. 1993. Gabaergic neurons and their role in cortical plasticity in primates. Cereb
2193 Cortex. 3:361–372.
2194 Jones EG, Dell'Anna ME, Molinari M, Rausell E, Hashikawa T. 1995. Subdivisions of
2195 macaque monkey auditory cortex revealed by calcium-binding protein
2196 immunoreactivity. J Comp Neurol. 362:153–170.
2197 Kaas JH. 1992. Do humans see what monkeys see? Trends Neurosci. 15:1–3.
2198 Kaas JH. 1995. The evolution of isocortex. Brain Behav Evol. 46:187–196.
2199 Kaas JH. 2003. Early visual areas: V1, V2, V3, DM, DL, and MT. In: Kaas JH,, Collins
2200 CE, editors. The primate visual system. London: CRC Press. p. 139–159.
2201 Kaas JH. 2005. The evolution of visual cortex in primates. In: Kremers J, editor. The
2202 primate visual system. John Wiley & Sons Ltd. p. 267–284.
2203 Katz LC, Gilbert CD, Wiesel TN. 1989. Local circuits and ocular dominance columns in
2204 monkey striate cortex. J Neurosci. 9:1389–1399.
2205 Kelly JG, Hawken MJ. 2017. Quantification of neuronal density across cortical depth
2206 using automated 3D analysis of confocal image stacks. Brain Struct Funct.
2207 222:3333–3353.
2208 Kennedy H, Bullier J. 1985. A double-labeling investigation of the afferent connectivity
2209 to cortical areas V1 and V2 of the macaque monkey. J Neurosci. 5:2815–2830.
2210 Kim HR, Angelaki DE, DeAngelis GC. 2015. A Functional Link between MT Neurons

and Depth Perception Based on Motion Parallax. J Neurosci. 35:2766–2777.

Kisvarday ZF, Cowey A, Smith a D, Somogyi P. 1989. Interlaminar and lateral excitatory amino acid connections in the striate cortex of monkey. J Neurosci. 9:667–682.

Kötter R. 2004. Online Retrieval, Processing, and Visualization of Primate Connectivity Data From the CoCoMac Database. Neuroinformatics. 2:127–144.

Kravitz DJ, Saleem KS, Baker CI, Mishkin M. 2011. A new neural framework for visuospatial processing. Nat Rev Neurosci. 12:217–230.

Kravitz DJ, Saleem KS, Baker CI, Ungerleider LG, Mishkin M. 2013. The ventral visual pathway: An expanded neural framework for the processing of object quality. Trends Cogn Sci. 17:26–49.

Kritzer MF, Cowey a, Somogyi P. 1992. Patterns of inter- and intralaminar GABAergic connections distinguish striate (V1) and extrastriate (V2, V4) visual cortices and their functionally specialized subdivisions in the rhesus monkey. J Neurosci. 12:4545–4564.

Landau ID, Egger R, Dercksen VJ, Oberlaender M, Sompolinsky H. 2016. The Impact of Structural Heterogeneity on Excitation-Inhibition Balance in Cortical Networks. Neuron. 92:1106–1121.

Landisman CEC, Ts'o DY. 2002. Color processing in macaque striate cortex: relationships to ocular dominance, cytochrome oxidase, and orientation. J Neurophysiol. 87:3126–3137.

Large I, Bridge H, Ahmed B, Clare S, Kolasinski J, Lam WW, Miller KL, Dyrby TB, Parker AJ, Smith JET, Daubney G, Sallet J, Bell AH, Krug K. 2016. Individual Differences in the Alignment of Structural and Functional Markers of the V5/MT Complex in Primates. Cereb Cortex. 26:3928–3944.

Larkman AU. 1991. Dendritic morphology of pyramidal neurones of the visual cortex of

2236 the rat: I. Branching patterns. J Comp Neurol. 306:307–319.
2237 Larkum M. 2013. A cellular mechanism for cortical associations: An organizing principle
2238 for the cerebral cortex. Trends Neurosci. 36:141–151.
2239 Larkum ME, Senn W, Lüscher HR. 2004. Top-down dendritic input increases the gain of
2240 layer 5 pyramidal neurons. Cereb Cortex. 14:1059–1070.
2241 le Gros Clark WE. 1941. The laminar organization and cell content of the lateral
2242 geniculate body in the monkey. J Anat. 75:419–433.
2243 Lee SH, Hjerling-Leffler J, Zagha E, Fishell G, Rudy B. 2010. The largest group of
2244 superficial neocortical GABAergic interneurons expresses ionotropic serotonin
2245 receptors. J Neurosci. 30:16796–16808.
2246 Lee WCA, Bonin V, Reed M, Graham BJ, Hood G, Glattfelder K, Reid RC. 2016.
2247 Anatomy and function of an excitatory network in the visual cortex. Nature.
2248 532:370–374.
2249 Lennie P, Movshon JA. 2005. Coding of color and form in the geniculostriate visual
2250 pathway (invited review). J Opt Soc Am A Opt Image Sci Vis. 22:2013–2033.
2251 LeVay S, Hubel D, Wiesel T. 1975. The Pattern of Ocular Dominance Columns in
2252 Macaque Visual Cortex Revealed by a Reduced Silver Stain. J Comp Neurol.
2253 159:559–576.
2254 Levitt JB, Kiper DC, Movshon JA. 1994. Receptive-Fields and Functional Architecture of
2255 Macaque V2. J Neurophysiol. 71:2517–2542.
2256 Levitt JB, Lund JS, Yoshioka T. 1996. Anatomical substrates for early stages in cortical
2257 processing of visual information in the macaque monkey. Behav Brain Res. 76:5–
2258 19.
2259 Levitt JB, Yoshioka T, Lund JS. 1994. Intrinsic cortical connections in macaque visual
2260 area V2: evidence for interaction between different functional streams. J Comp

Neurol. 342:551–570.

Li H, Fukuda M, Tanifuji M, Rockland KS. 2003. Intrinsic collaterals of layer 6 Meynert cells and functional columns in primate V1. Neuroscience. 120:1061–1069.

Li WH. 2015. A fast and flexible computer vision system for implanted visual prostheses. In: Lecture Notes in Computer Science. p. 686–701.

Livingstone M, Hubel D. 1988a. Segregation of form, color, movement and depth: anatomy, physiology and perception. Science. 240:740–749.

Livingstone MS, Hubel DH. 1984a. Anatomy and physiology of a color system in the primate visual cortex. J Neurosci. 4:309–356.

Livingstone MS, Hubel DH. 1984b. Specificity of intrinsic connections in primate primary visual cortex. J Neurosci. 4:2830–2835.

Livingstone MS, Hubel DH. 1988b. Do the relative mapping densities of the magno- and parvocellular systems vary with eccentricity? J Neurosci. 8:4334–4339.

Lu HD, Chen G, Tanigawa H, Roe AW. 2010. A Motion Direction Map in Macaque V2. Neuron. 68:1002–1013.

Lu HD, Roe AW. 2008. Functional organization of color domains in V1 and V2 of Macaque monkey revealed by optical imaging. Cereb Cortex. 18:516–533.

Luebke JI. 2017. Pyramidal Neurons Are Not Generalizable Building Blocks of Cortical Networks. Front Neuroanat. 11:Article 11.

Luebke JI, Medalla M, Amatrudo JM, Weaver CM, Crimins JL, Hunt B, Hof PR, Peters A. 2015. Age-related changes to layer 3 pyramidal cells in the rhesus monkey visual cortex. Cereb Cortex. 25:1454–1468.

Lund JS. 1973. Organization of neurons in the visual cortex, area 17, of the monkey (Macaca mulatta). J Comp Neurol. 147:455–495.

Lund JS. 1987. Local circuit neurons of macaque monkey striate cortex: I. Neurons of

laminae 4C and 5A. J Comp Neurol. 257:60–92.

Lund JS. 1988. Anatomical Organization of Macaque Monkey Striate Visual Cortex. Annu Rev Neurosci. 11:253–288.

Lund JS, Angelucci A, Bressloff PC. 2003. Anatomical substrates for functional columns in macaque monkey primary visual cortex. Cereb Cortex. 13:15–24.

Lund JS, Boothe RG. 1975. lnterlaminar Connections and Pyramidal Neuron Organisation in the Visual Cortex, Area 17, of the Macaque Monkey. J Comp Neurol. 159:305–334.

Lund JS, Griffiths S, Rumberger A, Levitt JB. 2001. Inhibitory Synapse Cover on the Somata of Excitatory Neurons in Macaque Monkey Visual Cortex. Cereb Cortex. 11:783–795.

Lund JS, Hawken MJ, Parker AJ. 1988. Local circuit neurons of macaque monkey striate cortex: II. Neurons of laminae 5B and 6. J Comp Neurol. 276:1–29.

Lund JS, Hendrickson AE, Ogren MP, Tobin EA. 1981. Anatomical organization of primate visual cortex area VII. J Comp Neurol. 202:19–45.

Lund JS, Lund RD, Hendrickson AE, Bunt AH, Fuchs AF. 1975. The origin of efferent pathways from the primary visual cortex, area 17, of the macaque monkey as shown by retrograde transport of horseradish peroxidase. J Comp Neurol. 164:287–303.

Lund JS, Wu CQ. 1997. Local circuit neurons of macaque monkey striate cortex: IV. Neurons of laminae 1-3a. J Comp Neurol. 384:109–126.

Lund JS, Yoshioka T. 1991. Local circuit neurons of macaque monkey striate cortex: III. Neurons of laminae 4B, 4A, and 3B. J Comp Neurol. 311:234–258.

Lund JS, Yoshioka T, Levitt JB. 1993. Comparison of intrinsic connectivity in different areas of macaque monkey cerebral cortex. Cereb Cortex. 3:148–162.

Lund JS, Yoshioka T, Levitt JB. 1994. Substrates for interlaminar connections in area V1

of macaque monkey cerebral cortex. In: Peters A,, Rockland KS, editors. Cerebral Cortex, Volume 10, Primary visual cortex in primates. New York: Plenum Press. p. 37–60.

Luo L, Callaway EM, Svoboda K. 2008. Genetic Dissection of Neural Circuits. Neuron. 57:634–660.

Mainen Z, Sejnowski T. 1995. Reliability of spike timing in neocortical neurons. Science. 268:1503–1506.

Malach R, Amir Y, Harel M, Grinvald A. 1993. Relationship between intrinsic connections and functional architecture revealed by optical imaging and in vivo targeted biocytin injections in primate striate cortex. Proc Natl Acad Sci. 90:10469–10473.

Malpeli JG, Lee D, Baker FH. 1996. Laminar and retinotopic organization of the macaque lateral geniculate nucleus: Magnocellular and parvocellular magnification functions. J Comp Neurol. 375:363–377.

Mansfield RJW. 1973. Latency functions in human vision. Vision Res. 13:2219–2234.

Marino L. 1998. A comparison of encephalization between odontocete cetaceans and anthropoid primates. Brain Behav Evol. 51:230–238.

Markov NT, Ercsey-Ravasz M, Ribeiro Gomes AR, Lamy C, Magrou L, Vezoli J, Misery P, Falchier A, Quilodran R, Gariel MA, Sallet J, Gamanut R, Huissoud C, Clavagnier S, Giroud P, Sappey-Marinier D, Barone P, Dehay C, Toroczkai Z, Knoblauch K, Van Essen DC, Kennedy H. 2014. A weighted and directed interareal connectivity matrix for macaque cerebral cortex. Cereb Cortex. 24:17–36.

Markov NT, Ercsey-Ravasz M, Van Essen DC, Knoblauch K, Toroczkai Z, Kennedy H. 2013. Cortical high-density counterstream architectures. Science. 342:1238406.

Markov NT, Misery P, Falchier A, Lamy C, Vezoli J, Quilodran R, Gariel MA, Giroud P,

Ercsey-Ravasz M, Pilaz LJ, Huissoud C, Barone P, Dehay C, Toroczkai Z, Van Essen DC, Kennedy H, Knoblauch K. 2011. Weight consistency specifies regularities of macaque cortical networks. Cereb Cortex. 21:1254–1272.

Markov NT, Vezoli J, Chameau P, Falchier A, Quilodran R, Huissoud C, Lamy C, Misery P, Giroud P, Ullman S, Barone P, Dehay C, Knoblauch K, Kennedy H. 2014. Anatomy of hierarchy: feedforward and feedback pathways in macaque visual cortex. J Comp Neurol. 522:225–259.

Markram H, Muller E, Ramaswamy S, Reimann MW, Abdellah M, Sanchez CA, Ailamaki A, Alonso-Nanclares L, Antille N, Arsever S, Kahou GA, Berger TK, Bilgili A, Buncic N, Chalimourda A, Chindemi G, Courcol JD, Delalondre F, Delattre V, Druckmann S, Dumusc R, Dynes J, Eilemann S, Gal E, Gevaert ME, Ghobril JP, Gidon A, Graham JW, Gupta A, Haenel V, Hay E, Heinis T, Hernando JB, Hines M, Kanari L, Keller D, Kenyon J, Khazen G, Kim Y, King JG, Kisvarday Z, Kumbhar P, Lasserre S, Le Be J V, Magalhaes BR, Merchan-Perez A, Meystre J, Morrice BR, Muller J, Munoz-Cespedes A, Muralidhar S, Muthurasa K, Nachbaur D, Newton TH, Nolte M, Ovcharenko A, Palacios J, Pastor L, Perin R, Ranjan R, Riachi I, Rodriguez JR, Riquelme JL, Rossert C, Sfyrakis K, Shi Y, Shillcock JC, Silberberg G, Silva R, Tauheed F, Telefont M, Toledo-Rodriguez M, Trankler T, Van Geit W, Diaz J V, Walker R, Wang Y, Zaninetta SM, DeFelipe J, Hill SL, Segev I, Schurmann F. 2015. Reconstruction and Simulation of Neocortical Microcircuitry. Cell. 163:456–492.

Markram H, Toledo-Rodriguez M, Wang Y, Gupta A, Silberberg G, Wu C. 2004. Interneurons of the neocortical inhibitory system. Nat Rev Neurosci. 5:793–807.

Markram H, Wang Y, Tsodyks M. 1998. Differential signaling via the same axon of neocortical pyramidal neurons. Proc Natl Acad Sci U S A. 95:5323-8.

2361 Mates SL, Lund JS. 1983. Neuronal composition and development in lamina 4C of
2362 monkey striate cortex. J Comp Neurol. 221:60–90.
2363 Maunsell JH, Gibson JR. 1992. Visual response latencies in striate cortex of the macaque
2364 monkey. J Neurophysiol. 68:1332–1344.
2365 Maunsell JH, Van Essen DC. 1983a. Functional properties of neurons in middle temporal
2366 visual area of the macaque monkey. II. Binocular interactions and sensitivity to
2367 binocular disparity. J Neurophysiol. 49:1148–1167.
2368 Maunsell JHR, van Essen DC. 1987. Topographic organization of the middle temporal
2369 visual area in the macaque monkey: Representational biases and the relationship to
2370 callosal connections and myeloarchitectonic boundaries. J Comp Neurol. 266:535–
2371 555.
2372 Maunsell JHR, Van Essen DC. 1983b. The connections of the middle temporal visual area
2373 (MT) and their relationship to a cortical hierarchy in the macaque monkey. J
2374 Neurosci. 3:2563–2586.
2375 Maunsell JHR, Van Essen DC. 1987. The topographic organization of the middle
2376 temporal visual area in the macaque monkey and its relationship to callosal
2377 connections. J Comp Neurol. 266:535–555.
2378 McFarland JM, Cumming BG, Butts DA. 2016. Variability and Correlations in Primary
2379 Visual Cortical Neurons Driven by Fixational Eye Movements. J Neurosci.
2380 36:6225–6241.
2381 McGuire BA, Gilbert CD, Rivlin PK, Wiesel TN. 1991. Targets of horizontal connections
2382 in macaque primary visual cortex. J Comp Neurol. 305:370–392.
2383 Medalla M, Luebke JI. 2015. Diversity of Glutamatergic Synaptic Strength in Lateral
2384 Prefrontal versus Primary Visual Cortices in the Rhesus Monkey. J Neurosci.
2385 35:112–127.

2386 Mejias JF, Murray JD, Kennedy H, Wang X-J. 2016. Feedforward and feedback
2387 frequency-dependent interactions in a large-scale laminar network of the primate
2388 cortex. Sci Adv. 2:e1601335.
2389 Merigan WH, Maunsell JHR. 1993. How Parallel are the Primate Visual Pathways? Annu
2390 Rev Neurosci. 16:369–402.
2391 Merlin S, Ichida J, Federer F, Schiessl I, Angelucci A. 2012. Systematic relationship
2392 between cytochrome oxidase (CO) blobs, orientation singularities and dendritic
2393 spines in macaque V1. In: Soc. Neurosci. Abstr. Online. p. 568.02.
2394 Miller KD, Troyer TW. 2002. Neural noise can explain expansive, power-law
2395 nonlinearities in neural response functions. J Neurophysiol. 87:653–659.
2396 Montero VM, Zempel J. 1986. The proportion and size of GABA-immunoreactive
2397 neurons in the magnocellular and parvocellular layers of the lateral geniculate
2398 nucleus of the rhesus monkey. Exp Brain Res. 62:215–223.
2399 Mortazavi F, Stankiewicz A, Zhdanova I. 2019. Looking through Brains with Fast Passive
2400 CLARITY: Zebrafish, Rodents, Non-human Primates and Humans. BIO-
2401 PROTOCOL. 9:e3321.
2402 Movshon JA, Adelson EH, Gizzi MS, Newsome WT. 1985. The Analysis of Moving
2403 Visual Patterns. In: Chagas C,, Gattas R,, Gross CG, editors. Pattern Recognition
2404 Mechanisms. Rome: Vatican Press. p. 119–151.
2405 Munk MH, Nowak LG, Girard P, Chounlamountri N, Bullier J. 1995. Visual latencies in
2406 cytochrome oxidase bands of macaque area V2. Proc Natl Acad Sci. 92:988–992.
2407 Nassi JJ, Callaway EM. 2006. Multiple Circuits Relaying Primate Parallel Visual
2408 Pathways to the Middle Temporal Area. J Neurosci. 26:12789–12798.
2409 Nassi JJ, Callaway EM. 2007. Specialized Circuits from Primary Visual Cortex to V2 and
2410 Area MT. Neuron. 55:799–808.

2411 Nassi JJ, Callaway EM. 2009. Parallel processing strategies of the primate visual system.
2412 Nat Rev Neurosci. 10:360–372.
2413 Nassi JJ, Lomber SG, Born RT. 2013. Corticocortical Feedback Contributes to Surround
2414 Suppression in V1 of the Alert Primate. J Neurosci. 33:8504–8517.
2415 Nauhaus I, Benucci A, Carandini M, Ringach DL. 2008. Neuronal Selectivity and Local
2416 Map Structure in Visual Cortex. Neuron. 57:673–679.
2417 Nauhaus I, Nielsen KJ, Disney AA, Callaway EM. 2012. Orthogonal micro-organization
2418 of orientation and spatial frequency in primate primary visual cortex. Nat Neurosci.
2419 15:1683–1690.
2420 Nealey TA, Maunsell JH. 1994. Magnocellular and parvocellular contributions to the
2421 responses of neurons in macaque striate cortex. J Neurosci. 14:2069–79.
2422 Nhan HL, Callaway EM. 2012. Morphology of superior colliculus- and middle temporal
2423 area-projecting neurons in primate primary visual cortex. J Comp Neurol. 520:52–
2424 80.
2425 Nienborg H. 2006. Macaque V2 Neurons, But Not V1 Neurons, Show Choice-Related
2426 Activity. J Neurosci. 26:9567–9578.
2427 Nieuwenhuys R. 1994. The neocortex. An overview of its evolutionary development,
2428 structural organization and synaptology. Anat Embryol. 190:307–337.
2429 Nowak LG, Bullier J. 1997. The timing of information transfer in the visual system. In:
2430 Rockland KS,, Kaas JH,, Peters A, editors. Cerebral Cortex. London: Plenum Press.
2431 p. 205–241.
2432 Nowak LG, Munk MH, Girard P, Bullier J. 1995. Visual latencies in areas V1 and V2 of
2433 the macaque monkey. Vis Neurosci. 12:371–384.
2434 Nurminen L, Merlin S, Bijanzadeh M, Federer F, Angelucci A. 2018. Top-down feedback
2435 controls spatial summation and response amplitude in primate visual cortex. Nat

2436 Commun. 9:Article number 2281.
2437 O'Kusky J, Colonnier M. 1982a. Postnatal changes in the number of neurons and
2438 synapses in the visual cortex (area 17) of the macaque monkey: A stereological
2439 analysis in normal and monocularly deprived animals. J Comp Neurol. 210:291–
2440 306.
2441 O'Kusky J, Colonnier M. 1982b. A laminar analysis of the number of neurons, glia, and
2442 synapses in the visual cortex (area 17) of adult Macaque monkeys. J Comp Neurol.
2443 210:278–290.
2444 Obermayer K, Blasdel GG. 1993. Geometry of orientation and ocular dominance columns
2445 in monkey striate cortex. J Neurosci. 13:4114–4129.
2446 Oga T, Elston GN, Fujita I. 2017. Postnatal dendritic growth and spinogenesis of layer-V
2447 pyramidal cells differ between visual, inferotemporal, and prefrontal cortex of the
2448 macaque monkey. Front Neurosci. 11:Article 118.
2449 Oga T, Okamoto T, Fujita I. 2016. Basal Dendrites of Layer-III Pyramidal Neurons do not
2450 Scale with Changes in Cortical Magnification Factor in Macaque Primary Visual
2451 Cortex. Front Neural Circuits. 10:Article 74.
2452 Olavarria JF, Van Essen DC. 1997. The global pattern of cytochrome oxidase stripes in
2453 visual area V2 of the macaque monkey. Cereb Cortex. 7:395–404.
2454 Pack CC, Hunter NJ, Born RT. 2005. Contrast Dependence of Suppressive Influences in
2455 Cortical Area MT of Alert Macaque. J Neurophysiol. 93:1809–1815.
2456 Palmer CR, Chen Y, Seidemann E. 2012. Uniform spatial spread of population activity in
2457 primate parafoveal V1. J Neurophysiol. 107:1857–1867.
2458 Perkel DJ, Bullier J, Kennedy H. 1986. Topography of the afferent connectivity of area 17
2459 in the macaque monkey: A double-labelling study. J Comp Neurol. 253:374–402.
2460 Peters A, Payne BR, Budd J. 1994. A numerical analysis of the geniculocortical input to

striate cortex in the monkey. Cereb Cortex. 4:215–229.

Peters A, Sethares C. 1991a. Layer IVA of rhesus monkey primary visual cortex. Cereb Cortex. 1:445–462.

Peters A, Sethares C. 1991b. Organization of pyramidal neurons in area 17 of monkey visual cortex. J Comp Neurol. 306:1–23.

Petruzza S, Venkat A, Gyulassy A, Scorzelli G, Federer F, Angelucci A, Pascucci V, Bremer PT. 2017. ISAVS: Interactive scalable analysis and visualization system. In: SIGGRAPH ASIA 2017.

Petruzza S, Venkat A, Gyulassy A, Scorzelli G, Federer F, Angelucci A, Pascucci V, Bremer PT. 2018. Scaling big data neuroscience: From interactive analytics to HPC platforms. Adv Parallel Comput. 33:53–68.

Polimeni JR, Balasubramanian M, Schwartz EL. 2006. Multi-area visuotopic map complexes in macaque striate and extra-striate cortex. Vision Res. 46:3336–3359.

Polimeni JR, Granquist-Fraser D, Wood RJ, Schwartz EL. 2005. Physical limits to spatial resolution of optical recording: Clarifying the spatial structure of cortical hypercolumns. Proc Natl Acad Sci U S A. 102:4158–4163.

Potjans TC, Diesmann M. 2014. The cell-type specific cortical microcircuit: Relating structure and activity in a full-scale spiking network model. Cereb Cortex. 24:785–806.

Povysheva N V, Zaitsev A V, Rotaru DC, Gonzalez-Burgos G, Lewis DA, Krimer LS. 2008. Parvalbumin-positive basket interneurons in monkey and rat prefrontal cortex. J Neurophysiol. 100:2348–2360.

Preuss TM. 2004. Specializations of the human visual system: The monkey model meets the human reality. In: Kaas JH,, Collins CE, editors. The primate visual system. London: CRC Press. p. 231–259.

2486 Rall W. 1962. Theory of physiological properties of dendrites. Ann N Y Acad Sci.
2487 96:1071–1092.
2488 Ramsden BM, Hung CP, Roe AW. 2014. Orientation domain diversity in macaque area
2489 V2. Eye Brain. 6:97–112.
2490 Rasch MJ, Schuch K, Logothetis NK, Maass W. 2011. Statistical Comparison of Spike
2491 Responses to Natural Stimuli in Monkey Area V1 With Simulated Responses of a
2492 Detailed Laminar Network Model for a Patch of V1. J Neurophysiol. 105:757–778.
2493 Reimann MW, King JG, Muller EB, Ramaswamy S, Markram H. 2015. An algorithm to
2494 predict the connectome of neural microcircuits. Front Comput Neurosci. 9:Article
2495 120.
2496 Ringach DL, Shapley RM, Hawken MJ. 2002. Orientation selectivity in macaque V1:
2497 diversity and laminar dependence. J Neurosci. 22:5639–5651.
2498 Rockland KS. 1985. A reticular pattern of intrinsic connections in primate area V2 (area
2499 18). J Comp Neurol. 235:467–478.
2500 Rockland KS. 1989. Bistratified Distribution Of Terminal Arbors Of Individual Axons
2501 Projecting From Area V1 To Middle Temporal Area (MT) In The Macaque Monkey.
2502 Vis Neurosci. 3:155–170.
2503 Rockland KS. 1994. The organization of feedback connections from area V2 (18) to V1
2504 (17). In: Peters A,, Rockland KS, editors. Cerebral Cortex, Volume 10, Primary
2505 visual cortex in primates. New York: Plenum Press. p. 261–299.
2506 Rockland KS. 1995. Morphology of individual axons projecting from area V2 to MT in
2507 the macaque. J Comp Neurol. 355:15–26.
2508 Rockland KS. 1997. Elements of cortical architecture: Hierarchy revisited. In: Rockland
2509 KS,, Kaas JH,, Peters A, editors. Cerebral Cortex Volume 12: Extrastriate cortex in
2510 primates. London: Plenum Press. p. 243–293.

2511 Rockland KS, Lund JS. 1983. Intrinsic laminar lattice connections in primate visual
2512 cortex. J Comp Neurol. 216:303–318.
2513 Rockland KS, Ojima H. 2003. Multisensory convergence in calcarine visual areas in
2514 macaque monkey. Int J Psychophysiol. 50:19–26.
2515 Rockland KS, Pandya DN. 1979. Laminar origins and terminations of cortical
2516 connections of the occipital lobe in the rhesus monkey. Brain Res. 179:3–20.
2517 Rockland KS, Virga A. 1989. Terminal arbors of individual “Feedback” axons projecting
2518 from area V2 to V1 in the macaque monkey: A study using immunohistochemistry
2519 of anterogradely transported Phaseolus vulgaris-leucoagglutinin. J Comp Neurol.
2520 285:54–72.
2521 Rockland KS, Virga A. 1990. Organization of Individual Cortical Axons Projecting From
2522 Area VI (area 17) to V2 (area 18) In The Macaque Monkey. Vis Neurosci. 4:11–28.
2523 Roe AW. 2004. Modular complexity of area V2 in the macaque monkey. In: Kaas JH,,
2524 Collins CE, editors. The primate visual system. London: CRC Press. p. 109–138.
2525 Roe AW, Lu HD, Hung CP. 2005. Cortical processing of a brightness illusion. Proc Natl
2526 Acad Sci. 102:3869–3874.
2527 Roe W, Ts’o DY. 1995. Visual Topography in Primate V2: Multiple Representation across
2528 Functional Stripes. J Neurosci. 15:3689–3715.
2529 Rosa MGP, Tweedale R. 2005. Brain maps, great and small: Lessons from comparative
2530 studies of primate visual cortical organization. Philos Trans R Soc B Biol Sci.
2531 360:665–691.
2532 Rudy B, Fishell G, Lee S, Hjerling-Leffler J. 2011. Three groups of interneurons account
2533 for nearly 100% of neocortical GABAergic neurons. Dev Neurobiol. 71:45–61.
2534 Saleem KS, Price JL, Hashikawa T. 2007. Cytoarchitectonic and chemoarchitectonic
2535 subdivisions of the perirhinal and parahippocampal cortices in macaque monkeys. J

Comp Neurol. 500:973–1006.

Sawatari A, Callaway EM. 2000. Diversity and cell type specificity of local excitatory connections to neurons in layer 3B of monkey primary visual cortex. Neuron. 25:459–471.

Sceniak MP, Ringach DL, Hawken MJ, Shapley R. 1999. Contrast's effect on spatial summation by macaque V1 neurons. Nat Neurosci. 2:733–739.

Schein SJ, de Monasterio FM. 1987. Mapping of retinal and geniculate neurons onto striate cortex of macaque. J Neurosci. 7:996–1009.

Schiller PH, Finlay BL, Volman SF. 1976. Quantitative studies of single-cell properties in monkey striate cortex. I. Spatiotemporal organization of receptive fields. J Neurophysiol. 39:1288–1319.

Schmidt M, Bakker R, Hilgetag CC, Diesmann M, van Albada SJ. 2018. Multi-scale account of the network structure of macaque visual cortex. Brain Struct Funct. 223:1409–1435.

Schmolesky MT, Wang Y, Hanes D, Thompson KG, Leutgeb S, Schall JD, Leventhal AG. 1998. Signal timing across macaque visual system. J Neurophysiol. 79:3272–3278.

Schwabe L, Obermayer K, Angelucci A, Bressloff PC. 2006. The role of feedback in shaping the extra-classical receptive field of cortical neurons: a recurrent network model. J Neurosci. 26:9117–9129.

Schwartz EL. 1980. Computational anatomy and functional architecture of striate cortex: A spatial mapping approach to perceptual coding. Vision Res. 20:645–669.

Schwartz EL. 1994. Computational studies of the spatial architecture of primate visual cortex. In: Peters A,, Rockland KS, editors. Cerebral Cortex, Volume 10, Primary visual cortex in primates. New York: Plenum Press. p. 359–411.

Sclar G, Maunsell JHR, Lennie P. 1990. Coding of image contrast in central visual

2561 pathways of the macaque monkey. Vision Res. 30:1–10.
2562 Self MW, van Kerkoerle T, Supèr H, Roelfsema PR. 2013. Distinct roles of the cortical
2563 layers of area V1 in figure-ground segregation. Curr Biol. 23:2121–2129.
2564 Shepherd GMG. 2013. Corticostriatal connectivity and its role in disease. Nat Rev
2565 Neurosci. 14:278–291.
2566 Shipp S. 2007. Structure and function of the cerebral cortex. Curr Biol. 17:R443–R449.
2567 Shipp S, Adams DL, Moutoussis K, Zeki S. 2009. Feature binding in the feedback layers
2568 of area V2. Cereb Cortex. 19:2230–2239.
2569 Shipp S, Zeki S. 2002a. The functional organization of area V2, I: specialization across
2570 stripes and layers. Vis Neurosci. 19:187–210.
2571 Shipp S, Zeki S. 2002b. The functional organization of area V2, II: The impact of stripes
2572 on visual topography. Vis Neurosci. 19:211–231.
2573 Shipp S, Zeki S, Shipp S. 1989. The organization of connections between areas V5 and
2574 V2 in macaque monkey visual cortex. Eur J Neurosci. 1:309–332.
2575 Shushruth S, Ichida JM, Levitt JB, Angelucci A. 2009. Comparison of spatial summation
2576 properties of neurons in macaque V1 and V2. J Neurophysiol. 102:2069–2083.
2577 Sincich LC, Adams DL, Horton JC. 2003. Complete flatmounting of the macaque
2578 cerebral cortex. Vis Neurosci. 20:663–686.
2579 Sincich LC, Horton JC. 2002. Divided by cytochrome oxidase: A map of the projections
2580 from V1 to V2 in macaques. Science. 295:1734–1737.
2581 Sincich LC, Horton JC. 2003. Independent projection streams from macaque striate
2582 cortex to the second visual area and middle temporal area. J Neurosci. 23:5684–
2583 5692.
2584 Sincich LC, Horton JC. 2005. The Circuitry of V1 and V2: Integration of Color, Form,
2585 and Motion. Annu Rev Neurosci. 28:303–326.

2586 Sincich LC, Park KF, Wohlgemuth MJ, Horton JC. 2004. Bypassing V1: a direct
2587 geniculate input to area MT. Nat Neurosci. 7:1123–1128.
2588 Skottun BC, De Valois RL, Grosof DH, Movshon JA, Albrecht DG, Bonds AB. 1991.
2589 Classifying simple and complex cells on the basis of response modulation. Vision
2590 Res. 31:1079–1086.
2591 Snodderly DM, Gur M. 1995. Organization of striate cortex of alert, trained monkeys
2592 (Macaca fascicularis): ongoing activity, stimulus selectivity, and widths of receptive
2593 field activating regions. J Neurophysiol. 74:2100–2125.
2594 Spear PD, Moore RJ, Kim CB, Xue JT, Tumosa N. 1994. Effects of aging on the primate
2595 visual system: spatial and temporal processing by lateral geniculate neurons in
2596 young adult and old rhesus monkeys. J Neurophysiol. 72:402–420.
2597 Stelzer EHK. 2015. Light-sheet fluorescence microscopy for quantitative biology. Nat
2598 Methods. 12:23–26.
2599 Stephan KE, Kamper L, Bozkurt A, Burns GAPC, Young MP, Kotter R. 2001. Advanced
2600 database methodology for the Collation of Connectivity data on the Macaque brain
2601 (CoCoMac). Philos Trans R Soc B Biol Sci. 356:1159–1186.
2602 Ta'afua SF, Federer F, Merlin S, Angelucci A. 2018. Parallel feedback pathways between
2603 macaque visual areas V2 and V1. In: Soc. Neurosci. Abstr. Online. p. 219.20.
2604 Tamamaki N, Tomioka R. 2010. Long-range GABAergic connections distributed
2605 throughout the neocortex and their possible function. Front Neurosci. 4:Article 202.
2606 Tanigawa H, Wang Q, Fujita I. 2005. Organization of horizontal axons in the inferior
2607 temporal cortex and primary visual cortex of the macaque monkey. Cereb Cortex.
2608 15:1887–1899.
2609 Tasic B, Yao Z, Graybuck LT, Smith KA, Nguyen TN, Bertagnolli D, Goldy J, Garren E,
2610 Economo MN, Viswanathan S, Penn O, Bakken T, Menon V, Miller J, Fong O,

2611 Hirokawa KE, Lathia K, Rimorin C, Tieu M, Larsen R, Casper T, Barkan E, Kroll
2612 M, Parry S, Shapovalova N V., Hirschstein D, Pendergraft J, Sullivan HA, Kim TK,
2613 Szafer A, Dee N, Groblewski P, Wickersham I, Cetin A, Harris JA, Levi BP, Sunkin
2614 SM, Madisen L, Daigle TL, Looger L, Bernard A, Phillips J, Lein E, Hawrylycz M,
2615 Svoboda K, Jones AR, Koch C, Zeng H. 2018. Shared and distinct transcriptomic
2616 cell types across neocortical areas. Nature. 563:72–78.
2617 Teichert T, Wachtler T, Michler F, Gail A, Eckhorn R. 2007. Scale-invariance of receptive
2618 field properties in primary visual cortex. BMC Neurosci. 8:Article 38.
2619 Thomson AM. 2002. Synaptic Connections and Small Circuits Involving Excitatory and
2620 Inhibitory Neurons in Layers 2-5 of Adult Rat and Cat Neocortex: Triple
2621 Intracellular Recordings and Biocytin Labelling In Vitro. Cereb Cortex. 12:936–953.
2622 Thomson AM, Destexhe A. 1999. Dual intracellular recordings and computational models
2623 of slow inhibitory postsynaptic potentials in rat neocortical and hippocampal slices.
2624 Neuroscience. 92:1193–1215.
2625 Thomson AM, Lamy C. 2007. Functional maps of neocortical local circuitry. Front
2626 Neurosci. 1:19–42.
2627 Tomioka R, Rockland KS. 2007. Long-distance corticocortical GABAergic neurons in the
2628 adult monkey white and gray matter. J Comp Neurol. 505:526–538.
2629 Tootell R, Silverman M, Switkes E, De Valois R. 1982. Deoxyglucose analysis of
2630 retinotopic organization in primate striate cortex. Science. 218:902–904.
2631 Tootell RB, Hamilton SL. 1989. Functional anatomy of the second visual area (V2) in the
2632 macaque. J Neurosci. 9:2620–2644.
2633 Tootell RB, Mendola JD, Hadjikhani NK, Ledden PJ, Liu AK, Reppas JB, Sereno MI,
2634 Dale AM. 1997. Functional analysis of V3A and related areas in human visual
2635 cortex. J Neurosci. 17:7060–7078.

2636 Tootell RBH, Silverman MS, De Valois RL, Jacobs GH. 1983. Functional organization of
2637 the second cortical visual area in primates. Science. 220:737–739.
2638 Tootell RBH, Silverman MS, Hamilton SL, Switkes E, De Valois RL. 1988. Functional
2639 anatomy of macaque striate cortex. V. Spatial frequency. J Neurosci. 8:1610–1624.
2640 Tootell RBH, Switkes E, Silverman MS, Hamilton SL. 1988. Functional anatomy of
2641 macaque striate cortex. II. Retinotopic organization. J Neurosci. 8:1531–1568.
2642 Trojanowski JQ, Jacobson S. 1976. Areal and laminar distribution of some pulvinar
2643 cortical efferents in rhesus monkey. J Comp Neurol. 169:371–392.
2644 Ts'o DY, Frostig RD, Lieke EE, Grinvald A. 1990. Functional organization of primate
2645 visual cortex revealed by high resolution optical imaging. Science. 249:417–420.
2646 Ts'O DY, Roe AW, Gilbert CD. 2001. A hierarchy of the functional organization for color,
2647 form and disparity in primate visual area V2. Vision Res. 41:1333–1349.
2648 Turrigiano GG. 2008. The self-tuning neuron: synaptic scaling of excitatory synapses.
2649 Cell. 135:422–435.
2650 Turrigiano GG, Leslie KR, Desai NS, Rutherford LC, Nelson SB. 1998. Activity-
2651 dependent scaling of quantal amplitude in neocortical neurons. Nature. 391:892–
2652 896.
2653 Ungerleider LG, Desimone R. 1986. Cortical connections of visual area MT in the
2654 macaque. J Comp Neurol. 248:190–222.
2655 Ungerleider LG, Mishkin M. 1979. The striate projection zone in the superior temporal
2656 sulcus of Macaca mulatta: Location and topographic organization. J Comp Neurol.
2657 188:347–366.
2658 Valverde F. 1978. The organization of area 18 in the monkey - A Golgi study. Anat
2659 Embryol (Berl). 154:305–334.
2660 Van Essen DC. 2003. Organization of visual areas in macaque and human cerebral cortex.

2661 In: Chalupa L,, Werner J, editors. Visual Neurosciences. MIT Press. p. 507–521.
2662 Van Essen DC, Glasser MF, Dierker DL, Harwell J. 2012. Cortical parcellations of the
2663 macaque monkey analyzed on surface-based atlases. Cereb Cortex. 22:2227–2240.
2664 Van Essen DC, Newsome WT. 1984. The visual field representation in the striate cortex
2665 of the macaque monkey: Asymmetries, anisptropies, and indiviual variability.
2666 Vision Res. 24:429–448.
2667 van Rossum MC, Bi GQ, Turrigiano GG. 2000. Stable Hebbian learning from spike
2668 timing-dependent plasticity. J Neurosci. 20:8812–8821.
2669 Venkat A, Christensen C, Gyulassy A, Summa B, Federer F, Angelucci A, Pascucci V.
2670 2016. A scalable cyberinfrastructure for interactive visualization of terascale
2671 microscopy data. In: 2016 New York Scientific Data Summit, NYSDS 2016 -
2672 Proceedings. p. doi: 10.1109/NYSDS.2016.7747805.
2673 Vidyasagar TR, Eysel UT. 2015. Origins of feature selectivities and maps in the
2674 mammalian primary visual cortex. Trends Neurosci. 38:475–485.
2675 Wandell BA, Dumoulin SO, Brewer AA. 2007. Visual field maps in human cortex.
2676 Neuron. 56:366–383.
2677 Wang HX, Movshon JA. 2016. Properties of pattern and component direction-selective
2678 cells in area MT of the macaque. J Neurophysiol. 115:2705–2720.
2679 Wang Y, Xiao Y, Felleman DJ. 2007. V2 thin stripes contain spatially organized
2680 representations of achromatic luminance change. Cereb Cortex. 17:116–129.
2681 Weller RE, Kaas JH. 1983. Retinotopic patterns of connections of area 17 with visual
2682 areas V-II and MT in macaque monkeys. J Comp Neurol. 220:253–279.
2683 Williams SR, Stuart GJ. 2002. Dependence of EPSP efficacy on synapse location in
2684 neocortical pyramidal neurons. Science. 295:1907–1910.
2685 Wiser A, Callaway E. 1996. Contributions of individual layer 6 pyramidal neurons to

2686 local circuitry in macaque primary visual cortex. J Neurosci. 16:2724–2739.
2687 Wiser AK, Callaway EM. 1997. Ocular dominance columns and local projections of layer
2688 6 pyramidal neurons in macaque primary visual cortex. Vis Neurosci. 14:241–251.
2689 Xiao Y, Casti A, Xiao J, Kaplan E. 2007. Hue maps in primate striate cortex. Neuroimage.
2690 35:771–786.
2691 Xiao Y, Wang Y, Felleman DJ. 2003. A spatially organized representation of colour in
2692 macaque cortical area V2. Nature. 421:535–539.
2693 Yabuta NH, Sawatari A, Callaway EM. 2001. Two functional channels from primary
2694 visual cortex to dorsal visual cortical areas. Science. 292:297–300.
2695 Yang Y, Liang Z, Li G, Wang Y, Zhou Y. 2009. Aging affects response variability of V1
2696 and MT neurons in rhesus monkeys. Brain Res. 1274:21–27.
2697 Yarch J, Federer F, Angelucci A. 2017. Local Circuits of V1 Layer 4B Neurons Projecting
2698 to V2 Thick Stripes Define Distinct Cell Classes and Avoid Cytochrome Oxidase
2699 Blobs. J Neurosci. 37:422–436.
2700 Yarch J, Larsen H, Chen M, Angelucci A. 2019. Morphological cell types projecting from
2701 V1 layer 2B to V2 thick and thin stripes. J Neurosci. epub ahead of print.
2702 Yoshioka T, Blasdel GG, Levitt JB, Lund JS. 1996. Relation between patterns of intrinsic
2703 lateral connectivity, ocular dominance, and cytochrome oxidase-reactive regions in
2704 macaque monkey striate cortex. Cereb Cortex. 6:297–310.
2705 Zeki S. 2015. Area V5—a microcosm of the visual brain. Front Integr Neurosci. 9:Article
2706 21.
2707 Zeki S, Shipp S. 1988. The functional logic of cortical connections. Nature. 335:311–317.
2708 Zhou H, Friedman HS, von der Heydt R. 2000. Coding of Border Ownership in Monkey
2709 Visual Cortex. J Neurosci. 20:6594–6611.
2710 Zhu Q, Vanduffel W. 2019. Submillimeter fMRI reveals a layout of dorsal visual cortex in

2711 macaques, remarkably similar to New World monkeys. Proc Natl Acad Sci U S A.
2712 116:2306–2311.
2713 Ziemba CM, Freeman J, Simoncelli EP, Movshon JA. 2018. Contextual modulation of
2714 sensitivity to naturalistic image structure in macaque V2. J Neurophysiol. 120:409–
2715 420.
2716